CONDUCTIVE ANODIC FILAMENT RELIABILITY OF FINE-PITCH THROUGH-VIAS IN ORGANIC PACKAGING SUBSTRATES

A Dissertation
Presented to
The Academic Faculty

by

Koushik Ramachandran

In Partial Fulfillment
of the Requirements for the Degree
Doctor of Philosophy in Materials Science in the
School of Materials Science and Engineering

Georgia Institute of Technology
December, 2013

CONDUCTIVE ANODIC FILAMENT RELIABILITY OF FINE-PITCH THROUGH-VIAS IN ORGANIC PACKAGING SUBSTRATES

Approved by:

Dr. Rao Tummala, Advisor
School of Materials Science and Engineering
Georgia Institute of Technology

Dr. Christopher Summers
School of Materials Science and Engineering
Georgia Institute of Technology

Dr. Jud Ready
School of Materials Science and Engineering
Georgia Institute of Technology

Dr. Preet Singh
School of Materials Science and Engineering
Georgia Institute of Technology

Dr. Rosario Gerhardt
School of Materials Science and Engineering
Georgia Institute of Technology

Dr. Venky Sundaram
School of Electrical and Computer Engineering
Georgia Institute of Technology

Date Approved: July 25, 2013

Dedicated to my parents

ACKNOWLEDGEMENTS

I would like to thank Prof. Rao Tummala, my advisor, who has been a constant source of motivation and inspiration. I will always be indebted for his belief in me and for providing me with the opportunity to work under his guidance. I am grateful to Dr. Venky Sundaram for his technical guidance and for being a great mentor, supporting me through thick and thin. I would like to thank Dr. Preet Singh, Dr. Christopher Summers, Dr. Rosario Gerhardt and Dr. Jud Ready for agreeing to serve on my reading committee and for providing valuable suggestions. Special thanks to Dr. Jud Ready for taking interest in this work, his help has been instrumental in shaping this thesis. Thanks are due to Dr. Preet Singh for sharing his expertise, always making time to meet to address my questions and also for providing access to his lab equipment. I would also like to express my gratitude to Prof. Rosario Gerhardt and Prof. Christopher Summers for their valuable technical inputs.

Thanks are due to Dr. Fuhan Liu for his guidance, caring attitude, and for training me on substrate fabrication processes. I would also like to express my gratitude to Dr. P. M. Raj for his technical inputs and help with experimental work. I would like to thank Mark Wilson (Dow Chemical Company) for initiating this project and for providing me with the opportunity to work with him. I would like to acknowledge Dr. Baik-Woo Lee, Dr. Himani Sharma and Nitesh Kumbhat for their help. I am thankful to Yuya Suzuki (Zeon Chemicals), Toshitake Seki (NTK-NGK) and Yoichiro Sato (AGC) for their help with experiments. I would also like to thank Yushu Wang for helping with impedance measurements, Ye Tian for helping with SEM, Daniel Pahner, Christian Ullman, Felix

Bergs from TU, Dresden and the interns at Georgia Tech for assistance with sample fabrication.

I would like to acknowledge Chris White, Jason Bishop, Hunter Chan, Charlie Russell (AVX Corp.) and Mike Toole for training and assistance with experiments. Thanks are also due to Dean Sutter, Traci Walden Monroe, Patricia Allen, Brian Mcglade, Christa Ernst, Karen May and Susan Bowman for administrative support. I am also thankful to the staff at MiRC for training me on characterization tools.

I would like to thank all my current and past lab mates for making my stay at Georgia Tech a pleasant and memorable one. I am also grateful to have had great friends who have never hesitated to offer help during times of need and have helped relieve stressful days. I would like to express my eternal gratitude to my family without which none of this would have been possible. I am extremely grateful for their unconditional love, belief and support.

TABLE OF CONTENTS

LIST OF TABLES

LIST OF FIGURES

LIST OF SYMBOLS AND ABBREVIATIONS

BT	Bismaleimide Triazine
CAF	Conductive Anodic Filament
CE	Cyanate Ester
CTE	Coefficient of Thermal Expansion
EDS	Energy Dispersive X-ray Spectroscopy
FR4	Flame Retardant Epoxy-Glass Fiber Composite
HAST	Highly Accelerated Stress Test
IC	Integrated Circuit
keV	Kilo Electron Volt
MTTF	Mean Time to Failure
PI	Polyimide
PTH	Plated Through Hole
PWB	Printed Wiring Board
RH	Relative Humidity
SEM	Scanning Electron Microscopy
T_g	Glass Transition Temperature
THB	Temperature-Humidity-Bias

SUMMARY

Organic substrates for packaging of semiconductors are migrating from halogenated-polymer composites with glass fiber reinforcement to halogen-free resins with glass microspheres and advanced glass fiber reinforcement to comply with environmental regulations and for improved reliability of microelectronic systems. Conductive copper plated-through-vias used for vertical interconnections in polymer-glass fiber composites are expected to reduce in spacings due to increasing component density and system integration, resulting in a via-to-via spacing of 50 – 100 μm in the next few years. Conductive anodic filament (CAF) failure is one of the most important challenges to overcome to ensure reliability of such high density organic packages. CAF is a specific type of electrochemical failure mode observed with conductive through-vias in glass fiber reinforced organic substrates in the presence of humidity and bias voltage. Several researchers have previously studied the reliability and mechanism of CAF formation in coarse-pitch through-vias in printed wiring boards, using brominated-resin glass fiber composites. However, the Reduction of Hazardous Substances (RoHS) directive, which specifies less than 900 ppm of bromine and chlorine concentration each, and lead-free solders for interconnections, has led to major changes in polymer compositions and flame retardants used in organic substrates. Therefore, there is a critical need for reliability study and fundamental understanding of failure mechanisms in fine-pitch through-vias in advanced organic packages to ensure long term reliability of future electronics.

This research reports for the first time CAF reliability of copper plated-through-vias with conductor spacings of 75 – 200 μm in thin glass fiber reinforced organic

packaging substrates with advanced epoxy-based and cyclo-olefin polymer resin systems. Reliability studies were conducted in halogenated and halogen-free substrates with improved test structure designs with different conductor spacing and geometry. Accelerated test condition (temperature, humidity and DC bias voltage) was used to investigate the effect of conductor spacing and substrate influence on insulation reliability behavior of the substrates. Characterization studies included gravimetric measurement of moisture sorption, extractable ion content analysis, electrical resistance measurement, impedance spectroscopy measurement, optical microscopy and scanning electron microscopy analysis. Elemental characterization was performed using energy dispersive x-ray spectroscopy. The accelerated test results and characterization studies indicated a strong dependence of insulation failures on substrate material system, conductor spacing and geometry. This study presents advancements in the understanding of failure processes and chemical nature of failures in fine-pitch through-vias in newly developed organic substrates and demonstrates potential methods to mitigate failures in high density organic packages.

CHAPTER 1

INTRODUCTION

1.1 Background and Future Needs for Microelectronic Packaging Substrates

Electronic packaging is used for interconnecting, powering, cooling, and protecting the integrated circuits (ICs) and system components in an electronic system [1]. Figure 1.1 shows the various levels of interconnections from the integrated circuit (IC), to packaging substrate to printed wiring board (PWB) in an electronic system. A typical electronic system consists of two types of components, (1) active components, (ICs) that perform computing, communication and other functions, and (2) passive components such as resistors, capacitors, etc. The packaging substrates interconnect the active and passive components to each other and to the PWB. The interconnections from IC to substrate are referred to as first-level interconnections, and are accomplished by wire bonding, or flip chip bumps of solder or copper. The packaging substrate is connected to the PWB using larger size solders, referred to as second-level interconnections. Copper plated-through-vias, also shown in Figure 1.1, act as electrical and thermal conduits, interconnecting the top side of the package to the bottom side. The interconnection pitch (center to center spacing) on the ICs decreases with increasing transistor density and is currently at 110 μm in area array format. The pitch of the second-level or the ball grid array (BGA) interconnection from package to board is larger and is currently at 400-500 μm. The packaging substrate, therefore, acts as a space transformer between the ICs and the PWBs, accommodating the smaller interconnection pitch of the ICs and the larger interconnection pitch of PWBs. The density of copper wiring and through-vias in the package is significantly higher than in the PWB. The size of interconnections, copper wiring and copper plated-through-vias are being continuously

scaled down to achieve a high density of input/outputs (I/Os) between active ICs and system [1].

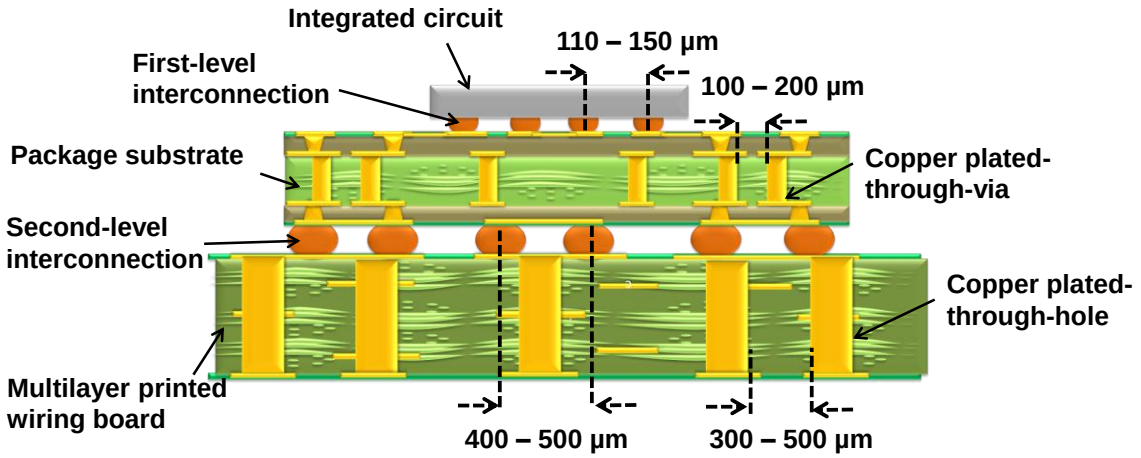

Figure 1.1. Cross-sectional schematic of an electronic packaging substrate showing plated-through-vias, chip-level interconnections on top and board-level interconnections on bottom.

1.2 Trends in Packaging Substrates: Fine-pitch Copper Plated-through-vias and Advanced Halogen-free Materials

The requirement for highly functional, smaller and reliable systems has resulted in two key technology drivers in microelectronic packages.

1. Need for smaller dimensions of conductors (copper plated-through-vias and surface-traces) in thin glass fiber reinforced organic substrates.
2. Need for novel halogen-free organic resin formulations with improved thermomechanical and electrical properties owing to environmental regulations on halogens and lead-based solders.

1.2.1 Need for Fine-pitch Copper Plated-through-vias

The continuous and aggressive scaling of conductor features in semiconductors is resulting in an ever widening gap between ICs and packages. Such aggressive scaling is continuously driving the need for high density wiring (plated-through-vias and surface-traces) capability in organic packages. The state-of-the-art dimensions for copper surface-traces and plated-through-vias in packages are defined in the International Technology Roadmap for Semiconductors (ITRS) [2]. A minimum through-via diameter of 100 µm with a minimum pitch of 300 µm, resulting in a minimum via to via spacing of 200 µm for high performance microelectronic packages (Table 1.1) is specified by ITRS. Based on the roadmap, the minimum spacing between the through-vias is expected to reduce to 160 µm by 2025. However, driven by 3D-IC stacking and system-on-packaging technology, the through-via diameters are shrinking rapidly and is expected to reach 30 - 50 µm and the spacings are expected to scale down to less than 100 µm in the next few years [3]. The limitations of organic packaging substrates in terms of achieving small through-via dimensions and surface-traces line width due to limitations such as dimensional stability and warpage with thinner substrates are being addressed by exploring alternate substrate materials such as glass and silicon.

Table 1.1. Projection for minimum wiring dimensions in packaging substrates [2].

Parameter	**2010**	**2015**	**2020**	**2025**
Min. through-via diameter (µm)	100	80	70	60
Min. through-via pitch (µm)	300	275	250	220
Min. line width/space (µm)	40/40	30/30	25/25	20/20

1.2.2 Need for Advanced Halogen-free Organic Resins

Reactive compounds based on halogens are integrated in the molecular network structure to provide flame retardant properties in traditional organic packaging substrates. However, there are environmental concerns associated with traditional halogen-based flame retardants in electronic systems. Halogenated aromatic compounds are undesirable because unregulated combustion of such materials can release toxic gases such as dioxins and furans into the environment. Dioxins and furans produced during recycling are considered as serious health risks because of reports on carcinogenicity and immunotoxicity. European directives such as Waste Electrical and Electronic Equipment Directive (WEEE) and Restriction of Hazardous Substances Directive (RoHS) restricted the use of certain halogenated materials in electrical and electronic components in 2006. Several halogen-free standards have been established since, such as IEC61249-2-21 and JPCA-ES01, and there is a continuous push towards using greener materials in electronics. Electronic industries across the globe have begun to adopt these standards, resulting in the development of a variety of halogen-free resin formulations for both packages and PWBs. The Institute for Printed Circuits (IPC) defines a maximum content of bromide and chloride less than 900 ppm each, with the total halogen content less than 1500 ppm for halogen-free materials (Table 1.2). Several non-halogenated substitutes have been identified, the most common of which are phosphorous-based, nitrogen-based and inorganic fillers. These compounds may also be used in combinations to achieve flame retardant properties [4], [5].

In addition to the trend towards implementing halogen-free resins, the restriction on lead-bearing solder alloys for chip-level and board-level interconnections has resulted in an increase in processing temperatures due to the higher melting temperature associated with lead-free solders. Organic substrates are subjected to peak temperatures of 250 - 260°C for assembly and therefore, traditional low T_g ($\leq$ 125°C) substrates are found to be incompatible for high temperature processes. The large thermal stresses

developed during such processes lead to reliability concerns. This in turn has driven the need for resin formulations with superior thermal stability and improved thermomechanical properties to withstand the high temperature processes [6].

Table 1.2. Halogen-free material specifications [5].

Halogen	Content (ppm)
Chlorine	≤ 900
Bromine	≤ 900
Total	≤ 1500

1.3 Reliability Challenges with Fine-pitch Copper Wiring and Through-vias in Advanced Halogen-free Organic Materials

The introduction of new halogen-free resin formulations with improved thermal, electrical properties, and the small dimensions of copper plated-through-vias and surface-traces can affect the long term reliability of electronic systems. Halogen-free resin formulations provide a solution to achieving greener electronic products that have minimal impact on environment. Additionally, resin systems with improved thermomechanical properties offer the required stability for lead-free assembly processes. However, the reliability performance of such newly developed materials, specifically the reliability of through-vias, has not yet been studied.

Copper is prone to electrochemical migration in the presence of humidity and bias voltage resulting in electrical insulation failures of systems. The magnitude of such failures increases drastically with decreasing conductor spacings; therefore, smaller spacings cause a reliability concern in terms of achieving high insulation reliability of through-vias in humid conditions. A specific mode of insulation failure driven by electrochemical migration of copper in glass fiber interface in organic substrates,

discovered by Bell Labs in late 1970s, is referred to as conductive anodic filament (CAF) failures [7].

1.4 Conductive Anodic Filament (CAF) Failures: A Reliability Concern

CAF failures have been recognized as a major barrier to miniaturization of electronic systems and it is one of the most important reliability concerns to overcome to achieve miniaturization and long term reliability [8]. CAF formation involves two steps [7], (a) interface degradation and (b) electrochemical migration.

a. Interface degradation

The first step involves degradation of the interface between the organic resin and the glass fiber reinforcement. This step is the path formation step and is the rate-limiting step for failures. Interfacial degradation is a result of several mechanisms such as drilling-induced fracture, high temperature processing resulting in thermal mismatch stresses and moisture diffusion induced swelling and hydrolysis of chemical bonds.

b. Electrochemical migration of copper

The second step is the electrochemical migration of copper from the anode. The copper conductors form the electrodes (anode and cathode), the diffused moisture acts as the electrolyte and the applied voltage is the driving potential for migration. The migration process is strongly dependent on the electric field between the conductors. Prior studies on CAF have reported a critical voltage gradient in the range of 0.1 – 0.4 V/μm for CAF failures. Therefore, the combination of applied DC voltage and small conductor spacing is a barrier for achieving miniaturization and CAF reliability in glass fiber reinforced organic substrates. Additionally, the presence of contaminants such as chloride and bromide ions is known to affect the failure mechanism by altering reaction kinetics and by forming insoluble corrosion products.

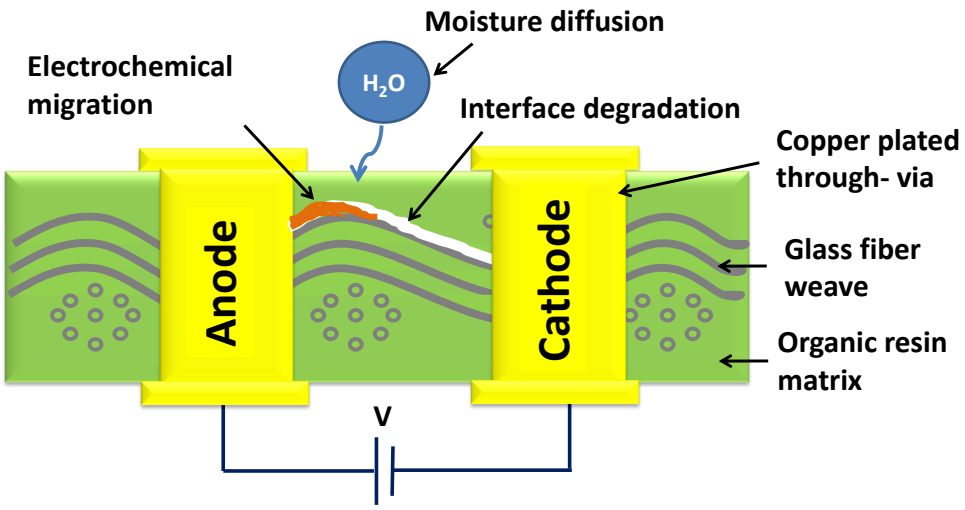

Figure 1.2. Simplified schematic showing the various steps involved in CAF failure.

1.5 Motivation Statement

CAF failures have been identified as a major threat for achieving miniaturization in electronic systems. Previous studies have focused on reliability investigation of plated-through-holes (PTHs) with conductor spacings (≥ 250 µm) in thick (800 - 1600 µm) glass fiber reinforced organic boards. However, organic packaging substrates for future electronic systems are expected to have conductor spacings less than 100 µm in thinner organic substrates (100 - 200 µm). There have been limited studies on reliability investigation of such small spacings in thin organic substrates and understanding of failure processes. Additionally, as stated previously the continuous push towards halogen-free and lead-free materials has driven the development of novel resin chemistries with improved thermal and electrical properties. Therefore, there is a necessity to investigate the reliability of small conductor spacings in newly developed organic resin system to obtain a fundamental understanding of the failure processes for

ensuring long term reliability of electronic products. The growing trend towards using halogen-free organic substrates and the demand for copper conductors with small spacings in next generation microelectronic packages are the main motivation for this study.

1.6 Research Objectives

The objective of this research is to investigate the reliability and understand failure mechanisms of fine-pitch copper plated-through-vias in organic packaging substrates. The specific objectives are stated as follows:

a. Investigate the effect of conductor spacings and conductor geometry in thin glass fiber reinforced organic substrates on insulation reliability in high temperature, humidity and DC bias conditions.
b. Study the influence of substrate material systems and material properties on insulation reliability using newly developed halogen-free substrate materials with improved properties and demonstrate a potential solution for achieving high reliability at small conductor spacings.

1.7 Technical Challenges

The technical challenges identified based on previous studies are described here.

a. Small conductor spacings have been found to drastically reduce mean time to failures in organic boards. Achieving high insulation reliability with small conductor spacings presents a major challenge for future microelectronic packages due to the critical voltage gradient required for CAF formation. Conductor spacings less than 250 μm in printed wiring boards have been previously reported to result in drastic reduction in failure times. There have been limited studies on small conductor spacings in thin packaging substrates.

b. Substrate material properties have been found to strongly influence CAF reliability. Traditional low-T_g epoxy-glass fiber composites with high moisture uptake have been observed to exhibit poor reliability in high temperature and humidity conditions; therefore, achieving reliable small conductor spacings in thin packages is a challenge for future electronic systems. This has led to the development of resin systems with significantly low moisture sorption, low CTE and high glass transition temperatures; the reliability of such materials have not been investigated. Ionic contaminants such as halides introduced during various stages of manufacturing have been reported to influence electrochemical migration and accelerate insulation failures. CAF reliability and chemical nature of failures in halogen-free materials have not been reported.

1.8 Research Tasks

Based on the technical challenges identified, the specific research tasks for this study are stated below.

a. Study reliability of small conductor spacings (75 – 200 μm) in thin (≤ 200 μm) glass fiber reinforced organic packaging substrates to understand the effect of small conductor spacing and geometry on insulation reliability. The research tasks include design of improved test structures with different conductor spacings and geometry, test structure fabrication, accelerated temperature-humidity-bias testing, insulation resistance measurements and failure analysis.
b. Investigate newly developed halogen-free substrate materials with improved properties such as low moisture absorption, low coefficient of thermal expansion (CTE) and high glass transition temperature (T_g) to establish substrate material influence on reliability behavior and chemical nature of failures. The research tasks include characterization studies including gravimetric measurements, extractable ion content analysis, and elemental characterization of failures.

CHAPTER 2

BACKGROUND AND LITERATURE REVIEW

2.1 Chapter Overview

This chapter provides background on glass fiber reinforced organic packaging substrates and conductive anodic filament (CAF) reliability. The discovery, mechanism of CAF and the effect of various parameters on CAF based on previous literature are discussed. Test structure design, testing conditions, parameters, detection techniques and chemical nature of CAF failures, and electrochemical mechanism leading to CAF formation will also be discussed.

2.2 Organic Packaging Substrates

The most common substrates used in microelectronic packages and printed wiring boards (PWBs) are organic composites with glass fiber reinforcement. Organic materials are widely used because of the ease of processability, low processing temperatures, low cost and the ability to tailor the properties by manipulating resin chemistries. Copper lines or traces on the surface and plated-through-vias form vertical interconnections, delivering signal and power from the integrated circuits (ICs) to the system boards (Figure 2.1). The individual components that constitute a substrate such as the organic resin matrix, glass fiber reinforcement, flame retardants, inorganic fillers, etc. and the functionalities of each of the components are briefly described in the following section.

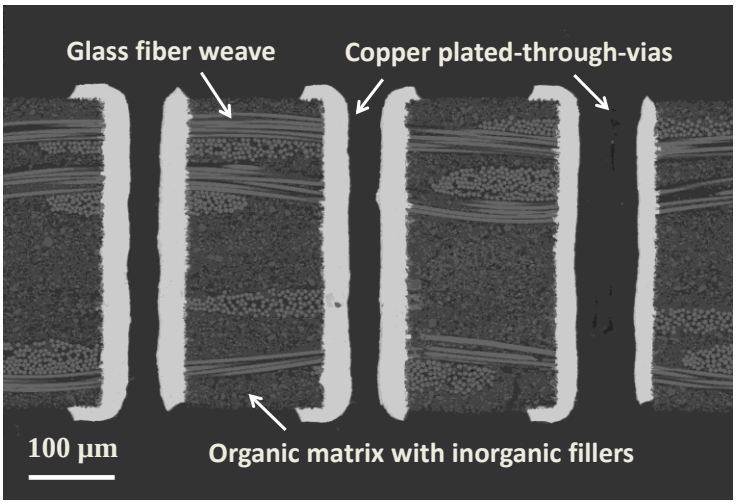

Figure 2.1. Cross-sectional SEM image of a glass fiber reinforced organic composite with copper plated-through-vias © 2013 IEEE [9].

2.2.1 Organic Resin

The organic resin system acts as a binder and load transferring agent. Organic resin matrices are reinforced with glass fibers and sometimes blended with inorganic filler particles to end up with the desired mechanical, electrical and thermal properties. Epoxy-based (FR4), bismaleimide triazine (BT), cyanate ester (CE) and polyimide (PI) are some of the most common resin systems. Epoxy based substrates (FR4) are most commonly used in packages and PWBs because of its electrical and mechanical properties. The epoxy resin matrix can consist of bi-, tetra- or multifunctional groups, which in turn results in different properties. FR4 substrates can have a wide range of glass transition temperatures [low T_g (< 140°C), mid T_g (140 - 165°C) and high T_g (> 165°C)], achieved using dicyandiamide (DICY) or phenolic curing agents. Curing agents enhance cross-linking of the epoxy resin, which affects thermal, mechanical and chemical properties of the substrate. Increased cross-link density in modified epoxies is known to increase the brittleness and reduce ease of processing. Phenolic-cured epoxies offer high thermal resistance, chemical resistance, lower moisture sorption but poor drillability compared to DICY cured-epoxy resins. Epoxy resins consist of accelerators such as

imidazole, organophosphine, etc. that increases reaction rates, reduces curing and controls the cross-linking density. Other resin systems such as BT (T_g > 200°C) , PI (T_g ~ 240 – 300°C), and CE (T_g ~ 260°C) exhibit better electrical performance compared to FR4 and are used especially for high speed applications due to higher cost [10].

2.2.2 Glass Fiber Reinforcement

The organic resin matrix is often reinforced with glass fibers to modify the coefficient of thermal expansion, elastic modulus, strength and electrical properties of the substrate. Sheets of prepregs consisting of organic resin reinforced with glass fibers are stacked layer by layer and subjected to head and pressure to make substrates. Glass fibers with different compositions, as shown in Table 2.1, are available and are chosen based on specific applications [1].

Table 2.1. Glass fiber compositions [1].

	E-glass	**S-glass**	**D-glass**
SiO_2	52 – 56	64 – 66	73 – 75
Al_2O_3	12 – 16	22 -24	0 – 1
CaO	15 – 25	< 0.01	0 – 2
MgO	0 – 6	10 – 12	0 – 2
B_2O_3	8 – 13	< 0.01	18 – 21

E-glass (electrical grade glass) is most commonly used because of its stable electrical characteristics combined with good mechanical properties. E-glass is also available at a low cost. S-glass and D-glass are high temperature glasses and are used when low CTE and low dielectric constant are preferred. However, S-glass and D-glass are expensive due to the high processing temperature and high silica content. Some of the newly developed organic substrates for next generation thin packages have utilized S-

glass fibers for achieving CTEs less than 5 ppm/°C. The CTE and dielectric properties of the different glass fiber are given in Table 2.2 [1].

Table 2.2. Glass fiber properties [1].

Glass	CTE (ppm/°C)	Dielectric constant (1 MHz)
E-glass	5.04	5.8
S-glass	2.80	4.52
D-glass	2.00	3.95

2.2.3 Silane Coupling Agents

Silane coupling agents are adhesion promoters between the inorganic glass fibers and the organic resin matrix. Silane coupling agents, also referred to as glass finish, vary between 0.1 µm to 10 µm in thickness. Silanes, represented using general chemistry, X_3SiRY (Y is an organofunctional group and X is a hydrolysable group), act as a bridge between the organic resin and inorganic fibers by forming chemical bonds. The hydrolysable group (X) attaches to the silicon through alkoxy or acyloxy linkage. This process is referred to as Silanization (Figure 2.2). If water is continuously removed during silanization, bonding of silane will continue until all the available sites on the glass surface are depleted. The bonding mechanism with inorganic surfaces involves the formation of hydrogen bonds with the hydroxyl groups on the surface of glass that later condense to form oxane bonds. The organofunctional group of the silane forms covalent bonds with the organic resin. Acids and bases are known to be powerful catalysts for hydrolysis and reformation of siloxanes bonds [11].

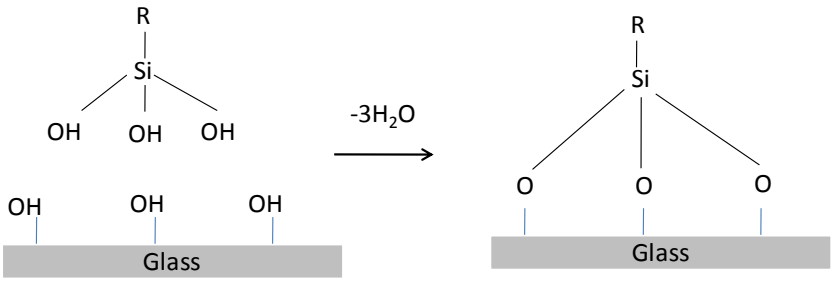

Figure 2.2. Schematic of glass silanization reaction.

2.2.4 Flame Retardants

Flame retardant capability is a requirement for all substrates used in electronics. In traditional organic packages and boards, reactive compounds based on halogens are polymerized with the resin and integrated in the molecular network structure to enable self-extinguish ability. Such compounds release reactive bromine atoms in to the flame upon combustion where they disrupt the oxidation reactions of flammable volatiles. However, such polybrominated compounds are considered undesirable because unregulated incineration of these materials can release dioxins and furans into the environment. Several environmental directives are driving halogen-free flame retardants. The Institute for Printed Circuits (IPC) defines halogen-free as materials with maximum chloride and bromide contents less than 900 ppm and a total halogen content less than 1500 ppm. This has led to the development of a variety of halogen-free substitutes [4].

Halogenated flame retardants are being replaced with phosphorus-based, nitrogen-based compounds and inorganic fillers. Flame retardant mechanisms are grouped into gas phase, char formation or release of water depending on the reactions that prevent combustion. Metal hydroxides are most commonly used, however, a large volume of fillers are required to achieve flame retardant properties. Increasing filler content to achieve flame retardant property affects the mechanical properties of the substrate. Therefore, a combination such as phosphorus doped resin and inorganic hydroxides are often used. The mechanism of phosphorus-based flame retardants

involves the formation of char on combustion, where the char forms an insulation layer between the substrate and flame preventing further combustion. Inorganic fillers such as aluminum hydroxides and magnesium hydroxide, on the other hand, release water on combustion at 200°C to 400°C (Equations 2.1 and 2.2), which absorbs the heat and cools the system [5].

$$2Al(OH)_3 \rightarrow Al_2O_3 + 3H_2O \quad (2.1)$$

$$Mg(OH)_2 \rightarrow MgO + H_2O \quad (2.2)$$

The mechanism of preventing combustion (gas phase, char formation or release of water) for the different types of flame retardants used in organic substrates is summarized in Table 2.3.

Table 2.3. Flame retarding mechanisms for different materials.

Type	**Mechanism**
Brominated	Gas phase
Phosphorus based	Char formation
Nitrogen based	Gas phase, Char formation
$Al(OH)_3$, $Mg(OH)_2$	Release of water

2.2.5 Inorganic Fillers

Inorganic fillers such as silicon dioxide and aluminum dioxide are blended with the organic resin for improving the thermomechanical property, specifically to lower the coefficient of thermal expansion (CTE) and increase the modulus of the substrate. Silica is most commonly used because of its ultra-low CTE (0.5 ppm/°C). Recently developed materials incorporate such fillers for increased modulus and reduced warpage in thin

substrates. However, high filler loading affects the mechanical properties of the substrates that in turn can affect processing [12], [13].

2.2.6 Copper Surface-traces and Plated-through-vias

Copper is the material of choice for circuitry in packages and PWBs owing to its superior electrical conductivity, thermal conductivity and mechanical properties. Copper surface-traces and plated-through-vias provide electrical and thermal interconnection between the ICs and PWBs, transmitting both signal and power. Through-vias in organic packages and boards are formed using mechanical or laser drilling process. After the formation of through-vias, electroless copper plating is used to form a thin conductive seed layer on the side walls, followed by electrolytic plating to achieve the desired thickness of copper [14].

2.3 Reliability

Reliability is defined as the ability of the system to perform its functions under a given condition for a specified period of time. Electronic systems are required to be highly reliable as they are constantly exposed to different conditions of usage. Moreover, some applications require are exposure to harsh environments such as high temperature and humid conditions. Accelerated life time tests are commonly used to evaluate and predict the long term reliability of components in electronic systems. Failure processes can be accelerated using conditions such as elevated temperature, humidity and bias voltage depending on the expected failure mode. As a result, the lifetime of a product under normal operating conditions can be determined. For instance, a temperature dependent failure process can be expressed using an Arrhenius relationship (Equation 2.3). The activation energy (E_a) can be determined from the reaction rates at two different temperatures.

$$k_T = k_O \exp\left[-\frac{E_a}{k_B T}\right] \quad (2.3)$$

Where k_T is the reaction rate, k_o is an empirical constant, E_a is the activation energy, k_B is the Boltzmann constant and T is the temperature. Similarly, for a failure mode dependent on humidity, Equation 2.4 expresses the effect at a certain humidity value (H).

$$k_H = k_O \exp[C.H^b] \quad (2.4)$$

Where k_H is the reaction rate, b is a constant found to be between 1 and 2. The experimental constant k_H and C can be determined from reaction rate at different humidity conditions. In order to extrapolate the lifetime of a product at normal operating conditions, an acceleration factor (AF) can be calculated using the following equation:

$$AF = \frac{S_s}{S_t} \quad (2.5)$$

Where S_s is the failure rate at service conditions and S_t is the failure rate under accelerated test conditions. For a failure process that involves temperature and humidity effects, the acceleration factor can be expressed using the following equation:

$$AF = \left(\frac{H_s}{H_t}\right).\exp\left[\frac{Ea}{k_b}.\left(\frac{1}{T_s}-\frac{1}{T_t}\right)\right] \quad (2.6)$$

2.4 Conductive Anodic Filament (CAF) Reliability

Conductive anodic filament (CAF) is a sub-surface electrochemical migration failure mode resulting in loss of insulation resistance of glass fiber reinforced organic

substrates [7]. CAF failures are different from metallic dendrite growth in the following ways:

- CAF is sub-surface failure mode, typically observed along the glass fiber-resin interface
- CAF is composed of a metallic salt as opposed to pure metal in case of dendritic growth.
- The direction of migration is from anode to cathode, hence the term anodic filament.

Silver migration in the presence of humidity and bias was reported as early as the 1930s [15]. CAF was first observed by researchers at Bell Laboratories in the 1970s when an unpredictable loss of insulation resistance occurred between conductors held at a potential difference. This type of failure mode due to electrochemical migration was termed as CAF [16]. Lahti et al. [17] observed CAF in epoxy-glass fiber composites (PWBs) with copper plated-through-holes (PTHs). The initiation of CAF mechanism was evident from visual enhancement due to the physical separation at the glass fiber/epoxy interface near the anode. It was also observed that the change in insulation resistance up to the point of failure was minimal, indicating a two-step failure process. Based on the observation, Lando et al. [7] proposed a two-step model for mechanism of CAF formation. The first step involves the degradation of resin and glass fiber interface. Once the interface degradation occurs, the second step is a rapid electrochemical migration step. The copper ions migrate from the anode to cathode along the epoxy-glass fiber interface causing a drastic reduction in insulation resistance. Such a system is analogous to an electrochemical cell where the copper conductors are the electrodes, the diffused water is the electrolyte and the applied voltage is the driving potential for electrochemical migration. A pH gradient is found to exist between the electrodes (anode and cathodes)

due to the generation of hydronium ions at the anode and hydroxide ions at the cathode. The pH gradient determines the corrosion behavior of copper under the given conditions. The electrochemical reactions occurring at the anode and cathode are given as follows.

Anode:

$$Cu \rightarrow Cu^{n+} + ne^{-} \quad (2.7)$$

$$H_2O \rightarrow \frac{1}{2}O_2 + 2H^{+} + 2e^{-} \quad (2.8)$$

Cathode:

$$Cu^{n+} + ne^{-} \rightarrow Cu \quad (2.9)$$

$$2H_2O + 2e^{-} \rightarrow H_2 + 2OH^{-} \quad (2.10)$$

A Pourbaix diagram [18] is an inter-relation of pH and corrosion to determine the thermodynamic behavior of metals under given conditions of pH. Pourbaix diagrams, also referred to as potential-pH diagrams are graphical representation of regions of thermodynamic stability of metal and the corresponding reaction products. Such diagrams are available for most metallic elements in water at 25°C. A representative Pourbaix diagram of copper is shown in Figure 2.3. It can be seen that in the region of pH between 7 and 11, copper is passivated and at pH values below 7 and potentials greater than 0.2 V, corrosion occurs. Similarly, corrosion occurs at a pH value greater than 11. Such diagrams are useful tools for understanding transition between active and passive state.

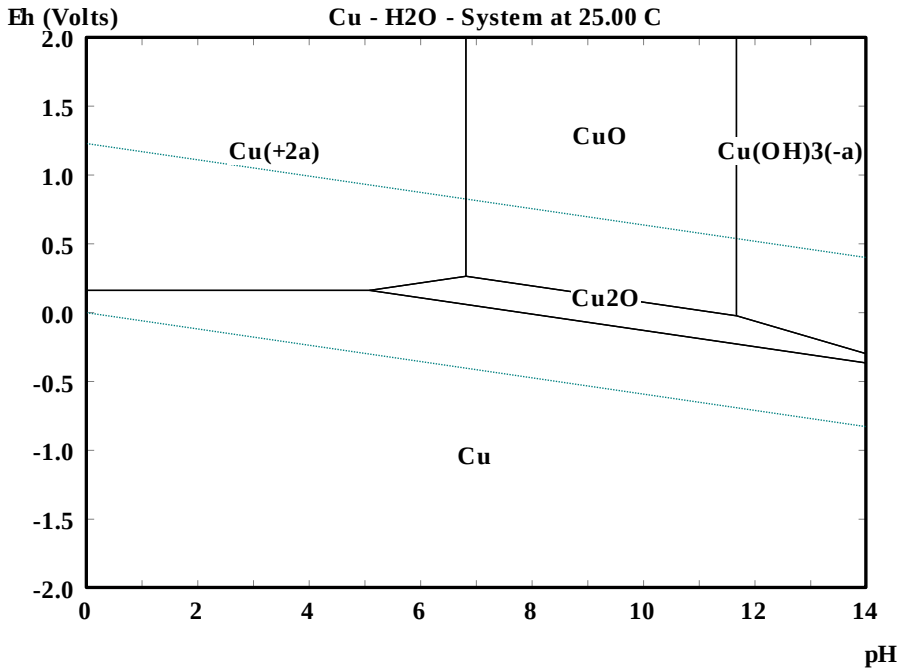

Figure 2.3. Pourbaix diagram for copper at 25°C.

2.5 Factors Influencing CAF Failures

Several factors have been identified to influence the formation of CAF. Some of the key factors include substrate material properties, conductor spacing, conductor configuration, voltage gradient, thermal excursion, humidity and processing variables such as flux formulation.

2.5.1 Substrate Material

Lando et al. [7] compared several fiber reinforced substrate materials including epoxy-based boards (FR4), non-fire retardant epoxy (G-10), polyimide, triazine, polyester and epoxy/Kevlar composites. Epoxy/Kevlar substrates were found to be most prone to CAF failures and triazine laminates were least susceptible to CAF failures. Rudra et al. [19] in 1994 compared the CAF behavior of three PWBs: epoxy-based (FR4), bismaleimide-triazine (BT) and cyanate ester (CE). BT was found to have the highest resistance to CAF formation because of its low moisture absorption and FR4

exhibited the lowest resistance to formation of CAF in their study. The three different laminates, FR4, BT and CE were found to absorb 1.15 wt%, 0.85 wt% and 0.65 wt% of moisture at 50°C and 70% RH, respectively. In addition to its lower moisture absorption, the higher T_g (195°C) of BT compared to FR4 (120°C), was also reported to have influenced the CAF failures. Similar observation was made by Liu et al. [20], who compared FR4, BT and Driclad (a proprietary high T_g substrate material), and found that FR4 exhibited the highest amount of moisture absorption. Driclad was found to have low moisture absorption due to the presence of lesser number of hydrophilic functional groups. Resin-rich substrates and cover-coated substrates were also investigated, either of which were observed to exhibit better CAF resistance than bare boards. The use of such cover-coated substrates provided an additional barrier to moisture diffusion thereby enhancing CAF resistance.

Ready [21] also investigated the effect of substrate materials on CAF failures using FR4, CEM-3 (G-10 with chopped glass) and MC-2 (blend of polyester with epoxy consisting of woven glass and chopped glass core). MC-2 was found to be most susceptible to failures in their study. BT, which was previously reported to be immune with large conductor spacings for PWBs, was recently found to suffer from insulation failures with smaller conductor spacings by Cohn and Kimbara [22]. Sauter [23] evaluated both CAF resistant and standard FR4 materials using CAF test. The CAF resistant materials were found to exhibit higher number failures at a closer spacing (< 0.500 µm) compared to standard FR4. This was attributed to the brittle nature of CAF resistant materials, which resulted in enhanced drilling-induced fracture at small via spacings. Research at National Physical Laboratory also compared CAF resistant and non-CAF resistant boards. Their results indicated CAF resistant laminates exhibited a longer time to failure compared to non-CAF resistant boards [24].

Chan [25] compared the CAF reliability of dicyanamide (DICY) and phenolic-cured epoxy boards using a voltage gradient of 0.4 V/µm and reported that DICY-cured

epoxy displayed better CAF resistance in comparison to phenolic-cured epoxy boards. The brittle nature of the phenolic-cured boards was reported to be the reason for higher number of failures in spite of its lower moisture absorption and higher thermal stability. Most previous studies have focused on reliability investigations in glass fiber reinforced organic boards. As discussed previously, the limitations in achieving smaller through-via diameters and spacings in organic substrates have led to the exploration of alternate substrate materials. Glass has recently gained attention as an alternative to organic substrate materials for high density packages. Glass substrates with thin polymer layers on either side with through-via spacing of 60 μm was reported to exhibit stable insulation resistance for 100 h in biased-highly accelerated stress testing [26].

2.5.2 Glass Fiber Reinforcement

CAF failures are also influenced by the type of reinforcement, glass fiber thickness, defects in fibers and surface finish. Hinds and Treanor [27] reported that thicker glass fibers required more force during drilling resulting in large mechanical stresses at the interfaces. Thicker glass styles such as 7628 (average thickness of 175 μm) required at least 2.5 times more force for drilling compared to 106 glass style (average thickness of 35 μm). Based on their study, thinner glass fibers are preferred for achieving smaller through-vias (100 μm) and for minimizing stresses resulting from the drilling process. However, several layers of thin glass fibers increase the cost of the substrate.

The direction of glass fiber was also found to have an effect on insulation resistance. Karavakis and Bertling [28] investigated laminates with through-via spacings ranging from 178 μm to 500 μm in both warp and fill direction. Their study revealed that the insulation resistance was lower for the fill direction for all conductor spacings. Johander et al. [29] showed that the distance between glass fibers has an important effect on CAF failures. The insulation resistance was one order of magnitude less for a length of 570 μm compared to a fiber length of 880 μm with a constant spacing between the

through-vias. They concluded that the smaller length increased the possible failure sites due to the high density of fibers along that direction.

2.5.2.1 Hollow Fibers

Researchers at CALCE identified the presence of hollow glass fibers in PWBs as a potential reliability issue due to filament formation failures. Their study utilized a technique, previously used to investigate leaks in fiber glass reinforced pressure vessels, to detect hollow fibers in PWBs. The number of hollow fibers in a woven glass fabric of dimension of 100 cm^2 varied from 0 to 3000. A typical multilayered laminate may consist of 15 layers of woven glass fabric; as such the presence of such hollow fibers was identified as potential failure sites due to conductive filament formation. The specification to prevent hollow fiber related failures is to have not more than one hollow fiber in a 10 cm x 10 cm sample, which reduced the failure possibility to less than 1% based on their models. An alternate guideline for hollow fibers specification is to have not more than four hollow fibers in a glass fabric with dimensions of 80.3 cm x 80.3 cm. Eliminating impurities and gas bubbles in molten glass were proposed as potential solution to prevent hollow fibers [30], [31].

2.5.3 Glass Surface Finish

Lando et al. [7] studied the reliability of boards with no-surface treatment and silane-treated glass fibers and reported that both the materials exhibited insulation resistance failures. However, they noted that the untreated sample indicated much more activity at the interface compared to the material with silane finish. Complete removal of glass fibers from the polymer matrix was therefore proposed as a method to reduce CAF related failures. However, this results in a loss of mechanical properties of the substrate. Therefore improving interfacial adhesion is an important consideration for reliability. In a recent study by Su et al. [32], amphiphilic oligomeric silane coupling agents (consisting of both hydrophobic and hydrophilic functional groups) were investigated to improve the

CAF behavior of epoxy-based laminates. The amphiphilic silanes resulted in lower moisture absorption at the interface due to its hydrophobic property, thereby, resulting in better CAF resistance. In another recent invention [33], hydrophobic silane coating mixed with the silane coupling agent was proposed a potential solution to prevent CAF formation. The silane composition consisted of a general structure R_1—S—$R_{(2,3,4)}$, where R_1 is a functional group that reacts with one or more surface silanols, and $R_{(2,3,4)}$ are each a functional groups that are hydrophobic and non-reactive with the surface silanol. The hydrophobic property of such coatings is expected to enhance the CAF resistance.

2.5.4 Moisture Sorption

Moisture sorption of the substrates is a critical factor for consideration in achieving high insulation reliability. In the presence of humidity, the moisture diffuses in to the substrate and affects resin-glass fiber adhesion in several ways in addition to providing an electrochemical pathway for ion migration. The moisture diffused in to the substrate can cause swelling of the resin adding stresses on interface, potentially resulting in interface degradation [8]. It is found that the majority of the diffused moisture remains as unbound liquid in the free volume of polymer. It can reach the interface and react with the silane coupling agents resulting in hydrolysis of chemical bonds. The bonds that form between the silane coupling agents and glass fibers, i.e. silicon and oxygen are 50% ionic in nature. The formation of such bonds depends on equilibrium constants and is reversible based on environmental condition [7]. Chemical bonding and debonding of silane coupling agents with glass fibers can be described using the general equation:

$$Si\text{-}O\text{-}Si + H_2O \Leftrightarrow Si\text{-}O\text{-}H + H\text{-}O\text{-}Si \qquad (2.11)$$

Substrates with lower moisture sorption are reported to exhibit better reliability. Liu et al. [34] reported that using a substrate with lower moisture uptake and a

hydrophobic coupling agent offered the high resistance to moisture induced failures. Takahashi [35] reported that the diffusion of water into the board was the rate-determining step for loss of insulation resistance based on AC impedance measurements in different conductor geometries on FR4. An abrupt and irreversible loss of adhesion in epoxy was observed by Lefebrve et al. [36] when the boards were equilibrated in air whose relative humidity exceeded the critical value. The moisture content in the board is traditionally evaluated using gravimetric method. However, gravimetric method of moisture absorption can result in significant errors in measuring thin samples, significant changes in moisture content can occur [37]. In a recent study by Su et al. [32], gravimetric measurements of water sorption in epoxy-glass fiber laminates consisting of an amphiphilic oligomeric silane were found to be consistent with the CAF behavior of the laminates. Gravimetric measurement can provide important information about moisture sorption of substrates, diffusion behavior, hygroscopic stresses, and interfacial adhesion.

2.5.5 Through-via Formation

Mechanical drilling remains the preferred low-cost method for forming through-vias or holes in substrates and boards. Mechanical drilling is typically restricted to a minimum through-hole diameter of 100 µm achieved using high speed drilling machines. A through-hole diameter of 200 µm is most commonly used for reducing the process cost. Recently, several advances have been made in this field. Murai et al. [38] reported that through-hole spacings between 50 µm to 100 µm can be achieved with great accuracy using 100 µm drill bits in thin boards. Another recent study reported that ultra-small through-vias with diameters less than 50 µm can be achieved using recently developed high speed (350,000 rpm) drilling machines [39]. However, there are certain limitations associated with mechanical drilling of composites. Since the drilling process involves physical displacement of the materials to form a hole, the process can result in

significant cracking and weakening of interfaces. The drill bits are capable of drilling only a specified number of holes (approximately 4000) before they wear out. The force required to drill increases with increasing drill bit wear, resulting in increased damage with time. The distance travelled by the drill bit into the board with each revolution is defined as chip load. An optimum chip load is required to avoid temperature build-up and to prevent drill bit wear. A lower chip load results in high drill bit wear while a higher chip load increases the force resulting in fracture. Aspect ratio is also an important consideration for mechanical drilling of substrates. Thicker boards result in greater drill bit wear because of the higher force exerted during the process [27]. The through-via diameter can also affect the reliability of the boards. Gopalakrishnan et al. [40] studied the effect of through-via diameter on a CAF resistant material using different drill bits. They reported that same spacing (495 µm) created using a larger drill bit (495 µm) revealed better reliability compared to smaller diameters (200 µm and 250 µm) in accelerated tests.

Drilling induced cracking has been noted as a reliability issue in printed wiring boards [8]. Ready and Turbini [41] noted the possibility of drilling-induced cracks of two closely spaced through-vias intersecting leading to degradation. Parry et al. [42] recommended a spacing of 350 µm for multilayer board design with a drilling tolerance of 75 µm. Caputo [43] recommended a minimum spacing of 500 µm for evaluation of CAF resistance. Through-via spacing of 500 µm was also utilized by Ready and Turbini [41] for investigating the CAF reliability. A minimum spacing of 270 µm is generally recommended for evaluation of CAF reliability of boards by IPC standards. The standards also specifies a minimum spacing of 150 µm for test structures in boards with very high CAF resistance [44]

The formation of drilling-induced micro cracks exposing the glass fibers can result in premature electrical shorts in accelerated tests. Drastic insulation failures in FR4 PWBs with spacings less than 100 µm were reported by Sood and Pecht [45], indicating

the possible presence of pre-existing defective sites. However, they reported that the through-hole tolerance was less than 25 µm. The exposed glass fibers act as preferred sites for filament formation, thereby accelerating insulation failures. In a recent invention [46], silane coating of the exposed glass fibers was proposed as a solution to enhance CAF resistance. The silane layer reacts with the silanols on glass to form siloxanes, which is further polymerized to form a barrier layer thereby resulting in an increased resistance to CAF formation. Zhang [47] also proposed a method to enhance CAF resistance, where the drilled through-holes are sputtered with a copper seed layer of sufficient thickness to provide a barrier layer against migration of ions.

Cohn and Kimbara [22] reported that the insulation property showed a strong dependence on the quality of through-vias and via formation method. Insulation failures were observed in mechanical-drilled through-vias with small through-via spacing, 100 µm and 150 µm in BT. They noted that there is a possibility of degradation along the entire length of the glass fibers between closely spaced vias during mechanical drilling. Substrates with laser-drilled vias with the 100 µm spacing were found to exhibit better reliability under the same accelerated test conditions. Chan [25] also compared the reliability of mechanically-drilled and laser-drilled vias and reported that laser-drilled vias performed better in accelerated test. The test structures studied were not exactly similar, resulting in differences in number of possible failure sites. Laser drilling is also reported to induce lower stress at the interface, and is suggested as an alternative to mechanical drilling for achieving fine-pitch through-vias. However, there are significant challenges associated with laser drilling of glass-fiber reinforced substrates including heat affected zone (HAZ), charring, redeposition and residues that can affect processing and reliability. Laser drilling processes require optimization for specific substrate systems because of the different ablation threshold energy density of resin, copper and glass fibers [48]. Additionally, electroless plating of laser drilled vias and achieving interfacial

adhesion between copper and side walls of laser-drilled through-vias remains a challenge [25].

2.5.6 Conductor Geometry, Spacing and Applied Voltage

CAF failures have been reported to occur in different conductor geometries. Failures can occur between two surface-traces, two through-vias or a through-via and a surface-trace. Different conductor geometries are shown in Figure 2.4 of which, the through-via to through-via geometry is found to exhibit the highest susceptibility to CAF followed by via-trace and trace-trace configurations by Lando et al. [7].

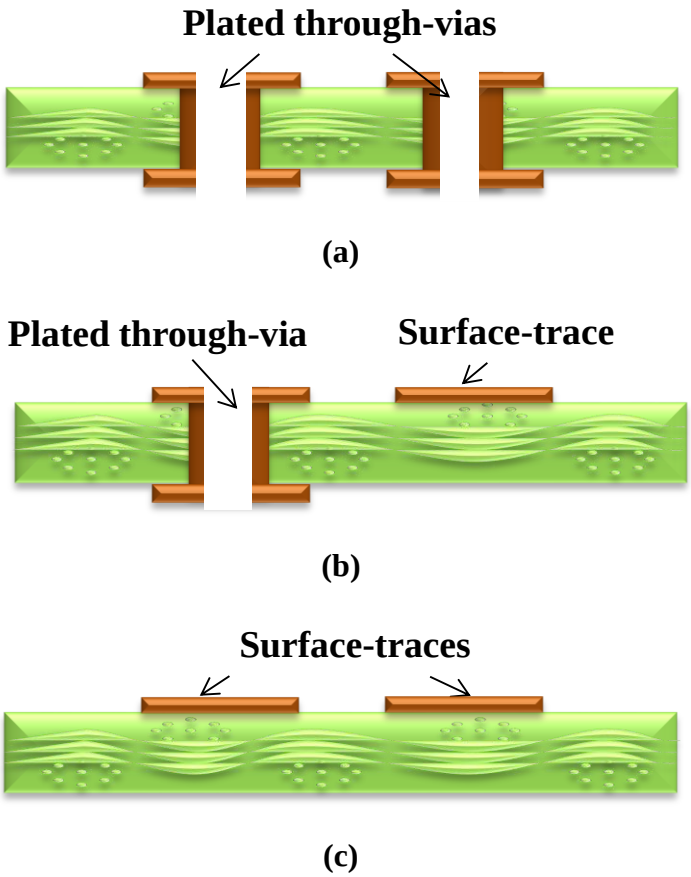

Figure 2.4. Conductor configurations: (a) through-via to through-via, (b) through-via to surface-trace, and (c) surface-trace to surface-trace.

Der Marderosian [49] investigated the reliability of multilayer PWBs under three different conditions: 100V DC, 100V AC and no bias. The boards, exposed to AC bias and no bias condition, were not found to exhibit failures. The boards exposed to 100V DC were found to exhibit failures, which were later shown to be CAF failures. The study indicated that CAF failures occurred only under DC bias voltage.

Lahti et al. [17] investigated PTHs with spacings ranging from 5 mils to 50 mils and reported a drastic reduction in failure times with 5 mil spacings. Rudra et al. [19] also investigated the spacing effect using different conductor geometries with spacings ranging from 5 mils to 65 mils (~125 µm to 1650 µm) with two different DC voltages, 300V and 800V. The test structures with 0.5 mm spacing were reported to exhibit a life of 450 h at 300V in comparison to life of 100 h at 800V. Ready and Turbini [41] investigated the effect of spacing in PTH-PTH geometry using two different spacings, 500 µm and 750 µm and developed a quantitative model for mean time to failure (MTTF) with spacing and voltage dependence, which is described in Section 2.7. Their study showed a critical voltage gradient of 0.325 V/µm for CAF failures. Chan [25] used a voltage gradient of 0.4 V/µm to investigate CAF failures in DICY-cured and phenolic-cured epoxy boards.

Driven by high circuit density demands, recent studies have focused on reliability of smaller conductor spacings [22], [45]. A strong dependence of insulation failures on conductor spacing in BT was observed by Cohn and Kimbara [22]. They reported insulation failures in test structures with mechanically-drilled through-vias with spacing of 100 µm and 150 µm in accelerated testing. Sood and Pecht [45] investigated the conductive filament formation reliability of four different FR4 laminates (thickness of approximately 1800 µm) with conductor spacings of 75, 100 and 150 µm respectively. The test vehicles were found to exhibit drastic insulation failures in accelerated life tests with some of the failures occurring within 1 min of application of bias voltage.

2.5.7 Temperature and Humidity

A temperature dependence of activation energy was reported by Bell Labs researchers. The activation energy (E_a) was found to be between 0.0 eV and 0.2 eV below 60°C and between 1.0 eV and 2.5 eV above 65°C [17]. Ready and Turbini [41] determined activation energies as 0.14 – 0.37 eV at three different temperatures (75°C, 85°C and 95°C) in FR4 for different flux formulation and also observed a reduction in MTTF with increasing aging temperatures. A higher reflow temperature was also found to increase thermal strains due to the CTE mismatch between the glass fibers and the epoxy resin. The effect of thermal cycling and lead-free reflow temperature (250°C) was investigated by the researchers at National Physics Laboratory [24]. Their study concluded that lead-free reflow process increased the susceptibility to CAF while thermal shock had a negligible effect on MTTF. CAF resistant and non-CAF resistant FR4 boards were subjected to thermal cycling and lead-free reflow and it was observed that higher reflow temperature increased the susceptibility to CAF. CAF resistant FR-4 boards delayed the time to failure in comparison to non-CAF resistant FR-4 boards.

Researchers at National Physical Laboratory also investigated the effect of thermal shock on FR4 boards. The boards were exposed to thermal cycling from -15°C to 120°C with 5 minutes at each temperature extreme with a total cycle of time of 15 minutes. The boards were also exposed to lead-free assembly temperature for three times. It was found that the lead-free reflow process increased the CAF susceptibility while thermal shock had minimal effect on CAF failures. In a second set of experiments, high and low T_g laminates were exposed to lead-free and lead-based reflow temperatures. The results indicated that higher reflow temperatures accelerated CAF failures in both low and high T_g laminates [24].

It has been identified that CAF failures do not occur in the absence of humidity. Augis et al. [50] reported the effect of relative humidity on the formation of CAF and

established that there is a threshold in relative humidity below which CAF will not occur. The percentage of CAF failures increased rapidly above certain humidity levels in step stress tests. This indicated that a material that performed poorly in accelerated conditions may have acceptable performance in normal operation conditions. Rudra et al. [19] also evaluated the effect of humidity and found that at 70% RH, the life in accelerated testing was 430 h while it reduced to 190 h at 85% RH in FR4 with conductor spacings of 500 μm.

2.5.8 Flux Formulation

Fluxes are used to remove the surface oxides and minimize oxidation of the base metal during assembly. The three main types are (a) rosin-based, (b) no clean, and (c) water soluble fluxes. Rosin fluxes liquefy and solidify trapping harmful contaminants and are generally used for high reliability applications. The cleaning step after fluxing can be avoided using no clean flux due to the low level of contaminations. Water soluble fluxes provide higher soldering yield and require a cleaning step with water. However, water soluble fluxes have been found to leave harmful contaminants that affect the reliability of the boards [43].

Jachim [51] demonstrated the effect of flux choice on CAF formation using IPC B-24 SIR coupons. The coupons processed with flux were found to exhibit more CAF failures than the coupons without flux. Bent and Turbini [52] later studied the effect of CAF formation with several water soluble fluxes using both lead-based and lead-free soldering conditions. The study showed that the magnitude of CAF failures were significantly higher for coupons processed with flux under lead-free conditions. Certain water-soluble flux residues were found to diffuse in to the board during the reflow process. Such residues are hydrophilic, resulting in enhanced moisture absorption and accelerating the time to failure.

Turbini et al. [53] studied the effect of water-soluble flux at 201°C and 240°C simulating the peak temperature for traditional lead-based and lead-free solder alloys, respectively. The study revealed that the susceptibility of CAF formation increased at higher processing temperatures. Ready et al. [54], [55] investigated the effect and formulation of flux on formation of CAF. The CAF filaments were found to contain chlorine or bromine and copper. It was reported that the presence of bromine detected by EDS may have come from a processing step. HBr was a solder flux constituent, which was identified as the source of bromide ions in CAF. It was also observed that presence of polyglycol in the flux enhanced the moisture absorption by diffusing in to the boards when the substrate is above its T_g during soldering. The longer the boards were exposed to temperatures above the glass transition temperature; there was an enhanced diffusion of polyglycol in to the board. It was also noted that during soldering process, glass fiber-epoxy delamination might also occur, leading to an increased possibility for delamination and formation of CAF. While CAF was found to form only at the epoxy/glass fiber interface for unprocessed boards, a copper and chlorine containing compound was found in the epoxy matrix for the boards processed with a flux. CAF morphology was also found to be different based on the type of flux used for processing the boards. The CAF appeared stratified in boards processed with a polyethylene polypropylene glycol (PEPG) flux (2 wt% bromide) and striated for boards processed with linear aliphatic polyether (2 wt% chloride).

Caputo et al. [43], [56] investigated the effect of polyethylene glycol (PEG) and polyethylene propylene glycol (PEPG) fluxing agents on CAF formation. For the coupons processed using PEPG flux with and without chloride; a copper-chloride compound was formed in the matrix. For the test coupons processed using PEG with and without chloride, CAF formed at the epoxy-glass fiber interface, however no copper chloride formed in the matrix. The PEG appeared to form a PEG-Cu-Cl complex binding the available copper and acting as a barrier to the formation of CuCl in the matrix.

Caputo et al. [43] also evaluated the effect of a high-bromide containing flux on CAF formation and detected the formation of a bromide containing CAF.

2.6 Chemical Nature of CAF

DerMarderosian [57] identified CAF failure mechanism as an electrochemical failure mode and proposed the chemical reactions (Equations 2.12 and 2.13) as cause of failures that was observed in copper conductors under DC bias. The failures were termed as "punch-thru", which were later found to be CAF failures.

$$Cu + 3H_2O = CuO + Cu(OH)_2 + 2H_2 \quad (2.12)$$

$$Cu(OH)_2 = CuO + H_2O \quad (2.13)$$

The mechanism proposed involved the formation of CuO and $Cu(OH)_2$ at the anode, and $Cu(OH)_2$ decomposed to CuO and H_2O in the presence of heat. Later investigations of CAF microstructure using elemental analysis techniques revealed that two types of CAF compound could form, chloride containing and bromide containing copper compound [43], [54].

2.6.1 Chloride Containing CAF

Ready et al. [58] investigated the microstructure of CAF using scanning electron microscopy and energy dispersive x-ray spectroscopy. The study revealed that CAF contained copper, chlorine and sometimes bromine. The formation of a chloride containing copper compound under the given conditions was explained based on a potential-pH diagram. As seen from the Pourbaix diagram of Cu-Cl-H_2O (Figure 2.5), the compound ($3Cu(OH)_2$. $CuCl_2$) forms in the presence of copper ions, water and chloride ions near the low pH region, which corresponds to the anodic region [41], [54].

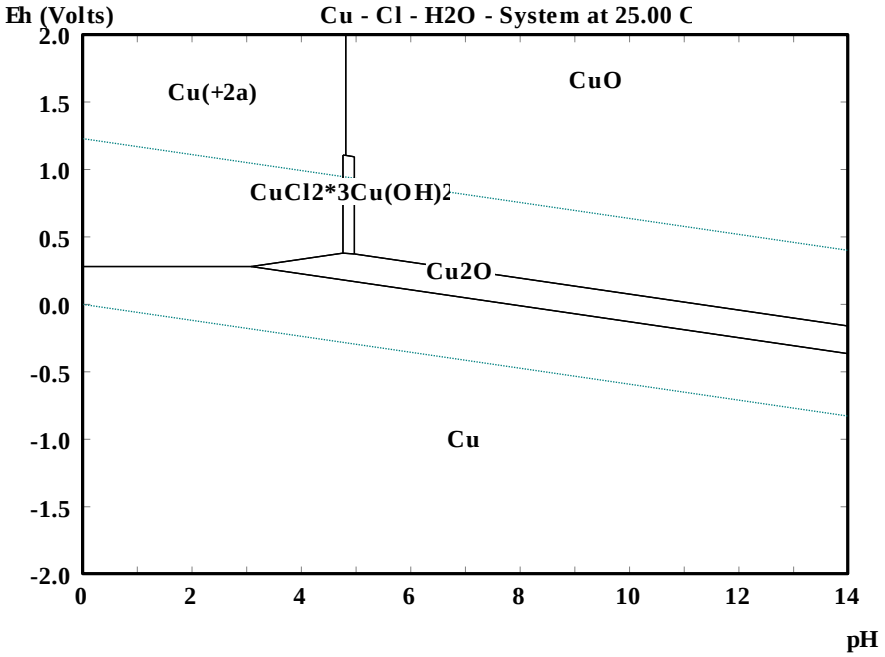

Figure 2.5. Pourbaix diagram for Cu-Cl-H_2O system with 35 ppm of Cl at 25°C.

Ready and Turbini [41], [54] identified the conductive filament as synthetic atacamite [$2CuCl_2.5Cu(OH)_2.H_2O$] based on powder diffraction data using transmission electron microscopy (TEM), as shown in Figure 2.6. In their study, they reported that synthetic atacamite or copper chloride hydroxide hydrate was detailed in card number 23-948 from the International Centre for Diffraction Data (ICDD). They also reported that synthetic atacamite is translucent and deep green in color and displayed a slender, striated and acicular to fibrous rhombic or orthorhombic crystal structure. The x-ray diffraction database for this compound was later found to have been replaced with the chemical formula, ($Cu_2(OH)_3Cl$).

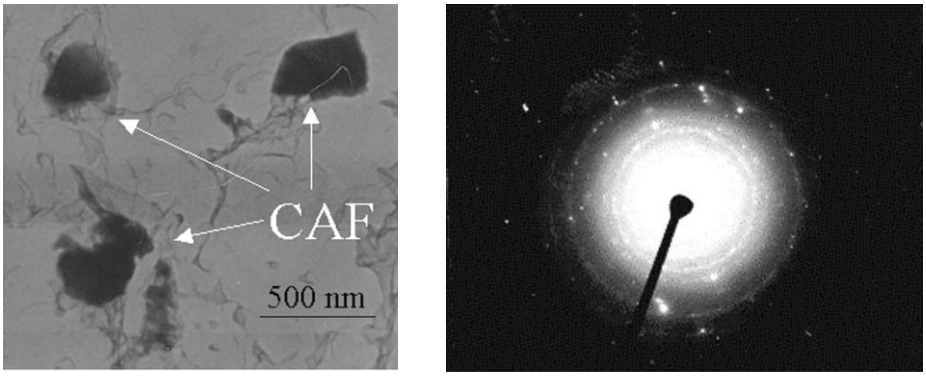

Figure 2.6. TEM image and electron diffraction pattern of chloride containing CAF [41].

Meeker and Luvalle [59] identified a failure causing chloride containing copper compound and proposed a kinetic model for formation, in which two competing reactions lead to two different chlorine containing compounds. Based on the model, one reaction leads to an innocuous trapped chloride compound while the other reaction lead to a failure causing chloride compound. However, later in a study by Caputo et al. [60], no evidence of innocuous chlorine containing compound was found in the matrix. Thus, it was concluded that the formation of ($Cu_2(OH)_3Cl$) from CuCl proceeded by a single non-reversible reaction that lead to CAF failures.

Copper corrosion in chloride medium has been reported by several researchers [61]-[66]. The difference is the initial dissolution step of copper depending on chloride concentration. May et al. [61] reported that copper dissolution occurred according to Equations 2.14 and 2.15 for chloride concentration in the range of 0.01 M to 0.03 M.

$$Cu + Cl^- \rightarrow CuCl + 1e^- \qquad (2.14)$$

$$CuCl \rightarrow Cu^{2+} + Cl^- + 1e^- \qquad (2.15)$$

A single-step electro-dissolution of copper can also occur according to the Equation 2.16. Copper was found to dissolve as $CuCl_2^-$ in NaCl solution with

concentrations of 0.124 M, 0.372 M, and 1.24 M at two temperatures, 29°C and 101°C [62]. Copper in LiCl with concentration ranging from 0.2M to 1 M was also found to form $CuCl_2^-$ according to the single-step dissolution process [63].

$$Cu + 2Cl^- \Leftrightarrow CuCl_2^- + 1e^- \qquad (2.16)$$

Based on previous studies on copper corrosion in chloride medium, $CuCl_2^-$ is favored for solutions with chloride concentration less than 0.75 M, while $CuCl_3^{2-}$ dominated for solutions with higher chloride concentrations. For chloride ion concentration less than 0.05 M, a considerable amount of copper was found to dissolve as Cu^{2+} ions. $CuCl_2^-$ was found to be dominant for chloride concentration less than 1M and $CuCl_3^{2-}$ for concentration higher than 1M [64]. However, Caputo [43] noted that the chloride concentration in PWBs is insufficient for the formation of $CuCl_2^-$. Further, the study identified the presence of CuCl in the matrix using XPS. Therefore, the formation of CAF was proposed to proceed according to the following reaction:

$$12CuCl + 6H_2O + 3O_2 \rightarrow 4Cu_2(OH)_3Cl + 4Cu^{2+} + 8Cl^- \qquad (2.17)$$

2.6.2 Bromide Containing CAF

Ready [21] have also observed formation of a bromide containing CAF. Caputo et al. [43], [67] also reported the formation of bromide containing CAF in boards processed with a high bromide containing hot air solder leveling (HASL) fluid. They reported that both chloride containing and bromide containing CAF was created in the boards processed with a flux with high bromide content (~15 wt%). Caputo et al. [43], [67] identified the bromide containing CAF as $Cu_2(OH)_3Br$ using TEM as seen in Figure 2.7 and also reported the formation of a bromide containing compound in the polymer matrix. The copper compound in the matrix was identified as CuBr using XPS. Ion

chromatography analysis was used to verify the source of bromide and diffusion of high bromide containing flux in to the board during reflow was identified as the main source of bromide ions.

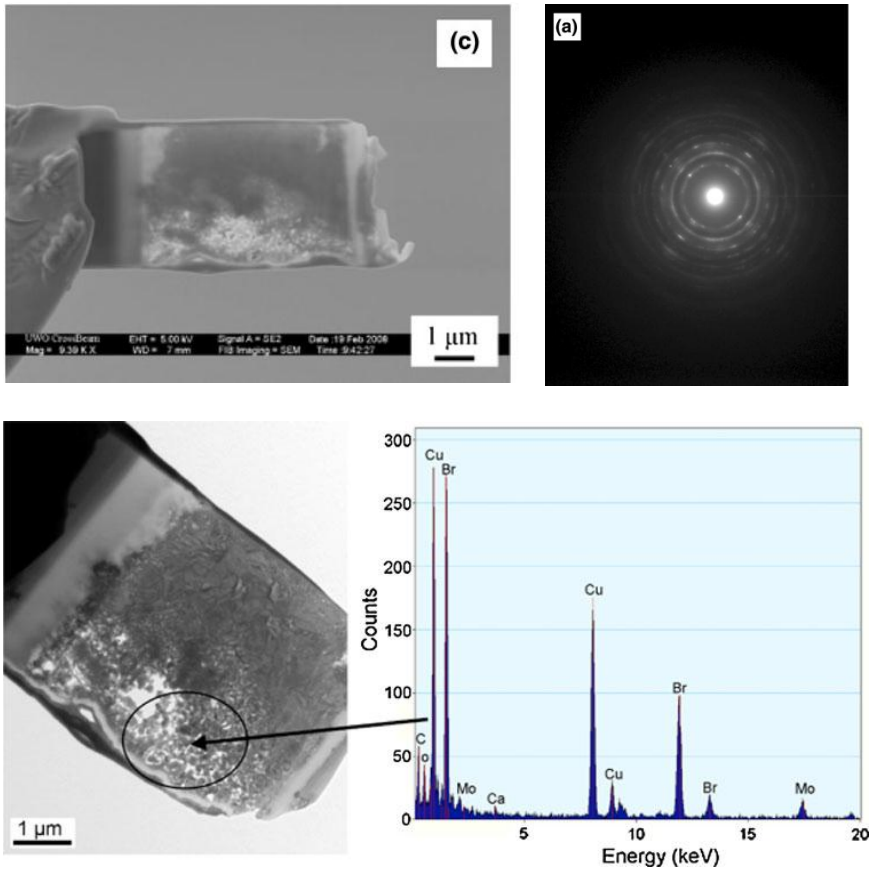

Figure 2.7. TEM image, electron diffraction pattern and EDS of bromide containing CAF [67].

The corrosion process for bromide containing CAF was reported to follow electrochemical mechanism similar to chloride containing compound formation. The dissolution of copper in presence of bromine is reported to occur in one of the several ways [68]-[70].

$$Cu + Br^- \rightarrow CuBr + e^- \quad (2.18)$$

$$Cu + 2Br^- \rightarrow CuBr_2^- + e^- \quad (2.19)$$

The presence of CuBr in the polymer matrix, verified using XPS, suggested that CuBr was forming near the anode. Therefore, similar to chloride containing CAF, the following electrochemical reaction was proposed for the formation of bromide CAF.

$$4CuBr + 4H_2O + O_2 \rightarrow 2Cu_2(OH)_3Br + 2Br^- + 2H^+ \qquad (2.20)$$

Similar to copper corrosion in the presence of chloride, corrosion behavior of copper in bromide media studies indicate that the system behaves in a similar fashion to copper-chloride system [68]. Based on thermodynamic calculations, Caputo [43] showed that the formation of $CuBr_2^-$ from the direct attack of bromide ions on copper is thermodynamically unfavorable. They reported that the formation of bromide containing CAF ($Cu_2(OH)_3Br$) is more likely to proceed from the formation of CuBr similar in a fashion to formation of chloride containing CAF [67].

2.6.3 Chloride vs. Bromide Containing CAF

Investigation of CAF by Ready and Turbini [41] suggested that chloride containing CAF was more favorable even in the presence of a bromide containing flux. The reasons hypothesized for such occurrence was that the large difference in electronegativity of copper and chlorine creates a favorable attraction in comparison to bromine. The ionic radius of chloride is also smaller than bromide and the ionic mobility of chloride ions is larger compared to bromide due to its lower ionic mass. Caputo [43] reported that the standard free energy of formation of chloride CAF is -1340.3 KJ/mol and that of bromide CAF is -1282 KJ/mol. Both the reactions were expected to be energetically favorable, however, thermodynamic calculations based on the proposed electrochemical mechanisms (Equations 2.16 and 2.20) resulted in a standard free energy change for a reaction -3287.4 KJ for chloride-CAF and -1420.4 KJ for bromide-CAF.

Hence it was concluded that high bromide content was required to form bromide CAF. This was consistent with experimental observation where only boards processed with HASL fluid containing approximately 15% of bromide ions resulted in the formation of a bromide containing CAF [43].

2.7 Quantitative Models for CAF failures

Based on the two-step model for CAF formation, models have been developed to predict the mean time of failure (MTTF) for CAF formation [41], [71]-[73]. Welsher et al. [71] proposed a two-step model consistent with the previously reported failure model for CAF. The first step, which is dependent on temperature and humidity, is expressed using the equation:

$$MTTF = a(H)^b \exp(E_a / RT) \tag{2.21}$$

The voltage dependent step is described using the following equation:

$$MTTF = c + d/V \tag{2.21}$$

In the equations above, E_a is the activation energy, T is the temperature, H is the relative humidity, R is the gas constant, V is the applied voltage, a, b c and d are material dependent constants. The combined equation to predict failure is given by,

$$MTTF = a(H)^b \exp(E_a / RT) + d(L^2/V) \tag{2.22}$$

Where d describes the temperature and humidity dependence and L is the conductor spacing. Mitchell and Welsher [72] further developed the model to

accommodate for different conductor geometries. The revised MTTF model is given by the equation

$$MTTF = \alpha\left(1 + \beta.\frac{L^n}{V}\right).H^{\gamma}.\exp\left(\frac{E_a}{RT}\right) \quad (2.23)$$

Where α and β are material dependent constants, γ is a humidity dependent factor and n relates to the orientation of the conductors. Gandhi et al. [73] showed that the voltage dependence is better represented by an inverse squared or cubed relationship rather than a linear dependence. A physics of failure approach has also been used to accommodate several factors such as humidity, temperature, voltage, laminate choice, spacing and geometry of the conductors in the failure model [19]. The time to failure model based on this approach is given by the following equation:

$$MTTF = \frac{a.f.(1000.k.L)^n}{V^m.(M - M_t)} \quad (2.24)$$

In the equation above, a is the acceleration factor for filament formation, f is a multilayer correction factor, k is the conductor shape factors, m is the acceleration factor for voltage V, M is the percentage moisture content, M_t is the percentage moisture content threshold. Ready and Turbini [41] modified Welsher's model to accommodate the effect of conductor spacing and voltage in hole to hole configuration. The equation for mean time to failure is given by,

$$MTTF = c\exp\left(\frac{E_a}{kT}\right) + \frac{d(L^4)}{V^2} \quad (2.25)$$

As seen from Equations 2.22 – 2.25, a consistent observation made by several researchers is the power law dependence of MTTF on conductor spacing (L) and the applied voltage (V). This is a critical because a drastic reduction in failure times can be expected with smaller conductor spacings.

2.8 CAF Test Structure

The test structure design for studying CAF reliability of boards is described in IPC-TM-650 2.6.25 test method (conductive anodic filament resistance x-y axis) [44]. The standards include two types of geometry (Figure 2.8), (a) in-line through-hole configuration and (b) staggered through-hole configuration. There are 210 through-holes in one test coupon in in-line through-hole configuration arranged in an alternate anode and cathode configuration. There are two rows of 42 through-vias that are positively biased and three rows of 42 through-vias that are negatively biased. Such a test design enables 168 possible in-line failure sites. The staggered through-hole design consists of three rows of 26 vias that are positively biased and four rows of 26 vias that are negatively biased, resulting in 312 possible failure sites. The smallest through-hole spacing for the staggered design is along the diagonal direction. The in-line through-hole spacing is smaller compared to the staggered through-hole design based on IPC test standards. Researchers have modified the test structures for investigating CAF reliability. Ready and Turbini [41] used a through-hole to through-hole test structure with four pairs of anodes and cathodes with spacings of 500 and 750 μm. Similar test vehicle was later used by Caputo [43] to investigate CAF reliability. Researchers at CALCE [45] modified the test structure design with 20 x 30 arrays of through-holes and 10 x 10 array of through holes for studying conductive filament formation reliability.

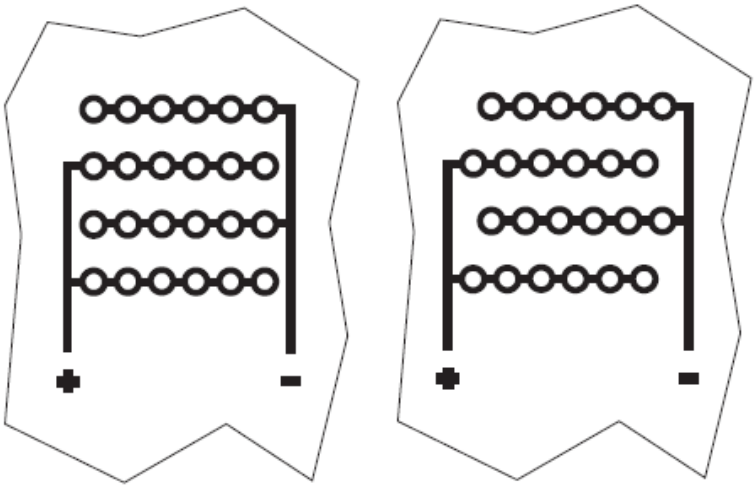

Figure 2.8. IPC CAF test board design: in-line and staggered through-hole design [44].

2.9 CAF Test Procedure

CAF reliability test is carried out using high temperature and humidity conditions in a controlled environmental chamber with a DC bias voltage. The test conditions based on different test standards are described below.

2.9.1 Temperature-Humidity-Bias (THB) Test

The test standards for evaluation of CAF resistance is specified in IPC-TM-650 test method 2.6.25 [44]. The test standard specifies a temperature of 65°C or 85°C with a relative humidity value of 85% for testing. A bias voltage of 100V DC is recommended for the test for accelerating the failure process. The coupons are placed in the environmental chamber in such a way that the air flows freely around the sample. The test also requires that the boards are preconditioned at 23±2°C and 50±5% RH prior to testing. After preconditioning, the boards are soaked for 96 hours at the test temperature and humidity before applying DC bias. The tests are typically run for 500 h with an additional 500 h if required. Resistance measurements are made every 24 h or 100 h. The

test standards recommend that the tests can be stopped when 50% of the parts have failed. Test duration of 500 h is a minimum standard for reporting CAF results.

2.9.2 Biased-Highly Accelerated Stress Test (B-HAST)

Some recent studies have utilized biased-highly accelerated stress test (B-HAST) for investigation of CAF reliability by using higher test temperatures to shorten the duration of the test [22], [74]. B-HAST is a recommended qualification test for microelectronic packages and the test has recently gained attention due to its shorter duration in comparison to THB test. Since B-HAST is also conducted under high temperature and high humidity condition, the test is reported to enable the same type of failure modes as observed in THB test. The test conditions for the highly accelerated test are available in JEDEC JESD22-A110, test method A110-B [75]. The difference in the test method is use of higher temperature, either 110°C or 130°C with higher pressure instead of 65°C or 85°C, which is standard for THB test. Based on JEDEC standards, a duration of 100 h in HAST is typically used for moisture-induced failure modes.

2.10 CAF Detection

An optical microscope equipped with a transmission light source has been utilized to identify CAF filaments. Small current flow through the filaments disrupts them, observation of filaments before burnout can be challenging [44]. Few researchers have been successful at isolating the conductive filaments [43], [54]. Researchers at CALCE used a superconducting quantum interface device (SQUID) to overcome the drawbacks of CAF identification techniques. A SQUID consists of a sensitive magnetometer to map the current distribution, which was applied to identify current leakage paths in test coupons with through-hole spacing of 3 mils and 4 mils. Based on SQUID analysis, multiple current leakage paths were identified in the test boards. They identified such

sites as a variant of conductive filament failures that formed when the spacing between the through-holes was less than 100 µm [76], [77].

2.11 Novel Test Circuit for CAF Detection

Ready et al. [78] recognized several limitations with the standard electrochemical migration test. The standard test method included insulation resistance measurements at widely separated intervals (24, 96 and 168 h) and the method does not terminate bias voltage when electrochemical migration occurs. Electrochemical migration occurred intermittently which could not be effectively captured using discrete measurements. The researchers compared daily and hourly measurement for detecting insulation resistance failures and found that increasing frequency of measurement improved success in detecting surface dendrites but was insufficient for detecting sub-surface shorts. They recognized the need for visual examination of circuit boards to observed sub-surface filaments and a need for more sensitive electrical reliability method. A "linear circuit" (LC) was therefore developed (Figure 2.9) to overcome the deficiency of the standard test method. The linear circuit terminated the current to the dendrite or CAF, thereby preventing it from blow out. The LC operated at a voltage 10-12V and could be remotely connected to a test pattern in an environmental chamber. The circuit utilizing a switching arrangement was shown to successfully identify dendritic shorts, which were otherwise difficult to detect using standard insulation measurement method. However, they identified a limitation with the novel test circuit, most the semiconductor devices operated at a voltage of 10-15V and therefore was not sufficient for CAF formation, which required a much higher voltage gradient.

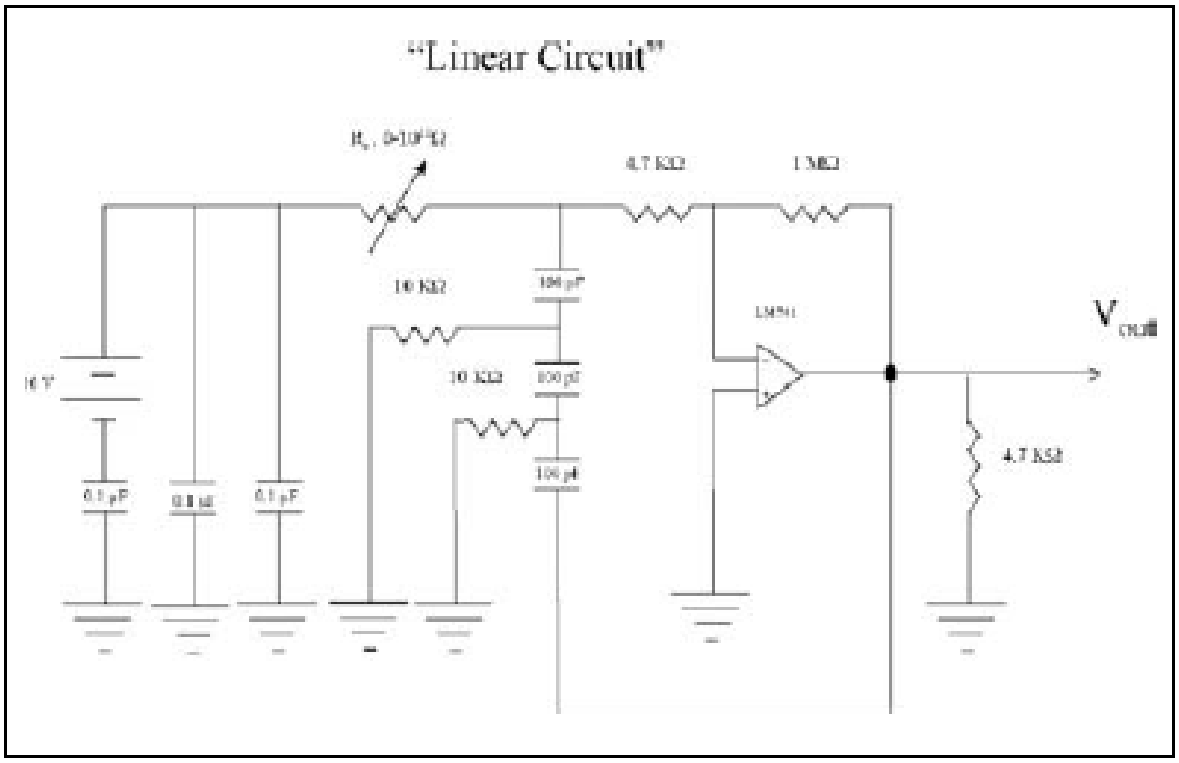

Figure 2.9. Electrical schematic of linear circuit [78].

2.12 Chapter Summary

This chapter presented the required background to CAF related failures in glass fiber reinforced substrates including its discovery, influence of factors such as substrate material properties, processing variables, temperature, humidity, applied voltage, conductor geometry and spacing on CAF.

CHAPTER 3

RESEARCH METHODOLOGY

3.1 Chapter Overview

This chapter will present an overview of the materials and test structures studied, fabrication processes, accelerated test conditions and characterization tools used in this study.

3.2 Organic Substrate Materials

The reliability of four substrate systems was investigated in this study. The glass fiber reinforced organic composites were based on the following resin chemistries:

- Halogenated epoxy (mid-T_g)
- Halogen-free epoxy (mid-T_g)
- Halogen-free epoxy (high-T_g)
- Halogen-free cyclo-olefin polymer (high-T_g)

3.3 Gravimetric Measurement of Moisture Sorption

Gravimetric measurement method was used to investigate the moisture sorption of the different substrates. Five samples of each substrate material with dimensions of 50 mm x 50 mm were prepared for gravimetric measurement. The samples were first dried at 125°C for 24 h and exposed to temperature and humidity in an environmental chamber, same conditions as used for CAF test. The samples were removed periodically and weighed using an analytical balance with a least count of 0.1 mg (M-310, Denver Instruments). Average moisture sorption wt% (M_t) of the substrate at time t, was calculated using the following equation:

$$M_t(wt.\%) = \frac{W_f - W_i}{W_i} X\ 100 \qquad (3.1)$$

Where W_f is the weight after exposure to humidity and temperature, and W_i is the initial dry weight of the sample.

3.4 Extractable Ion Content

The extractable ion content (chloride and bromide ions) in the substrates was analyzed using capillary electrophoresis. The extraction procedure for measuring ionic residues was based on IPC-TM-650 2.3.28 test standards (ionic analysis of circuit boards, ion chromatography method) [79]. Extraction was carried out using a solution containing 50/50 v/v of isopropyl alcohol (IPA) and deionized (DI) water solution. The substrates were immersed in the solution, sealed and placed in a water bath at 80°C for one hour. The solvent was evaporated and the extract solution was further diluted using 2 ml of DI water and then the mixture was sonicated for 30 minutes. A final injection volume of 2 ml was used for the analysis. A control containing only IPA and DI water was also analyzed for baseline measurement. The extracted solution was analyzed using capillary electrophoresis (Agilent CEG 1600). The surface area was calculated from sample dimensions and the results are expressed as micrograms of ions per square centimeter ($\mu g/cm^2$) using Equation 3.2 of the sample based on the extraction volume.

$$Ion\ content = \frac{ppm * final\ volume}{surface\ area} \tag{3.2}$$

3.5 Test Structure Design

The test structure design used in this study was created using a printed circuit board design software (CAM 350 version 8.7). All test structures studied consisted of two metal layers and consisted of through-vias with different conductor spacings. Different test structures were used in this study for the substrate materials investigated. The test structure design also consisted of two different conductor geometries, (a) through-via to through-via and (b) through-via to surface-trace. Additionally, two variations of the

through-via to through-via design was used in this study. The test structure specifications are explained in the following chapters (Chapters 4 and 5).

3.6 Through-via Formation

The through-vias for this study were formed using mechanical drilling process (Bit Shop Inc., CA). Copper clad substrates with dimensions of approximately 15 x 15 cm^2 with 12 µm of copper on either side were used. The through-vias were drilled using a spindle speed of 160,000 rpm at a feed rate of 49 ipm. The through-via diameter was fixed at 150 µm for all test structures studied.

3.7 Test Structure Fabrication

The test structures were fabricated using either subtractive etching or semi-additive plating method. The fabrication process was chosen based on the minimum critical spacing between the copper features in the test structure. The process flow for both the processes is described.

3.7.1 Subtractive Etching

Subtractive etching was used for fabricating the test structures where the minimum feature size between the conductors was larger than 50 µm. The process flow for subtractive etching is shown in Figure 3.1. After through-via drilling, the copper on the laminates was thinned down from 12 µm to approximately 3-5 µm using an etchant solution. The substrates were then subjected to electroless plating to form a conductive copper seed layer on the exposed side walls of the through-vias, followed by electrolytic plating of copper. The final copper thickness was approximately 15-20 µm. A dry film photoresist was then laminated on both sides, and patterned with ultra-violet (UV) lithography using a negative mask. The exposed part of the photoresist cross-link under exposure to light. The photoresist was developed in a basic solution to remove the

unexposed photoresist. The substrates were then subjected to copper etching and stripping of the photoresist to form the final test structures.

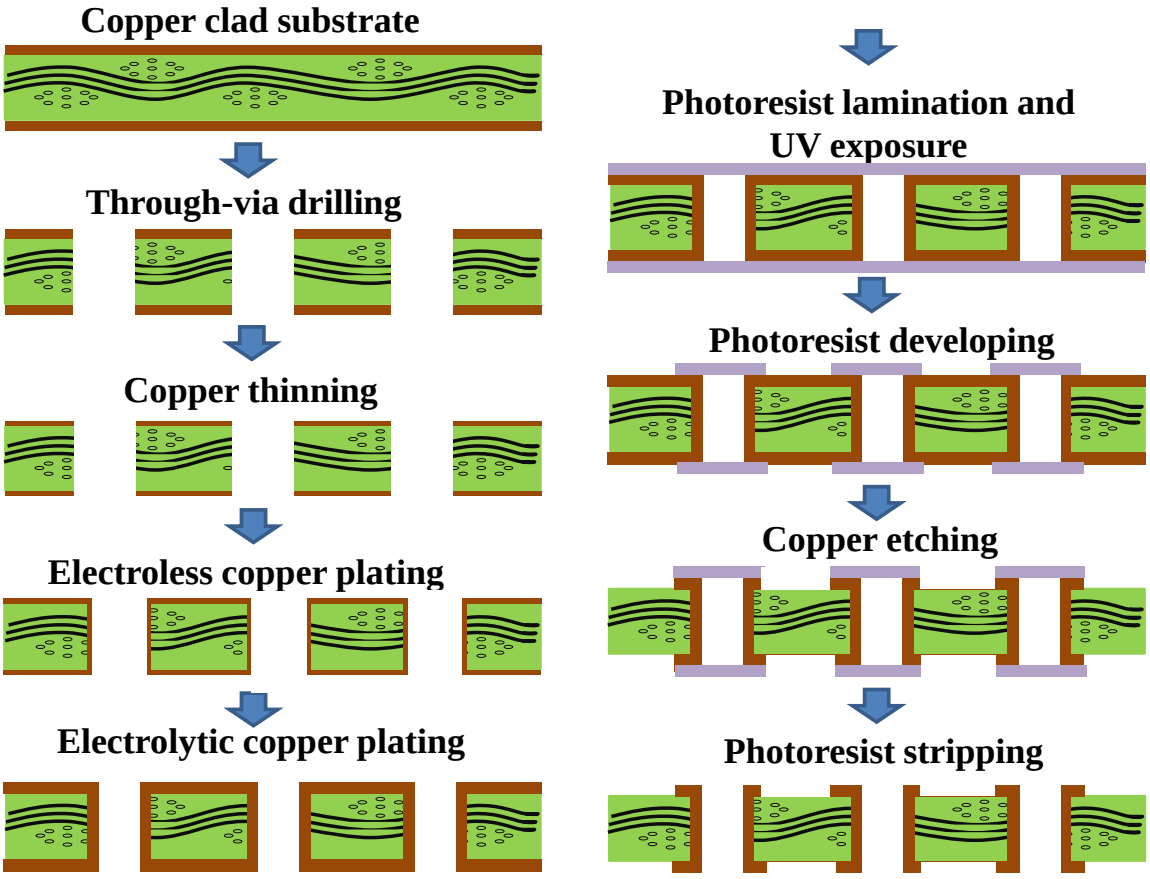

Figure 3.1. Process flow for subtractive etching process for test structure fabrication.

3.7.2 Semi-additive Plating

The process flow for semi-additive plating is shown in Figure 3.2. This process was used for test structures where the minimum spacing between the copper features was less than 40 µm. In this process, the copper was completely removed using an etchant solution after through-via drilling process. A dry film photoresist was then laminated on both sides, and patterned using a positive mask with ultra-violet (UV) lithography. The exposed part of the photoresist cross-link under exposure to light. The photoresist was

developed in a basic solution to remove the unexposed photoresist. The substrates were then subjected to electrolytic plating of copper to achieve a copper thickness of approximately 15-20 μm only in the exposed region. The photoresist was later stripped using a stripper solution and the copper seed layer was removed using a copper etchant to form the final test structures.

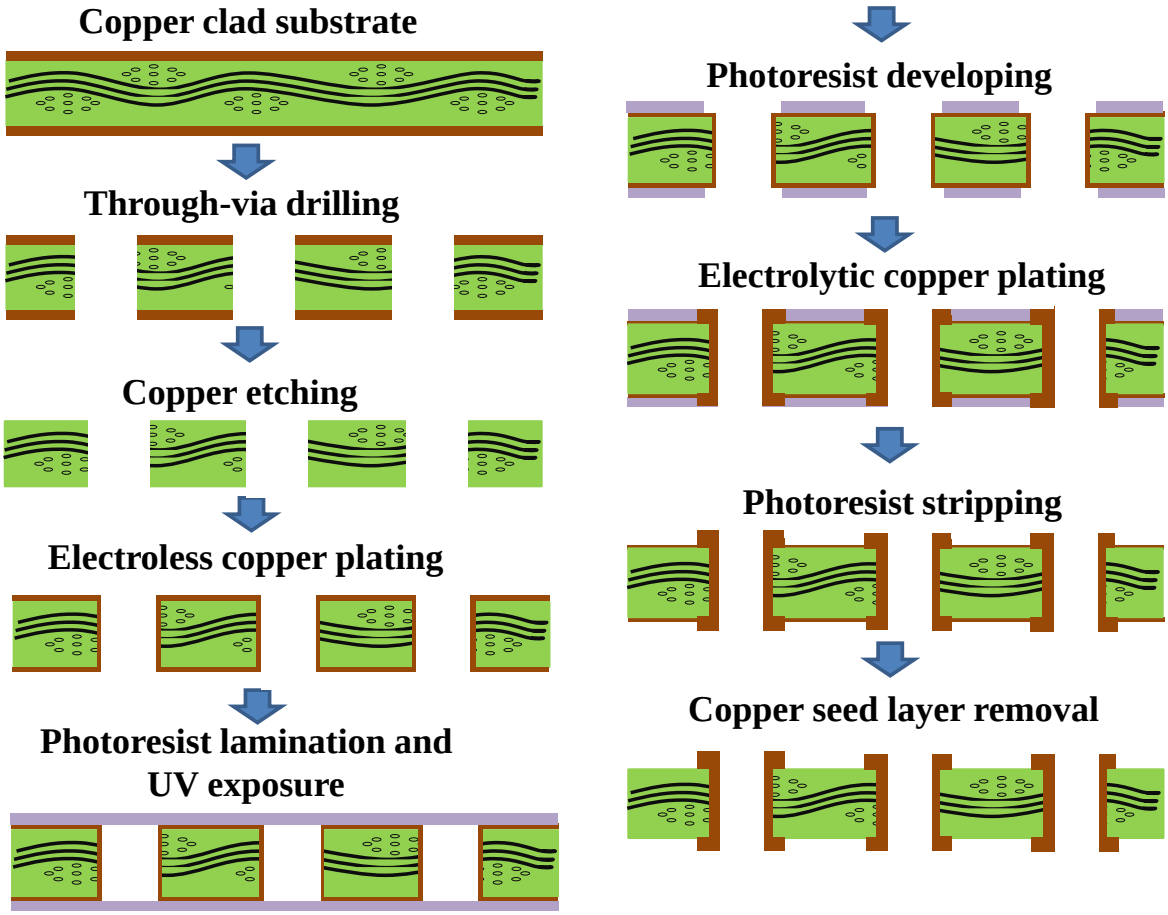

Figure 3.2. Process flow for semi-additive plating process for test structure fabrication.

3.8 Preconditioning and Lead-free Reflow

The fabricated test coupons were subjected to preconditioning. The preconditioning step is a standard process used for electronic packages. The purpose of preconditioning is to simulate the assembly process the boards undergo in actual manufacturing. Preconditioning consisted of three steps 1) baking to remove moisture, 2) temperature/humidity soak to introduce controlled amount of moisture in to the package and 3) exposing the boards to thermal shock to simulate the assembly process. The first step involved baking the test coupons for 24 h at 125°C. The second step was exposing the samples to 60°C and 60% RH for 40 h in an environmental chamber (JEDEC MSL-3). The final step is three times-reflow at a peak temperature of 260°C to simulate lead-free assembly process. A typical reflow profile used in this study is shown in Figure 3.3 [80].

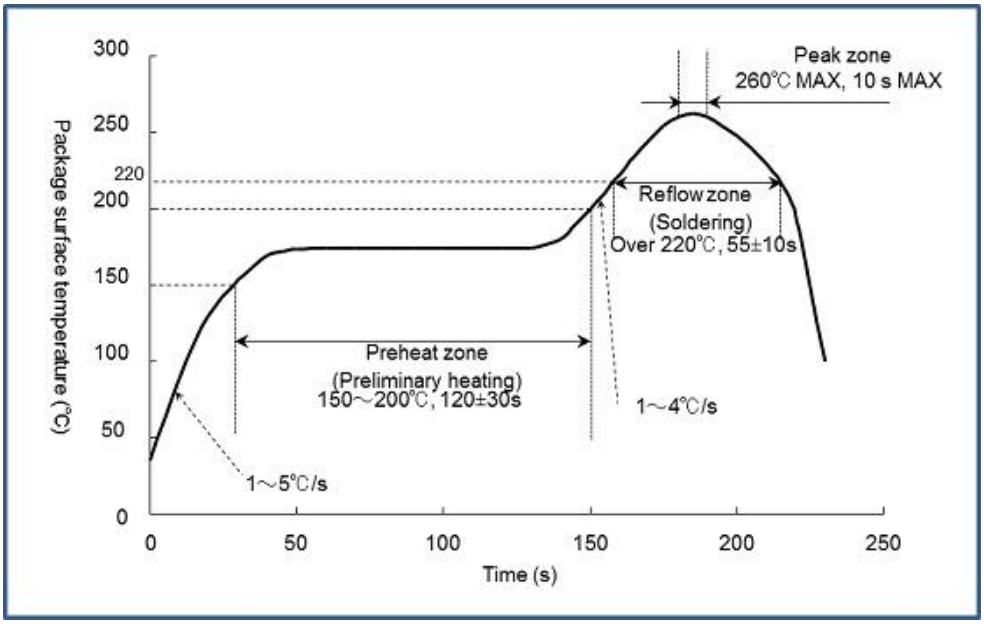

Figure 3.3. Temperature profile used for simulating lead-free reflow process [81].

3.9 Accelerated Test Setup

The test structures were exposed to high temperature, humidity and bias voltage in an environmental chamber. The bias voltage was fixed at 100V DC and the humidity was set at 85% RH for all test structures investigated in this study. The schematic of the test setup used for CAF test is shown in Figure 3.4.

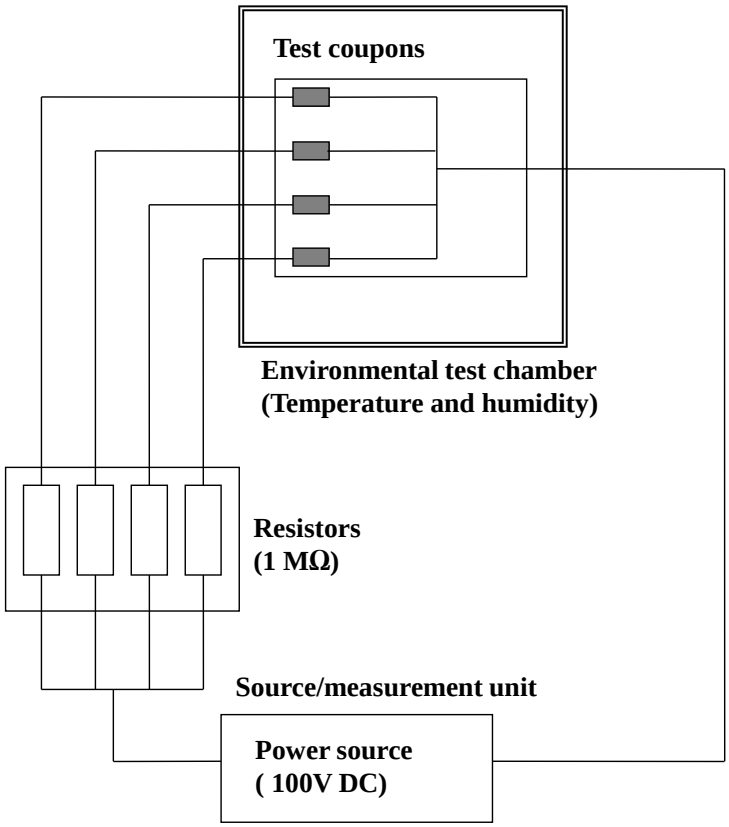

Figure 3.4. Test setup used for reliability study.

3.9.1 Temperature-Humidity-Bias (THB) Test

All test structures in this study were subjected to temperature-humidity-bias test. The test parameters (temperature, humidity and DC bias voltage) were chosen based on IPC-TM-650 2.6.25 test method recommendations [44]. The temperature was set at 85°C and the relative humidity was set at 85% RH. An environmental chamber (Thermotron) with an ability to produce required temperature and humidity condition required for the

test was used. The temperature was first increased to the required value and the humidity was increased in steps to prevent condensation on the test samples. The tests were carried out for a maximum period of 1000 h (approximately 42 days) or until all test coupons failed as specified in IPC standards. The test coupons were allowed to soak in at 85 °C and 85% RH before applying the DC bias. A high voltage power source (Keithley 236-source/measurement device) was used for applying 100V DC and also for measuring the output current. Insulation resistance of each test coupon was measured every 24 h and a drop in insulation resistance to 1 MΩ was chosen as the failure criterion.

3.9.2 Biased-Highly Accelerated Stress Temperature Humidity Test (B-HAST)

Some test structures in this study were also subjected to biased-highly accelerated stress temperature humidity test (B-HAST). The test conditions for the highly accelerated test were chosen based on standards established in JEDEC JESD22-A110, test method A110-B [75]. The test set up consisted of an environmental chamber (Espec) to produce 130°C and 85% RH required for the test. The tests were carried out for a maximum period of 100 h as per JEDEC recommendations. A bias voltage of 100V DC was used for the test. Insulation resistance of each test coupon was measured every 24 h and a drop in insulation resistance to 1 MΩ was recorded as an insulation failure.

3.10 Optical Microscopy

The test coupons were inspected using an optical transmission microscope (Nikon Eclipse E200) before and after the accelerated tests. The magnification range of the microscope is 5X to 50X. The failure sites were identified using a transmission lighting source. The optical images were recorded using a camera attached to the microscope. The optical microscope was insufficient to visually observe CAF in the test coupons, a high resolution digital microscope (Keyence VHX-2000) was also used for some of the test structures to record high resolution digital images. The digital microscope has a larger

depth of field with a maximum magnification up to 5000X. The images were recorded using a maximum magnification of 5000X with a high resolution zoom lens (VH-Z500).

3.11 Cross-sectional Analysis

After identification of failure sites using an optical microscope, the samples were cross-sectioned for further analysis. CAF cross-sections were carried out in a direction perpendicular to the growth of CAF. Some of the test coupons that exhibited burn out failures were cross-sectioned in a direction parallel to the failures. The samples were mounted using a fast curing molding compound and polished using a variable speed grinder-polisher (Ecomet 6). Polishing papers with grit size ranging from 320 to 4000 were used for the sample preparation. The final polishing step was carried out using alumina powders suspension with particle size ranging from 1 μm down to 0.03 μm. The final polishing was with a speed of 100 rpm using the slurry to ensure a smooth surface finish for characterization.

3.12 Scanning Electron Microscopy and Energy Dispersive X-ray Spectroscopy

A scanning electron microscopy (Zeiss Ultra60 FE-SEM) was used for failure analysis and elemental characterization. The mounted cross-sections were coated with a thin conductive layer of gold before observation in SEM. Gold coating was carried out using a gold/carbon sputter coater (EMS 150T). The typical deposition rate for Au is 7 nm/min with a deposition current of 20 mA. In this study, a deposition time of 15-20 seconds was used to coat a very thin layer of gold. The SEM images were recorded in secondary electron or in-lens mode. All SEM images were recorded using an accelerating voltage of 20 kV. Elemental analysis was carried out using energy dispersive x-ray spectroscopy (Oxford x-sight), which was attached to the SEM. Elemental analysis was either performed on a spot or over an area to verify the elements present and elemental

mapping was done in the site of interest. A working distance of 8.5 mm and accelerating voltage of 20 kV was used for energy dispersive x-ray spectroscopic analysis (EDS).

3.13 Impedance Spectroscopy

Impedance spectroscopy measurements were carried out after the test structures were exposed to different conditions (temperature, humidity and bias voltage). Impedance was measured in response to a 50 mV amplitude alternating current (AC) signal with frequency ranging from 10^{-1} to 10^{5} Hz using Gamry Reference 600 potentionstat equipment. Applied potential, current response, and relative phase angle were recorded using impedance spectroscopy software. Impedance was measured between adjacent rows of copper plated-through-vias (anodes and cathodes) in test structures with through-via spacing of 100 µm. Test structures under different conditions of exposure were analyzed to investigate the effect of exposure conditions on impedance response.

3.14 Chapter Summary

This chapter presented an overview of the materials and test structures studied. Fabrication processes, accelerated test parameters, characterization methods and tools used for characterization and failure analysis were discussed.

CHAPTER 4

RELIABILITY OF FINE-PITCH THROUGH-VIAS IN HALOGENATED-EPOXY GLASS FIBER SUBSTRATES

4.1 Chapter Overview

This chapter will discuss the reliability study of through-vias in a glass fiber reinforced brominated-epoxy substrate of 200 µm thickness. The test structures studied included three conductor spacings: 100 µm, 150 µm and 200 µm. Two different accelerated test conditions were used to investigate reliability. Test structure details, accelerated test results, failure analysis and elemental characterization of failures will be discussed.

4.2 Substrate Material

The substrate consisted of an epoxy matrix composed of polymerized diglycidyl ether of bisphenol A (DGEBA) with Tetrabromobisphenol A (TBBA) cured with dicyandiamide (DICY) (Figure 4.1). Tetrabromobisphenol A provides the substrate with flame retardant property and the organic matrix is reinforced with one layer of glass fiber weave.

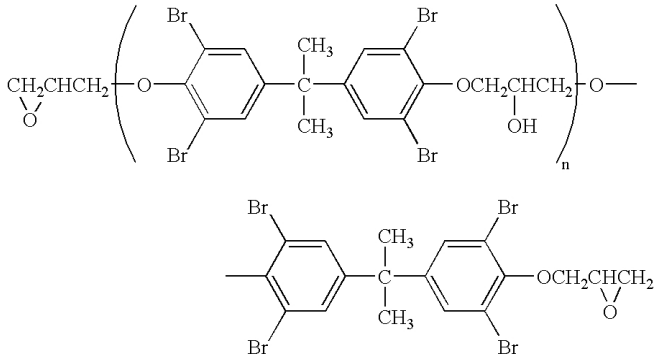

Figure 4.1. Chemical structure of brominated epoxy resin [82].

The substrate thickness was 200 µm with approximately 15-20 µm of copper. The key properties of the substrate material are summarized in Table 4.1.

Table 4.1. Material property of brominated epoxy substrate.

Parameter	**Value**
CTE (ppm/°C)	18
T_g (°C)	150
Dk (1 GHz)	4.4

The organic resin matrix was reinforced with one layer of E-glass fiber. The glass fabric style used is 7628, with an approximate thickness of 180 µm. The fiber count is 44 along the warp direction and 31 along the fill direction. The diameter of an individual fiber is approximately 9 µm. A cross-sectional SEM image of the substrate is shown in Figure 4.2.

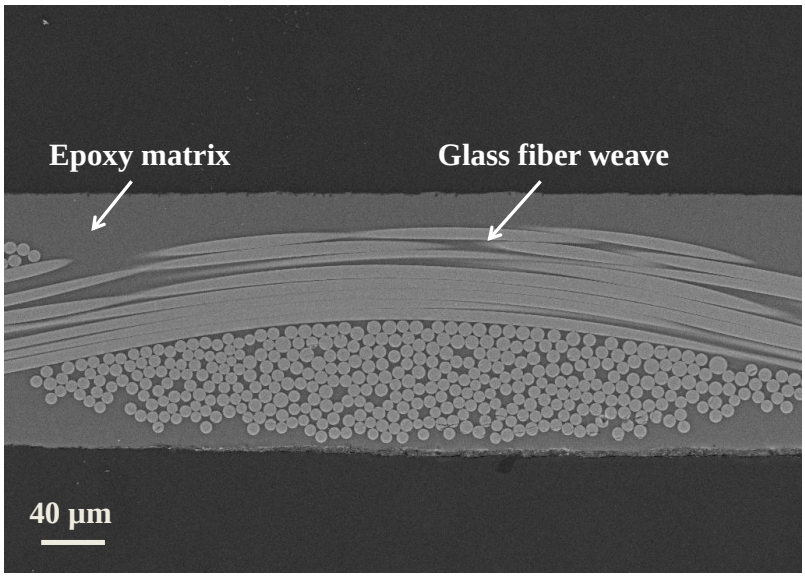

Figure 4.2. Cross-sectional SEM image of epoxy-glass fiber substrate.

4.3 Moisture Sorption

The moisture sorption behavior of the substrate was investigated using gravimetric measurement (Section 3.3). The measurement was done at two different test temperatures corresponding to the accelerated test conditions used for CAF study. The average moisture content increase with time for samples exposed to 85°C and 85% RH is shown in Figure 4.3. Gravimetric measurement of moisture sorption can result in significant errors during measurement of thin substrates due to desorption of moisture [37]. The errors were minimized in this study by reducing the time interval between removing the samples out of the temperature-humidity chamber and measurements before significant desorption can occur.

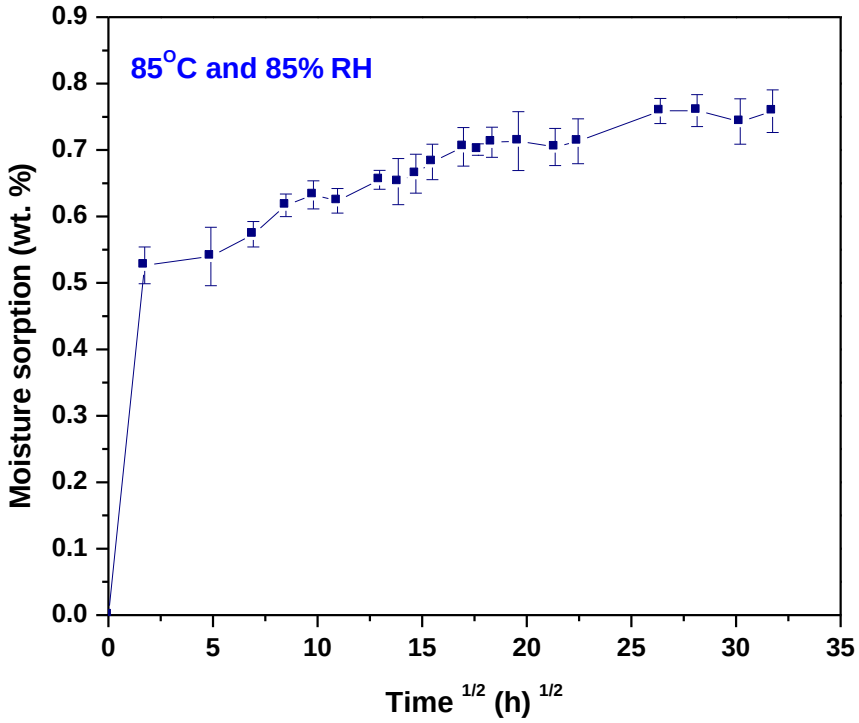

Figure 4.3. Moisture sorption of brominated epoxy substrate at 85°C and 85% RH.

Gravimetric measurement carried out on samples exposed to a higher temperature (130°C) in a HAST chamber for a maximum duration of 100 h is summarized in Table 4.2. The moisture content (wt%) after exposure at 24 h and 100 h at 130°C is compared with the measurement results at 85°C and 85% RH.

Table 4.2. Moisture sorption at 85% RH and two test temperatures.

Temperature (°C)	**Moisture sorption [M_t (wt%)]**		
	24 h	**100 h**	**1000 h**
85	0.54 ± 0.04	0.63 ± 0.02	0.74 ± 0.03
130	0.83 ± 0.03	0.88 ± 0.03	-

4.4 Extractable Ion Content

The results of ion analysis performed using the procedure described in Section 3.4 are summarized in Table 4.3. There are possible errors associated with quantitative determination of extractable ion content as a small number (n = 2 or 3) of test structures were used due to the destructive nature of ion analysis procedure as the substrates are extracted using isopropyl alcohol and deionized water. Possible differences in the total extractable ion content can come from variation between substrates, effectiveness of cleaning step and extraction procedure.

Table 4.3. Extractable ion content in brominated epoxy substrate.

Sample	**Br^- (µg/cm^2)**	**Cl^- (µg/cm^2)**
Epoxy substrate	< 0.01	0.229

4.5 Test Structure Design

A two-metal layer through-via to through-via geometry was used for this study. The test structure design is shown in Figure 4.4a, b and c.

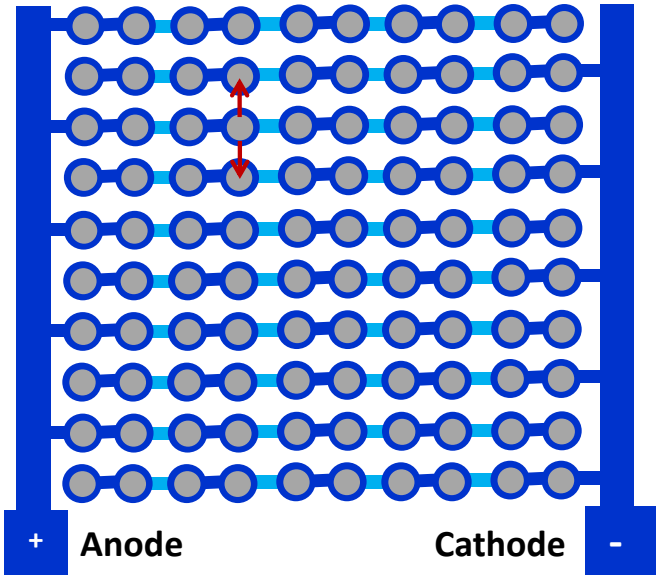

(a)

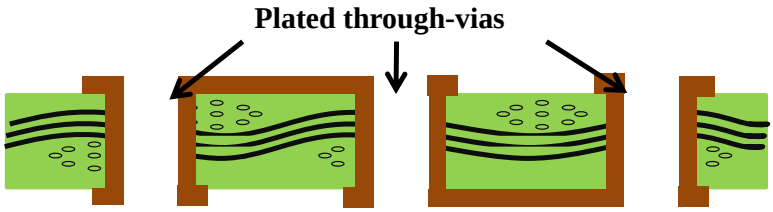

(b)

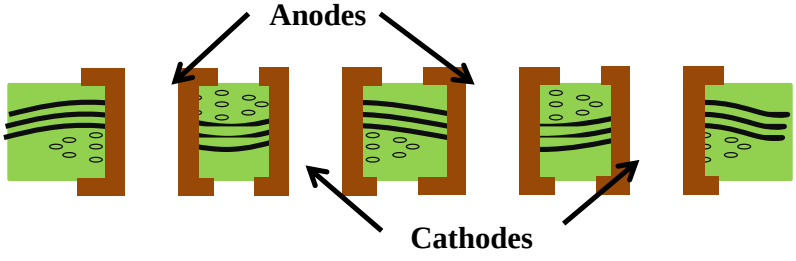

(c)

Figure 4.4. Through-via to through-via test structure design: (a) surface schematic, (b) cross-section along the row, and (c) alternate electrode configuration.

The test design is modified from IPC in-line PTH-PTH test structure design (Section 2.8) with lesser number of through-vias. The test structures consisted of 100 through-vias arranged in an alternate anode (5 rows with 10 through-vias each) and cathode (5 rows with 10 through-vias each) configuration as shown in Figure 4.4a. The test structures consisted of three through-via to through-via spacings: 100 µm, 150 µm and 200 µm. The spacing between the through-vias within each row was fixed constant at 500 µm for all three conductor spacings. The number of possible failure sites for such a test structure is given by the following expression:

$$No.of\ possible\ failure\ sites = m(n-1) \qquad (4.1)$$

Where m is the total number of rows and n is the total number of columns. The design provides 90 in-line failure possibilities in each test coupon.

4.6 Test Structure Fabrication

The test coupons were fabricated using subtractive etching process. The fabrication process steps are described in Section 3.7.1. Optical images of the fabricated test coupon and cross-section of a test coupon showing the copper plated-through-vias are shown in Figure 4.5a and b. Figure 4.5a shows part of the surface image of the fabricated test coupon and Figure 4.5b shows the cross-section with plated-through-vias arrange in an alternate anode and cathode configuration.

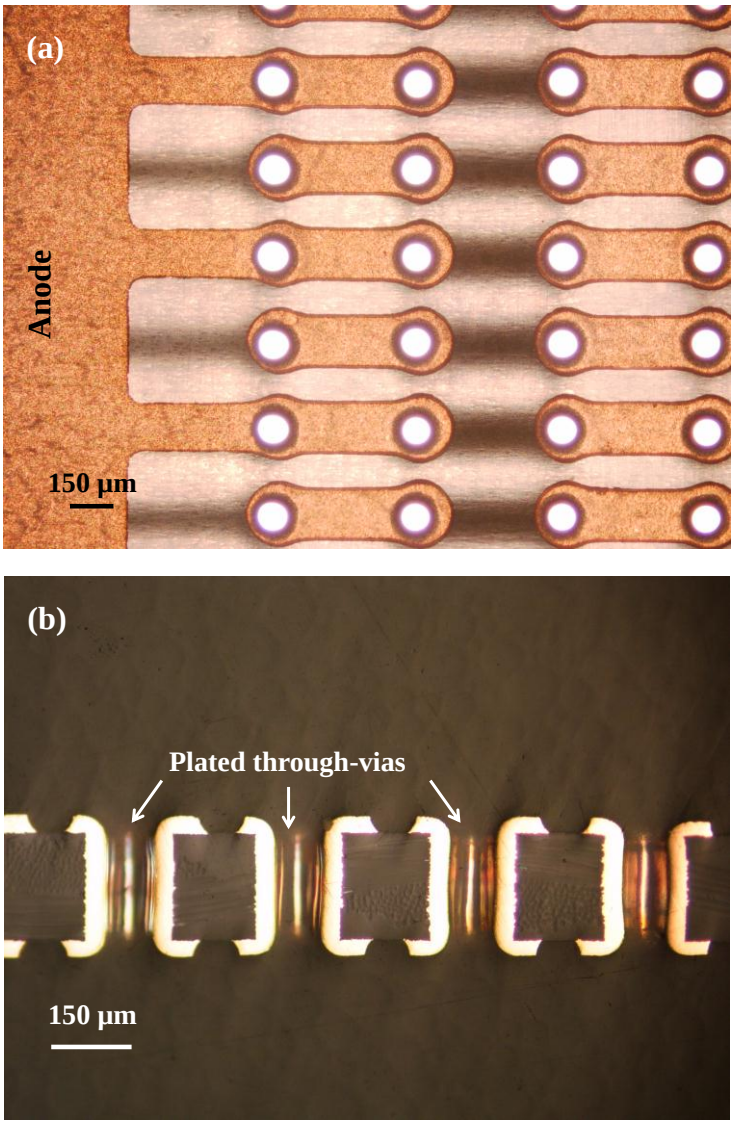

Figure 4.5. Optical images of the fabricated test structures: (a) surface image and (b) cross-sectional view of alternate through-via configuration.

4.7 Accelerated Testing

The accelerated test parameters are as follows.

1. Five test samples each with three through-via spacings (100, 150 and 200 µm) were subjected to THB test (85°C and 85% RH with 100V DC bias) for a maximum duration of 1000 h (Section 3.9.1).

2. Five test samples each with two through-via spacings (100 and 200 µm) were subjected to B-HAST (130°C, 85% RH and 2 atm with 100V DC) for a maximum duration of 100 h (Section 3.9.2).

4.8 Accelerated Testing Results

The insulation resistance of each test coupon was measured in-situ every 24 h during the test and a resistance drop to 1 MΩ was chosen as the failure criterion. Table 4.4 summarizes the total number of insulation failures for each conductor spacing observed during in-situ resistance measurement.

Table 4.4. Insulation measurement results based on a failure criterion of 1 MΩ in accelerated testing.

Through-via spacing (µm)	No. of failures/ total no. of coupons	
	THB	B-HAST
100	5/5	2/5
150	2/5	-
200	0/5	0/5

In THB Test, all test structures with through-via spacing of 100 µm exhibited failures. Two coupons with 150 µm spacing showed insulation failures and the test structures with 200 µm spacing did not reveal any insulation failures. For the test structures with 100 µm spacing, the insulation failures were found to occur between 120 - 624 h. For the test structures with 150 µm spacing, the two failures occurred at 364 h and 644 h, respectively.

In B-HAST, the test structures with 100 µm were found to exhibit two failures. The first insulation failure occurred within the first 48 h and the second failure within 72 h. The test structures with 200 µm via spacing did not show any failures.

4.9 Discussion

The insulation measurements indicated that the test structures with 100 µm spacing exhibited short failure times. The through-via test vehicles with 150 µm exhibited better reliability and test structures with spacing of 200 µm did not show any insulation failures in either accelerated tests. The results from either accelerated tests indicate a strong dependence on spacing on failure times. The effect of conductor spacing on through-hole geometry on CAF failures was previously discussed. The mean time to failure (MTTF) for CAF failures has been previously found to exhibit a power law dependence on applied voltage and spacing. As described in Section 2.7, the conductor spacing effect on failure time is described using L^n (L: conductor spacing), where n can take a value of 2 or 4 [41], [71]-[73]. Therefore, test structures with larger via spacings can exhibit considerably longer time to failures. Considering a spacing dependence of $L^{4,}$ the failure times can be approximately 16 times higher for a conductor spacing of 200 µm compared to 100 µm. However, a large deviation in MTTF was observed for 100 µm, possible reasons for such deviation are explained in the failure analysis discussion (Section 4.10).

CAF failures occur in the presence of humidity; therefore moisture is required at the fiber-resin interface for creating an electrochemical pathway and the saturation step has been recognized as a critical step for CAF failures [35]. Gravimetric measurements indicated a rapid initial moisture sorption followed by a slow increase in moisture content (Figure 4.3). A maximum sorption occurred within 3 h of exposure to temperature and humidity at 85°C and 85% RH. The moisture uptake process is rapid due to thinner boards compared to the thick PWBs previously studied as the diffusion varies with square

of thickness of the boards [35]. Additionally, a two-stage moisture sorption behavior was observed in the substrate (Figure 4.3). The first stage indicates diffusion in to the free volume, where the moisture diffuses through the interconnected pores inherent to epoxy resins. The free volume of the resin is reported to dominate the diffusion process for several polymer systems. This is due to the inaccessibility of hydrogen bonding sites. The second stage is likely due to the polymer relaxation processes. Epoxy resins consist of polar hydroxyl groups created by ring opening reactions. The polar groups in water can hydrogen bond with the hydroxyl groups in epoxy, disrupting the interchain hydrogen bonding. However, moisture contribution to swelling is reported to be significantly less in comparison to the total moisture uptake [83], [84]. Swelling increases over time leading to further degradation as it reduces mechanical interlocking between glass fiber and resin. The substrates were also found to exhibit significantly higher moisture content at the higher test temperature (Table 4.2). The average increase after 100 h exposure to at 130°C was higher than at 85°C. Increasing temperature results in increase in availability of free volume and increases the rate of chemical reactions [84]. Therefore, a higher moisture content was observed at a higher temperature.

4.9.1 THB vs. B-HAST

A higher number of CAFs was observed under optical inspection in samples in B-HAST within 100 h compared to samples subjected to THB test. Significant changes in insulation resistance changes ($10^7 – 10^8$ Ω) were also observed for the test structures with spacings of 100 µm in B-HAST. The results indicated that the test conditions used for the B-HAST test significantly accelerated interface degradation and CAF formation. Interface degradation, which is the rate-determining step for CAF, can include contributions from both thermal and hygroscopic strains. The coefficient of thermal expansion (CTE) of the epoxy resin (~50 ppm/°C) is approximately 8 - 10 times higher than glass fibers (5.5 ppm/°C). The thermal mismatch strain is a function of the

difference in CTE and change in temperature. Ready [54] reported an increase in thermal mismatch strains between the epoxy matrix and glass fibers with increasing process temperatures, similarly increasing test temperature results in higher mismatch thermal stresses at the interface. The other contribution is hygroscopic strains due to swelling of the resin from moisture sorption in humid conditions. The hygroscopic strain is a function of the coefficient of hygrothermal expansion and the change in moisture concentration. As seen from gravimetric measurements (Table 4.2), moisture content at 130°C was significantly higher compared to at 85°C. The increase in thermal and hygroscopic strain is likely reason for weakening of the epoxy and glass fiber interface leading to degradation. The other reason is the small difference between the test temperature and the glass transition temperature (~150°C) and the test temperature (~130°C), possibly resulting in softening and degradation. Additionally, the increased moisture content at the interface can result in loss of adhesion due to chemical debonding of interfacial bonds. Leung et al. [85] reported that the rate of hydrolysis of interfacial bonds is a function of both the moisture content at the resin-glass fiber interface and temperature. Therefore, the rate of chemical reactions can also be expected to be higher with higher moisture content at the higher test temperature. Further, an increase in moisture content is known to result in reduction of glass transition temperature in epoxies. Therefore, when the wet T_g of the substrate is close to the test temperature, which can lead to reduction in glass fiber-resin adhesion, resulting in formation and propagation of microcracks along the interface [83].

4.10 Failure Analysis and Characterization

The test structures subjected to accelerated tests were inspected using a backlit optical microscope after the accelerated tests. As seen from the Figure 4.7, a dark region was visible using the transmission light source. This type of burnout failure mode is known to be caused by the current flowing through the conductive filaments, which are

typically semiconducting copper compounds, resulting in localized melting and charring in the failure region [54]. Similar observation was made during cross-sectional analysis in one test structure that exhibited failure (Figure 4.8), where the cross-section revealed a formation of a hole in the failure region resulting from localized melting.

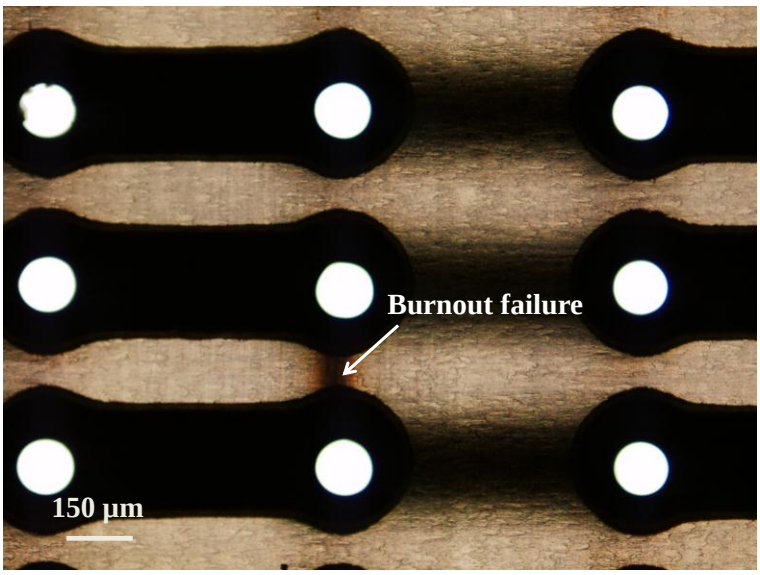

Figure 4.7. Backlit optical microscopy image of test coupon with burnout failure.

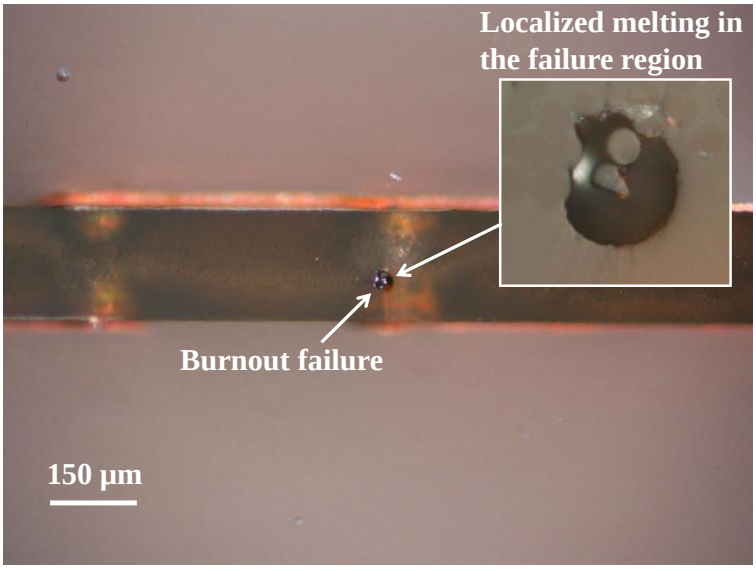

Figure 4.8. Cross-sectional optical image along the perpendicular direction of a burnout failure showing localized melting in the failure region.

Another observation from accelerated tests was the large difference in time to failures for the test structures. A cross-section of a failed test coupon which exhibited an initial failure is shown in Figure 4.9. The cross-sectional analysis revealed copper wicking in to the glass fiber between the two through-vias as a result of drilling-induced fracture. Cracks introduced during the drilling process lead to copper plating within the fractured interface and result in a decrease of effective spacing between the through-vias, which is the reason for the short failure times. A SEM cross-section image of the same sample is shown in Figure 4.10, where copper penetration can be seen (verified using EDS) in to the glass fibers. However, since the polishing direction was parallel to the failures, CAF could not be precisely located.

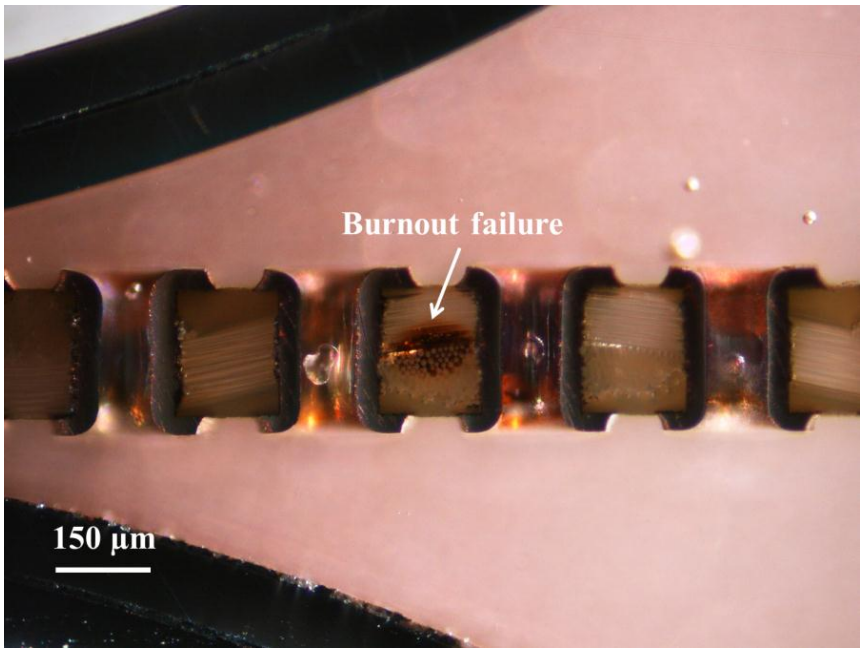

Figure 4.9. Cross-sectional optical image along the parallel direction of a burnout failure.

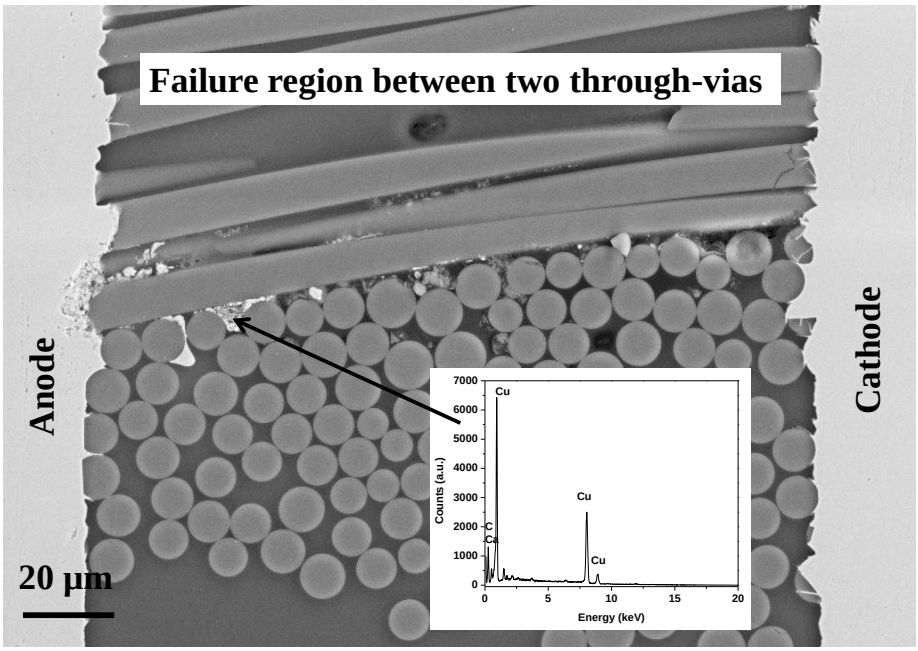

Figure 4.10. Cross-sectional SEM image of failure region and EDS showing copper wicking along the glass fiber interface.

Copper wicking defects were difficult to detect based on initial measurement of electrical resistance, as all coupons exhibited an average initial resistance higher than 10^{10} ohms (measured using 100V DC). The drilling induced fracture appeared to be significantly large with the smallest through-via spacing (100 µm) as seen from the higher number of insulation failures. The test structures with 100 µm subjected to B-HAST revealed a high number of CAF formation, result of the higher test temperature and enhanced degradation with smaller spacings. Optical microscopy images of CAF growth before electrical shorting are shown in Figure 4.11a and b. The appearance of CAF is similar to that previously observed by Ready et al. [58] who observed that CAF was thicker at the anode, becoming thinner as it migrated towards the cathode using microtomography. It was also observed that CAF growth occurred in two orientations, (1) between two through-vias and (2) between a through-via and a surface trace.

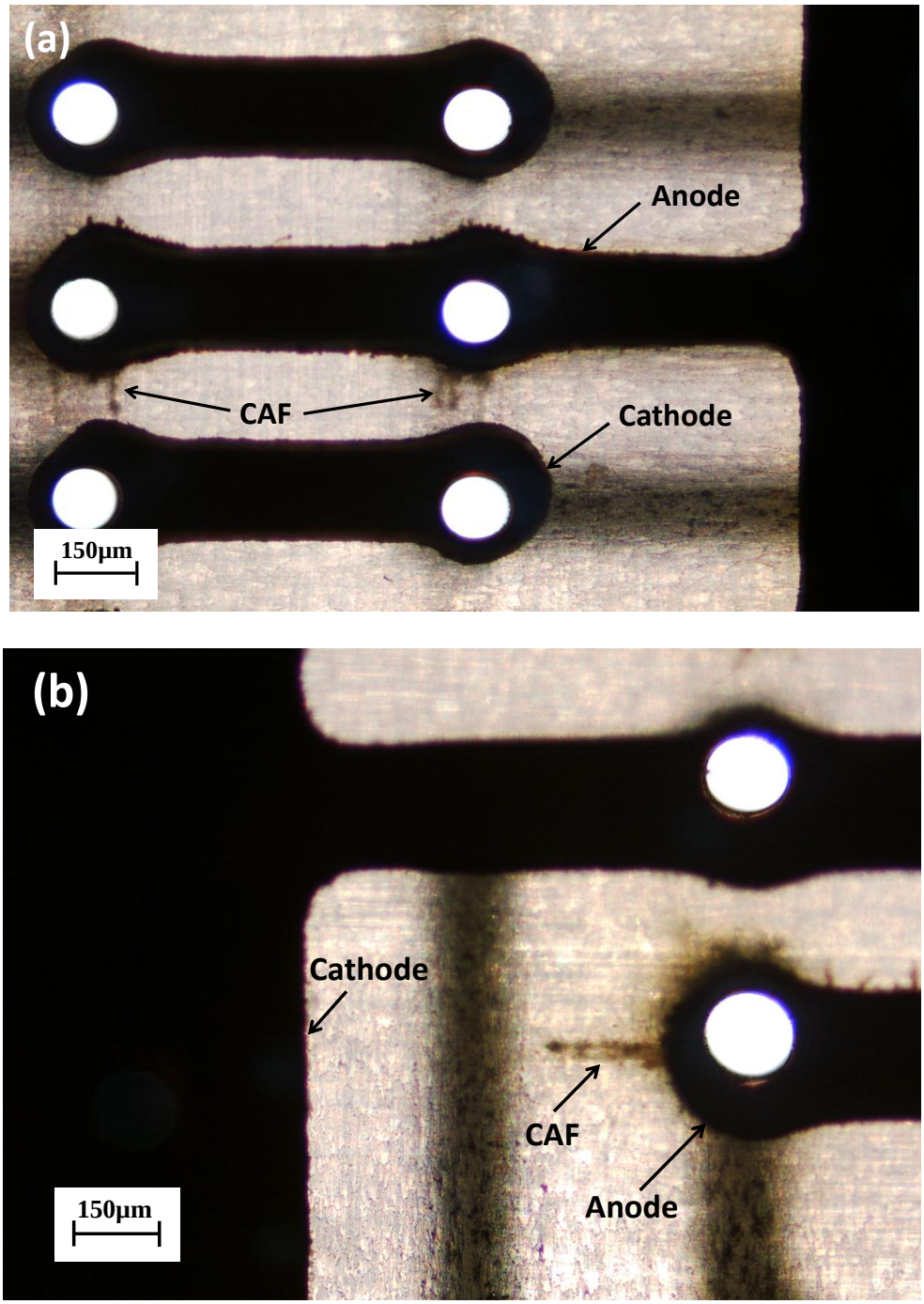

Figure 4.11. Optical image of CAF formation in test structures with 100 µm recorded using transmission light: (a) between through-vias, and (b) between through-via and a surface-trace [86].

Filament formation in the perpendicular direction, similar to observed in Figure 4.11b, was previously observed in test vehicles by Ready [54]. A possible reason was the orientation of the glass fibers. The machine or the warp direction of the fiber weave is under tension from the residual stresses compared to the fill direction. Therefore, the glass fabric along this orientation is more prone to fracture during drilling. Also, the glass fibers along the warp direction are denser with more number of fibers compared to the fill direction, thereby increasing the probability of fracture during drilling. Additionally, it was hypothesized that a fiber bundle close to the surface will absorb moisture faster resulting in a non-tortuous pathway. The other possible reason was the concentration of the electric field around two through-via conductors, graphically represented using Figure 4.12. A large electric field is observed along the perpendicular direction and CAF formation will be preferred along this direction.

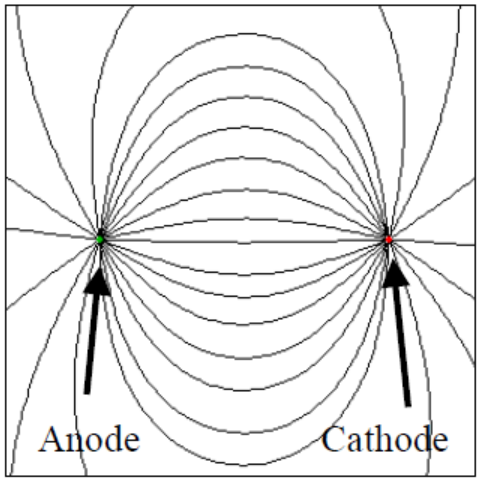

Figure 4.12. Simulation of electric field near the anode and cathode [52].

In this study, as seen from the cross-sectional image (Figure 4.2), the glass fibers in this substrate are also close to the surface traces due to the thin substrates. This might create a faster path as moisture diffuses to the outermost layers of glass fibers. The substrate does not include a butter-coat or a thin layer of resin that separates the glass

fibers from the copper surface-traces; there is additional electric field between the surface-trace and through-vias which could influence CAF growth along that orientation.

4.10.1 CAF Characterization

The test coupons with CAF formation (Figure 4.11) were mounted and cross-sectioned perpendicular to the direction of CAF growth. A high resolution digital image of the cross-sectioned sample showing CAF along the interface at a magnification of 5000x is shown in Figure 4.13. The arrows indicate the presence of a compound along the glass fiber-resin interface.

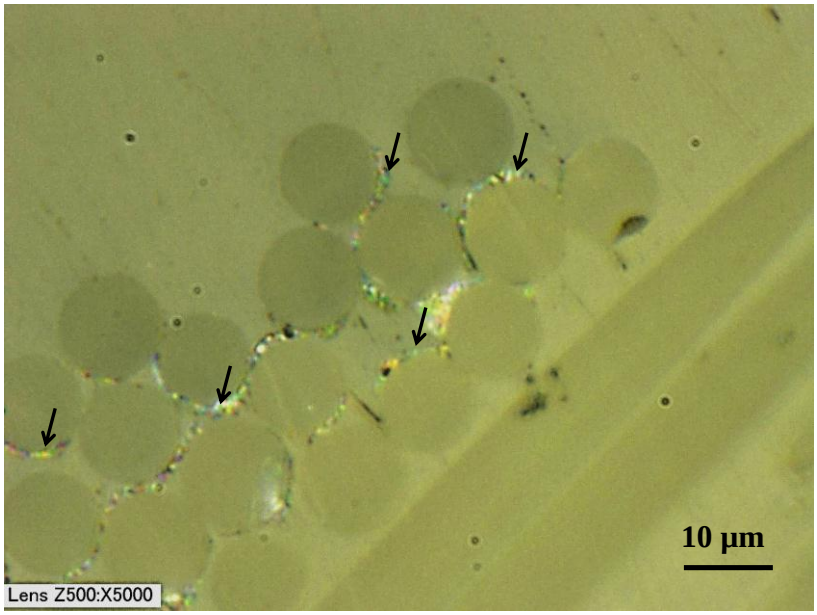

Figure 4.13. Optical image of CAF in the glass fiber-resin interface.

Cross-sectional SEM images of CAF along the interface of the resin and glass fibers is shown in Figure 4.14a and b. Figure 4.14b shows the separation between the resin and the glass fiber interface where CAF is present.

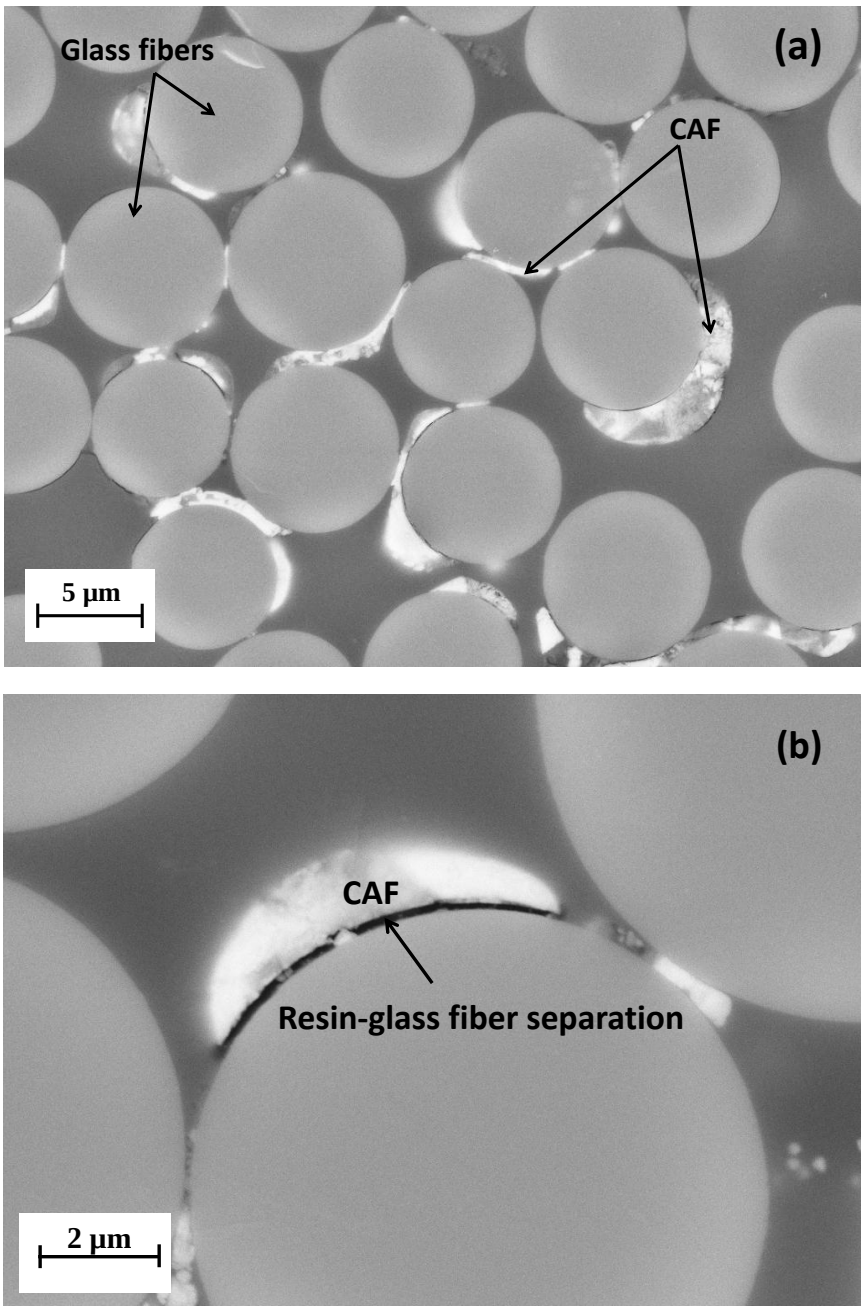

Figure 4.14. SEM images: (a) and (b) CAF in the glass fiber-resin interface at different magnifications [86].

Elemental spectra were obtained from the epoxy resin matrix and the CAF region in the cross-section, shown in Figure 4.15a and b, for characterization of CAF compound. The spectrum (Figure 4.15a) obtained from the epoxy resin revealed carbon, oxygen, and

bromine peaks, which are expected from the substrate. The EDS spectrum (Figure 4.15b) obtained from the CAF shows numerous peaks as a result of the interaction volume with CAF, the glass fibers and the resin. The calcium and silicon peaks in the spectra are expected from the oxides in the glass fiber weave. The copper and chlorine peak are expected in in case of a chloride containing copper CAF compound.

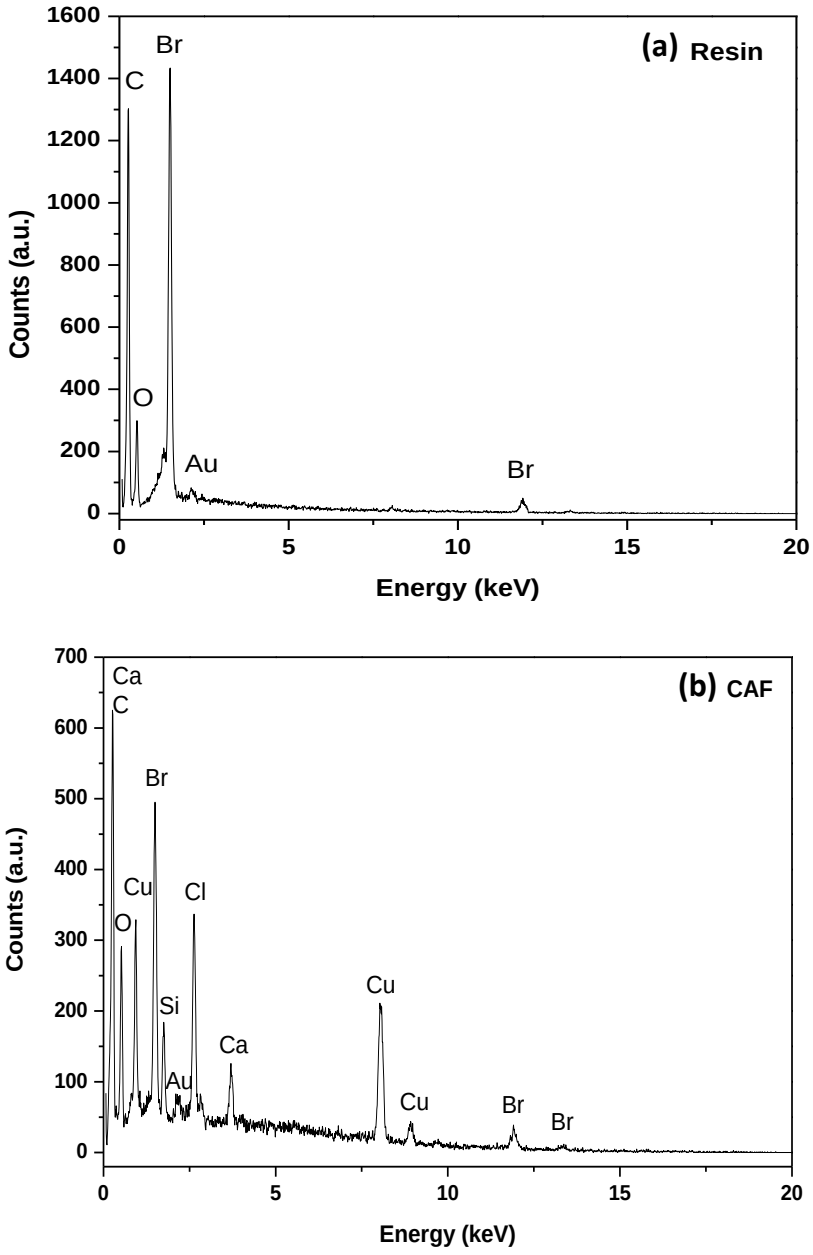

Figure 4.15. EDS characterization: (a) resin and (b) CAF region.

Elemental mapping was also performed in the CAF region to verify the association of copper and chlorine in CAF (Figure 4.16). The mapping results indicated a high concentration of chlorine where copper was found around the glass fibers in the CAF region.

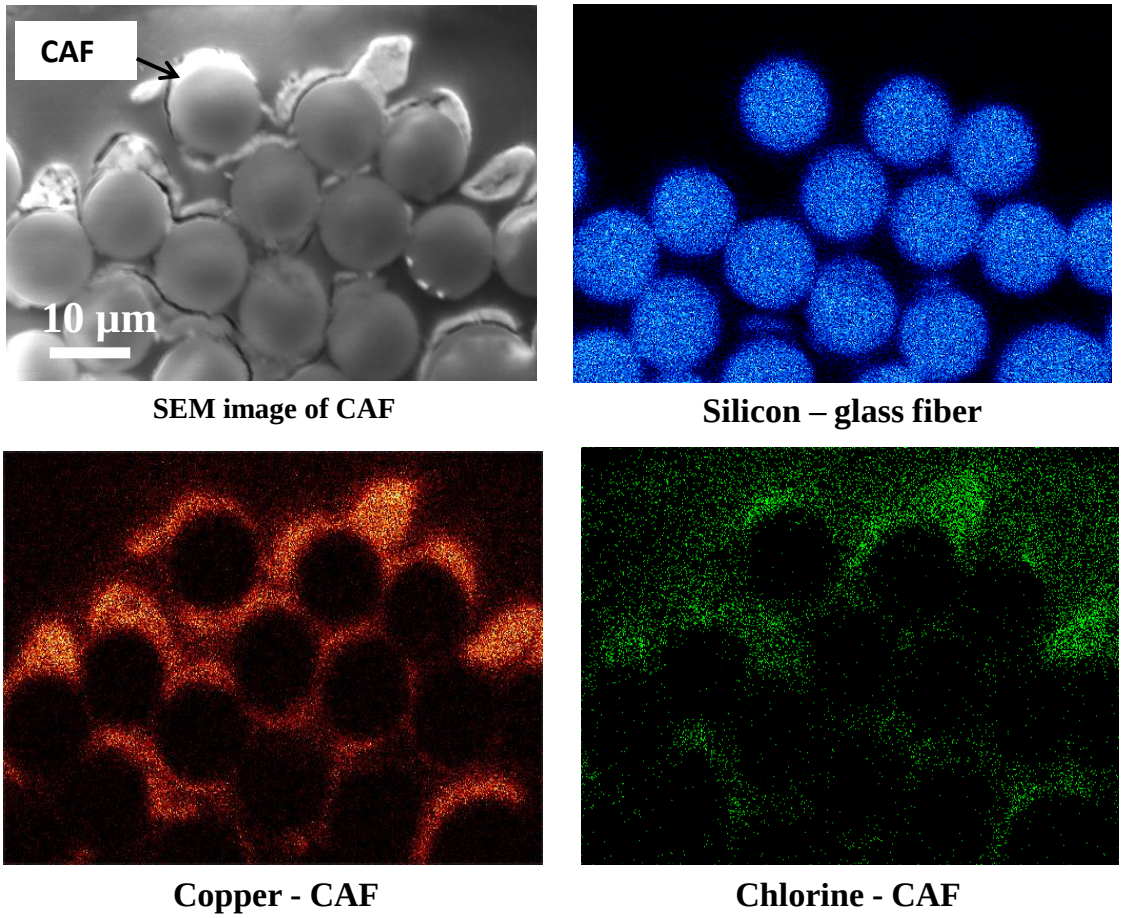

Figure 4.16. EDS map of silicon, copper, and chlorine in CAF region.

Cross-sectional analysis of the samples with CAF formation also revealed copper corrosion near the copper surface-traces that penetrated in to the epoxy matrix. SEM image of corrosion and EDS spectrum obtained from this region is shown in Figure 4.17a and b. The EDS spectrum obtained from the corrosion region also revealed the presence

of copper and chlorine in addition to carbon, oxygen and bromine peaks from the epoxy resin matrix.

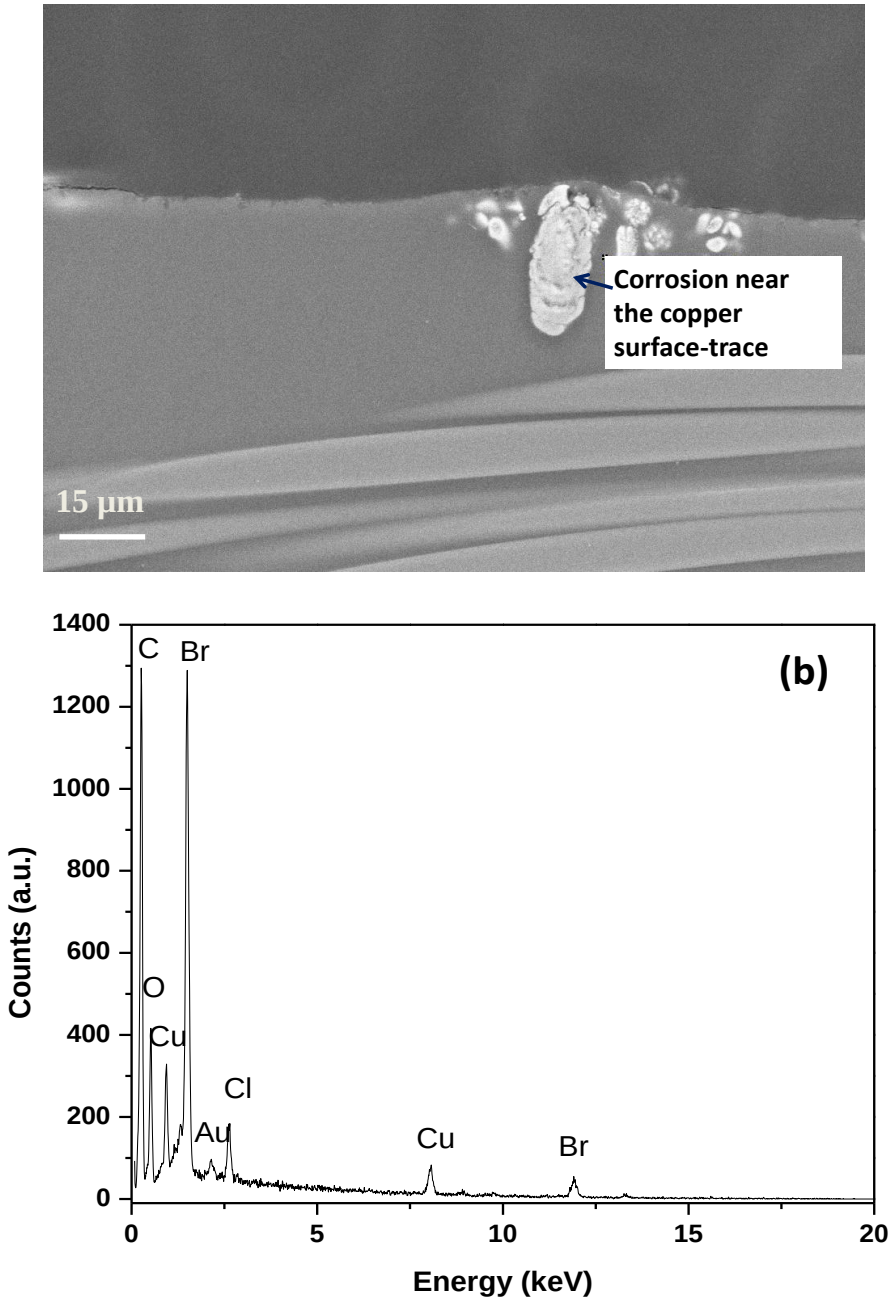

Figure 4.17. Corrosion near surface-trace: (a) SEM image and (b) EDS characterization of the corrosion compound.

The EDS characterization consistently revealed the presence of copper and chlorine in the corrosion region. As reported previously, the copper and chlorine peaks are expected in chloride containing CAF, which was previously shown to be synthetic atacamite by Ready and Turbini [41], [54]. The electrochemical mechanisms for the formation of $Cu_2(OH)_3Cl$ were described in Section 2.6.1. Ready [21] have also observed bromine containing copper compound in their study, which was later identified as $Cu_2(OH)_3Br$ by Caputo et al. [43], [67]. Ion content analysis (Table 4.3) performed on the substrates revealed lower extractable bromide ion content in comparison to the extractable chloride content. The presence of chlorine peaks in the CAF region and the corrosion region indicates a possible chloride containing CAF in the halogenated epoxy substrates. Also, as discussed previously, a bromide content threshold appears to exist below which bromide CAF is not favored. Ready and Turbini [41], [54] observed chloride containing CAF in unprocessed epoxy boards and the substrates used in this study were also unprocessed, indicating a possibility of a similar chloride containing copper-CAF compound.

4.11 Impedance Spectroscopy

AC impedance was measured in the test structures between the through-vias exposed to different conditions of temperature, humidity and bias. The measurement parameters are described in Section 3.13 and all measurements were carried out after exposure to the temperature and humidity conditions. Measurements were carried out on three different test structures with conductor spacing of 100 µm. The samples included (a) a control test structure not exposed to DC bias voltage, (b) a test structure with CAF initiation, and (c) a test structure that exhibited failure during the accelerated test. The impedance of three test structures over the frequency range was measured under two exposure conditions (a) baking at 125°C for 6 h to completely remove moisture from the

substrate and (b) exposing the samples to 85°C and 85% RH for 200 h to investigate the effect of moisture sorption on impedance response for the different test structures. From gravimetric measurements (Figure 4.3), moisture sorption after 200 h exposure at 85°C and 85% RH is 0.65 ± 0.03 wt% for the substrates.

Impedance spectroscopy involved the measurement of current, and phase angle with an AC voltage of 50 mV over a frequency range of 10^{-1} to 10^{5} Hz. The magnitude of the impedance vector (Zmod) can be described using the following equation:

$$Zmod = [Z'^{2} + Z''^{2}]^{\frac{1}{2}} \qquad (4.2)$$

In Equation 4.2, Z' is the real and Z" is the imaginary impedance. The data obtained were plotted in frequency-explicit format, referred to as Bode plot. Plots of magnitudes of impedance and frequency are useful tools for assessing the presence of different circuit components such as resistor ($Z^* = R$), capacitors ($Z^* = 1/j\omega C$) or inductors ($Z^* = j\omega L$). In plots of frequency and magnitude of impedance, the impedance of resistive components are flat with frequency, impedance of capacitive components decrease with increasing frequency and the impedance of inductive components increase with increasing frequency [87]. The impedance response (Zmod) as a function of frequency of measurement for the three different samples under two exposure conditions are shown in Figure 4.18a, b and c.

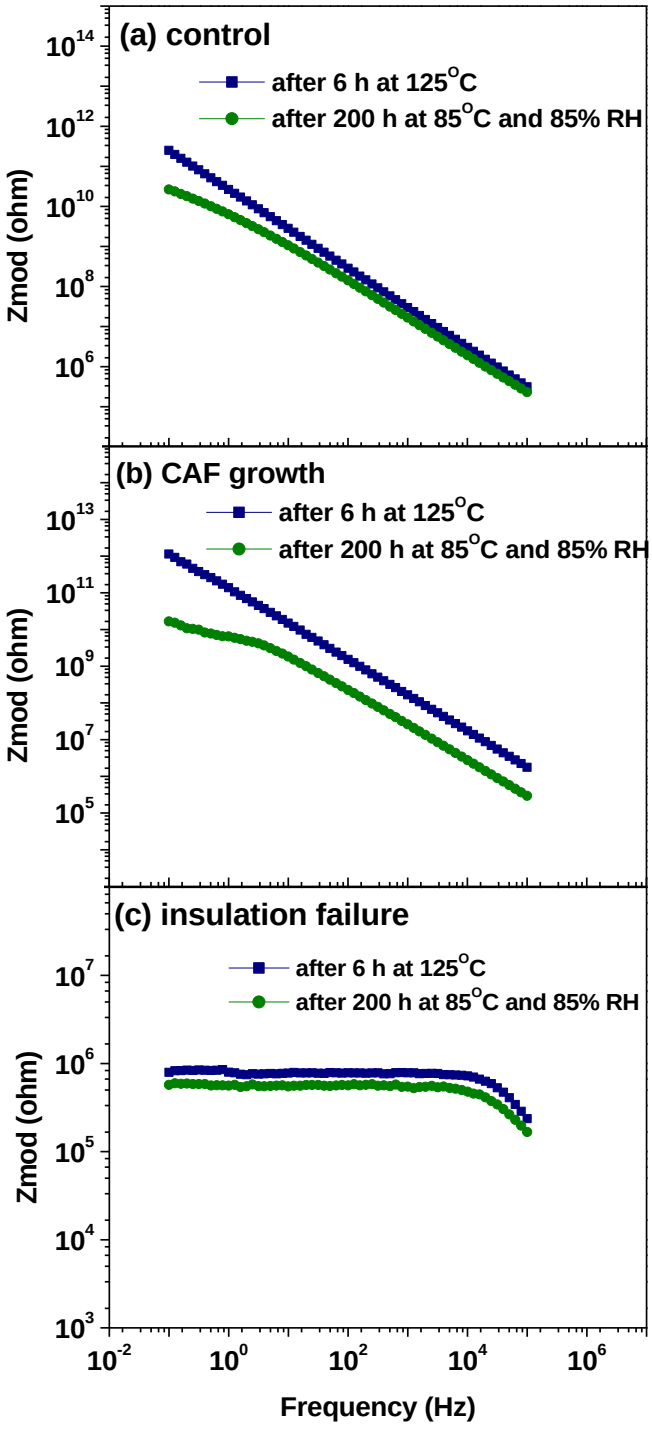

Figure 4.18. Impedance measurements in test structures with spacing of 100 µm: (a) control sample, (b) sample in which CAF growth initiated, and (c) sample which exhibited insulation failure during accelerated test.

For the control samples, the impedance behavior under dry condition (after baking at 125°C) is similar to that of an insulator. The impedance decreases with increasing frequency. For the same sample after exposure to humidity, the impedance at low frequency dropped by approximately 1 order of magnitude due to moisture penetration in to the substrate (Figure 4.18a). The linear region at higher frequency in the plot indicated that the capacitance is not a strong function of the absorbed moisture. The impedance response of the sample appeared to be similar under the two different exposure conditions. Takahashi [35] conducted impedance measurements between two through-holes, two surface-traces on one side and two surface-traces on both sides of the boards to investigate the different conduction mechanisms that exist in epoxy boards. It was reported that conduction through epoxy was weak and a primary conduction path existed along the glass fiber-epoxy interface as seen from impedance measurements. The impedance at low frequencies contained contributions from purely ohmic resistance, charge-transfer resistance and Warburg parameter, where the charge transfer resistance was found to be relatively insignificant, the ohmic resistance and Warburg parameter decreased, decaying to asymptotic values with long duration of humidity exposure [35]. The impedance measurements in this study for the control sample are similar to that observed by Takahashi [35] where impedance at low frequencies decreased with increasing duration of humidity exposure.

For the sample where CAF growth initiated (Figure 4.18b), the impedance response after removal of moisture after baking is similar to the control sample indicating that impedance recovered during drying. The magnitude is comparable to control samples, indicating high impedance in spite of formation of a conductive filament along

the epoxy-glass fiber interface. After exposure to humidity, however, impedance decrease is observed over the range of frequencies studied. This measurement response is different from the control sample, where the difference was observed only at the low frequency range. The impedance change over the frequency range is likely due to the change in the inter-electrode spacing (between the through-vias) resulting from the formation of conductive filaments along the glass fibers. Since the primary conduction path was reported to exist along the glass fiber-resin interface, the formation of filaments is found to influence the impedance response over the frequency range investigated. For the samples that exhibited insulation failure during the accelerated test (Figure 4.18c), impedance is several orders of magnitude (approximately ~$10^6\ \Omega$) lower compared to the control samples and similar to a pure resistor at low frequencies (relatively flat with frequency) [87]. At high frequencies, a decrease in impedance is observed. Impedance measurements for the insulation failure sample under the two exposure condition (after baking and humidity exposure) also indicated that the impedance did not recover due to removal of moisture. Therefore, it can be found that once a conduction path, moisture sorption did not play a major role in influencing impedance. This observation is similar to that of Takahashi [35] who reported drastic reduction in impedance value from catastrophic failure in through-hole geometry due to the application of a 50V DC bias. The DC resistance behavior of the samples during accelerated temperature-humidity-bias testing is characterized by minimal change in resistance up to the point of failure. A drastic and irrecoverable change in insulation resistance occurs after the filaments bridge the two electrodes.

4.12 Chapter Summary

In summary, the reliability of fine-pitch through-vias with spacing of 100, 150 and 200 μm in a 200 μm thick brominated-epoxy substrate with glass fiber reinforcement was investigated. Two different accelerated test conditions were used to investigate insulation reliability. A strong dependence of failures with via spacing was observed in either test condition. The test structures with 100 μm spacing were found to exhibit insulation failures in either test conditions. The test structures also exhibited short failure times, which were found to be driven by enhanced drilling-induced fracture because of the smaller separation distances. An increased number of CAFs at the higher test temperature (130°C) condition was observed due to the enhanced thermal and hygroscopic stresses at the epoxy-glass fiber interface. Impedance spectroscopy measurements revealed differences in frequency response for the test structures under different conditions before and after exposure to humidity. Elemental characterization of CAF using EDS consistently revealed the presence of copper and chlorine in the failure region indicating the formation of a chloride containing CAF compound in the halogenated-epoxy substrates.

CHAPTER 5

RELIABILITY OF FINE-PITCH WIRING IN HALOGEN-FREE EPOXY-GLASS FIBER SUBSTRATES

5.1 Chapter Overview

This chapter will discuss the results of reliability study conducted in two different glass fiber reinforced halogen-free epoxy substrates blended with inorganic fillers. The substrates included different epoxy resin systems with different filler content. The test structures for investigating reliability included, (1) an improved through-via to through-via design with conductor spacings of 100 and 150 µm, and (2) through-via to surface-trace geometry with a conductor spacing of 75 µm. The test structure design specifications, accelerated test results, substrate material property and geometry effects on failures, failure analysis and elemental characterization will be discussed in this chapter.

5.2 Substrate Materials

The substrate materials included two different halogen-free epoxy resin systems (material A and material B) of 100 µm thickness each. Flame retardant properties were achieved using a modified epoxy resin formulation and aluminum hydroxide ($Al(OH)_3$) filler particles in the matrix. Such an approach replaces the traditional brominated resin approach. Material B also incorporated SiO_2 particles in the resin matrix to achieve a much lower CTE and for improving the modulus. The properties of the substrate materials (material A and material B) are summarized in Table 5.1.

Table 5.1. Material properties of halogen-free epoxy substrates.

Property	Material A	Material B
T_g (TMA, °C)	145	165
CTE (ppm/°C)	17	13
Dk (1 GHz)	4.4	4.5

The organic resin matrices for both material A and B were reinforced with one layer of E-glass fiber. The total thickness of the glass fiber weave is approximately 90 µm and the diameter of an individual fiber is approximately 6 µm. The glass fiber weave consisted of a fiber count of 60 in the warp direction and 58 in the fill direction. A cross-sectional SEM image of the glass fiber reinforced substrate (material A) showing fillers and glass fiber reinforcement in the epoxy resin matrix is shown in Figure 5.1.

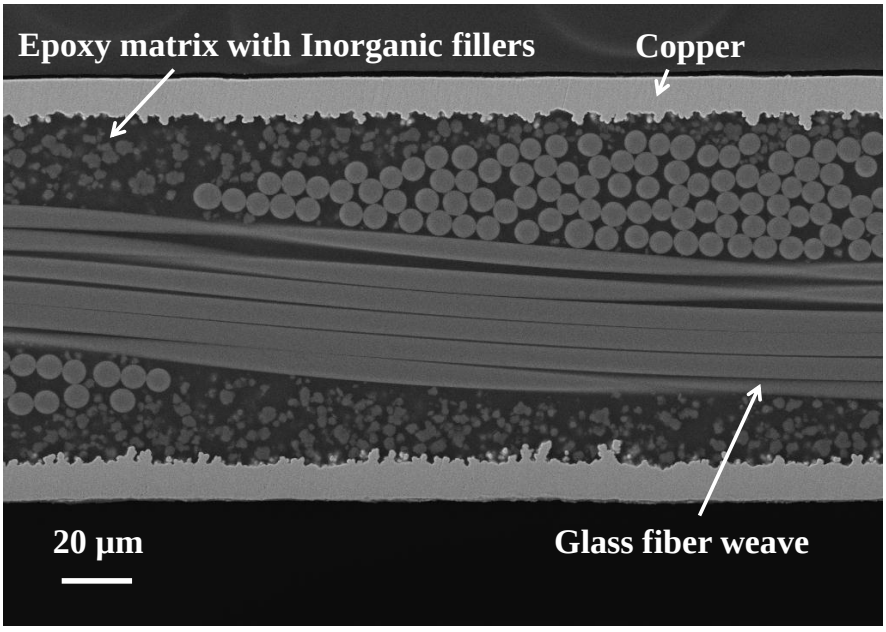

Figure 5.1. Cross-sectional SEM image of halogen-free epoxy substrate.

5.3 Moisture sorption

The moisture sorption behavior of the two substrates was investigated using gravimetric measurement (Section 3.3). The average moisture sorption content increase for the two substrates with time at 85°C and 85% RH is shown in Figure 5.2.

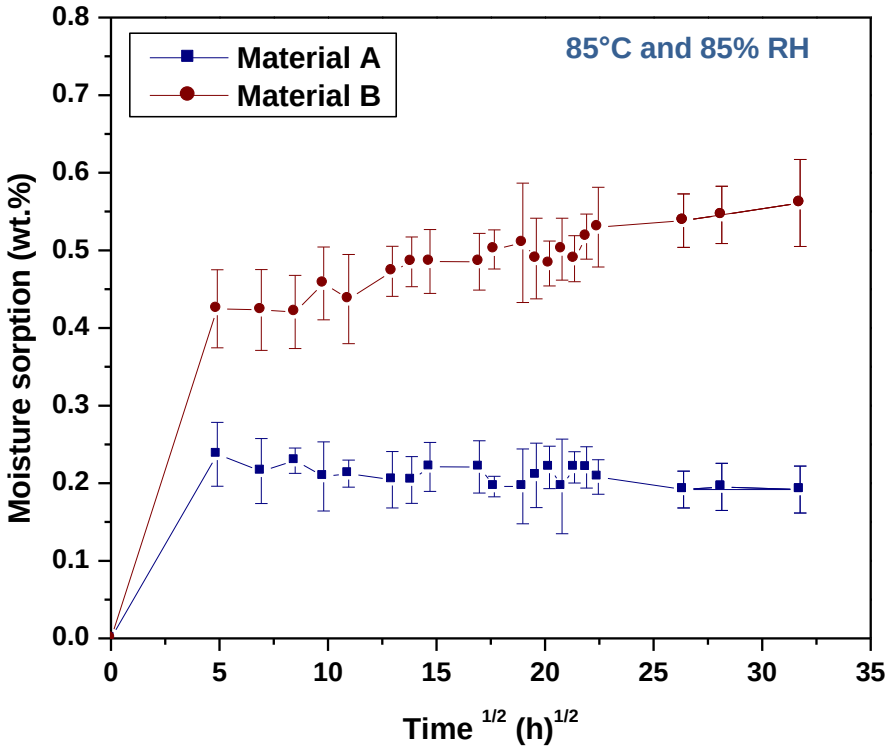

Figure 5.2. Moisture sorption of the halogen-free epoxy substrates at 85°C and 85% RH.

The average moisture content after exposure to 85°C and 85% RH for the two halogen-free epoxy substrate materials is summarized in Table 5.2.

Table 5.2. Moisture sorption at 85% RH and 85°C for the two halogen-free epoxy substrate materials.

Substrate Material	Moisture sorption [M_t (wt%)]		
	24 h	100 h	1000 h
Material A	0.24 ± 0.04	0.21 ± 0.04	0.19 ± 0.03
Material B	0.42 ± 0.05	0.45 ± 0.05	0.56± 0.06

Based on gravimetric measurements, the moisture sorption of material A appeared to decrease with time. However, this is likely due to the errors from measuring small moisture content in thin samples. The moisture content appears to be relatively constant after the initial sorption. For material B, however, an increase in moisture content was observed with exposure time, this behavior was similar to the sorption behavior of halogenated-epoxy substrate (Section 4.3).

5.4 Extractable Ion Content

Ionic constituents (chloride and bromide ions) in the halogen-free epoxy substrates were analyzed using the procedure described in Section 3.4. The extractable chloride and bromide content is given in Table 5.3. Possible errors associated with determination of extractable ion content were discussed previously in Section 4.4.

Table 5.3. Extractable ion content in halogen-free epoxy substrates.

Sample	Br^- (µg/cm^2)	Cl^- (µg/cm^2)
Material A	< 0.01	0.067
Material B	< 0.01	0.061

5.5 CAF Test Structure Design

Two different conductor geometries were studied, (a) through-via to through-via geometry and (b) through-via to surface-trace geometry. The test structure details are described as follows.

5.5.1 Through-via to Through-via Geometry

The 2-metal layer through-via to through-via test structure design is shown in Figure 5.3. The test structure consisted of 100 through-vias arranged in a 10 x 10 array in an alternate anode (5 rows) and cathode (5 rows) configuration. The positively biased vias (anodes marked with +) and the negatively biased vias (cathodes marked with -) were connected in such a fashion to increase the total number of possible failure sites in either orientations. The arrows in Figure 5.3 indicate four possible failure sites for one anodic through-via. The total number of possible failure sites for such type of design is given by

$$Number\ of\ failure\ sites = 2n\ (n-1) \qquad (5.1)$$

Where *n* is 10 for this design, resulting in 180 possible via-via failure sites with 100 through-vias in one test coupon. Test structures with two different spacings, 100 µm and 150 µm, were studied.

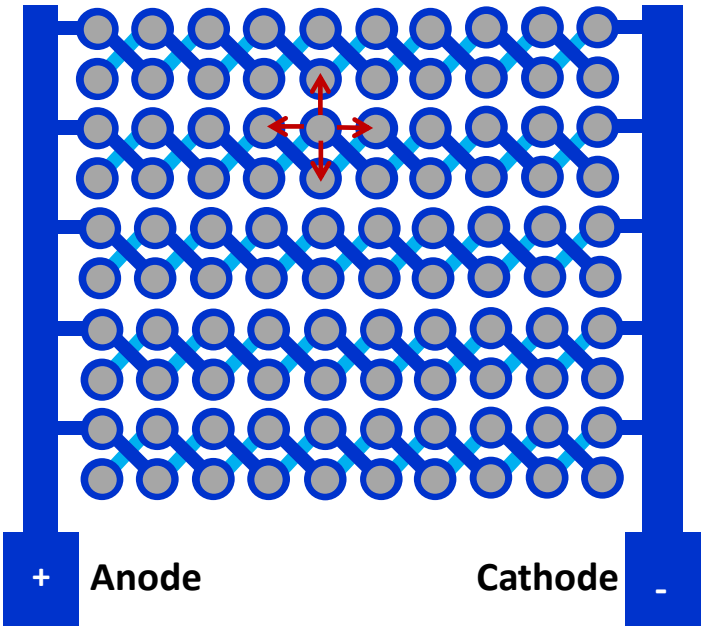

Figure 5.3. Schematic of through-via to through-via test structure.

The test structure described offers two key advantages in comparison to previously described test structures (Section 4.5).

1. The test structure increases the number of possible failure sites. There are 180 possible failure sites with 100 through-vias compared to 90 failure sites with 100 through-vias in IPC design. The standard test structure (Section 2.8) enables 168 failure sites with 210 through-vias. Therefore, the total number of samples can be reduced.
2. The test structure design enables failure sites in either through-via orientation. IPC test standard recommendation is to have test coupons at both 0° and 90° orientation to the board to study the preferred failure direction. Therefore, a number of test structures in either direction may be required for evaluation. In the test design described above, the preferred failure direction can be established without having test coupons in either orientation.

5.5.2 Through-via to Surface-trace Geometry

The purpose of this test structure is to study the susceptibility of CAF formation in such geometry in thin substrates where the glass fibers are closer to the copper surface-traces. The test structure design for the through-via to surface-trace is shown in Figure 5.4. The through-via to surface-trace geometry consisted of 60 through-vias. The through-vias and the surface-traces were arranged in an alternate anode and cathode configuration. The through-vias were positively biased such that the copper anode is in direct contact with the glass fibers. The spacing between the through-via and surface-trace was 75 µm. The spacing between two nearest through-vias was 300 µm and the width of the surface-traces was 150 µm. This test structure geometry consisted of surface-traces on only one side of the substrate. The arrows in Figure 5.4 indicate two possible failure sites for one anodic through-via and 110 such failure sites are possible with this test structure design.

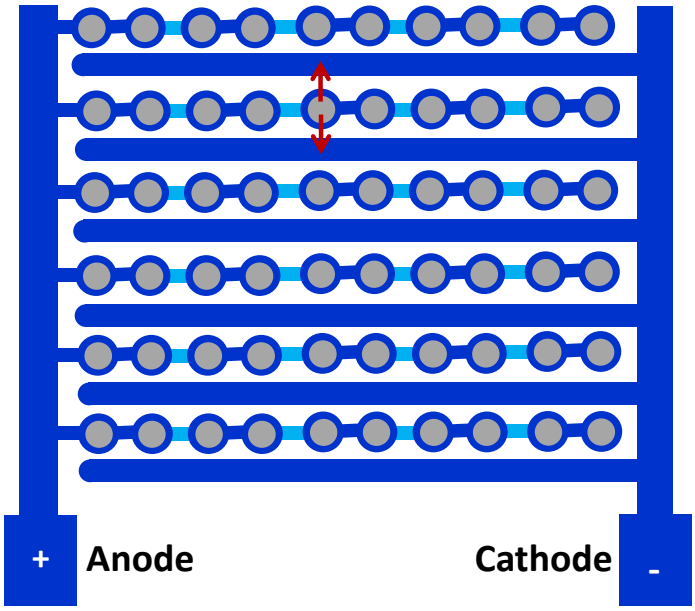

Figure 5.4. Schematic of through-via to surface-trace test structure.

5.6 Test Structure Fabrication

The test structures were fabricated using semi-additive plating method, (Section 3.7.2). Semi-additive plating method was used for fabrication as the spacing between the smallest features in the through-via to surface-trace test structures was 40 µm. Optical and cross-sectional SEM images of the fabricated test structures with both conductor geometries are shown in Figure 5.5a and b.

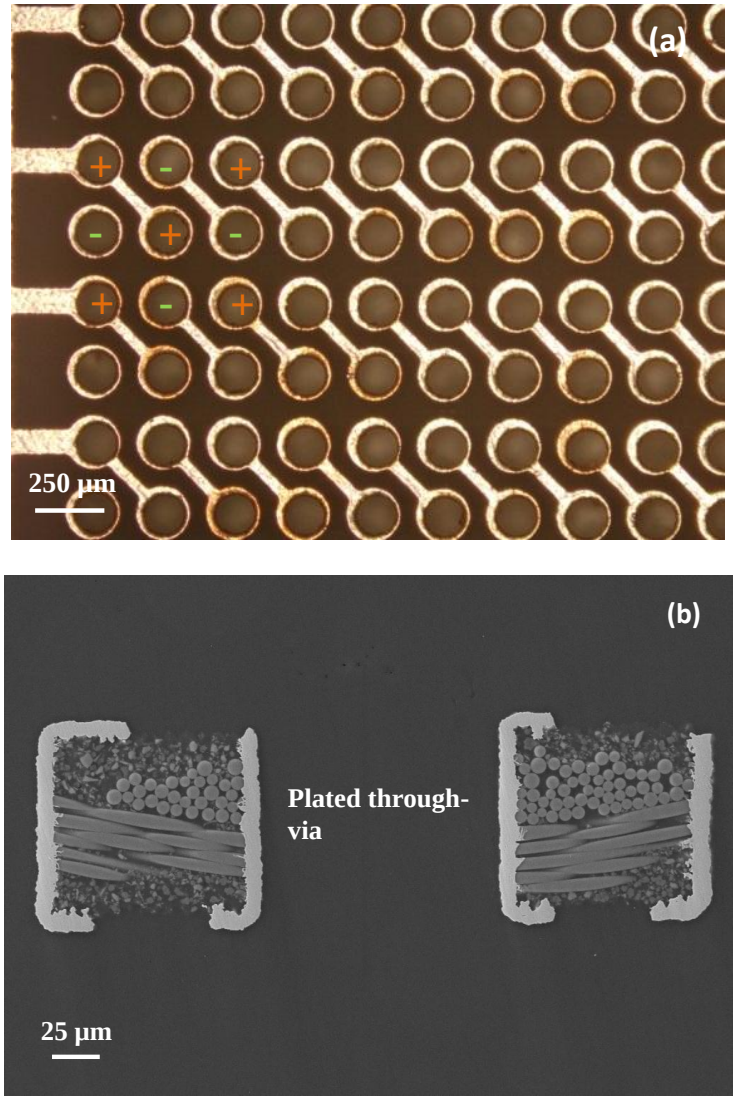

Figure 5.5. Through-via to through-via test structure: (a) optical image of surface and (b) cross-sectional SEM image.

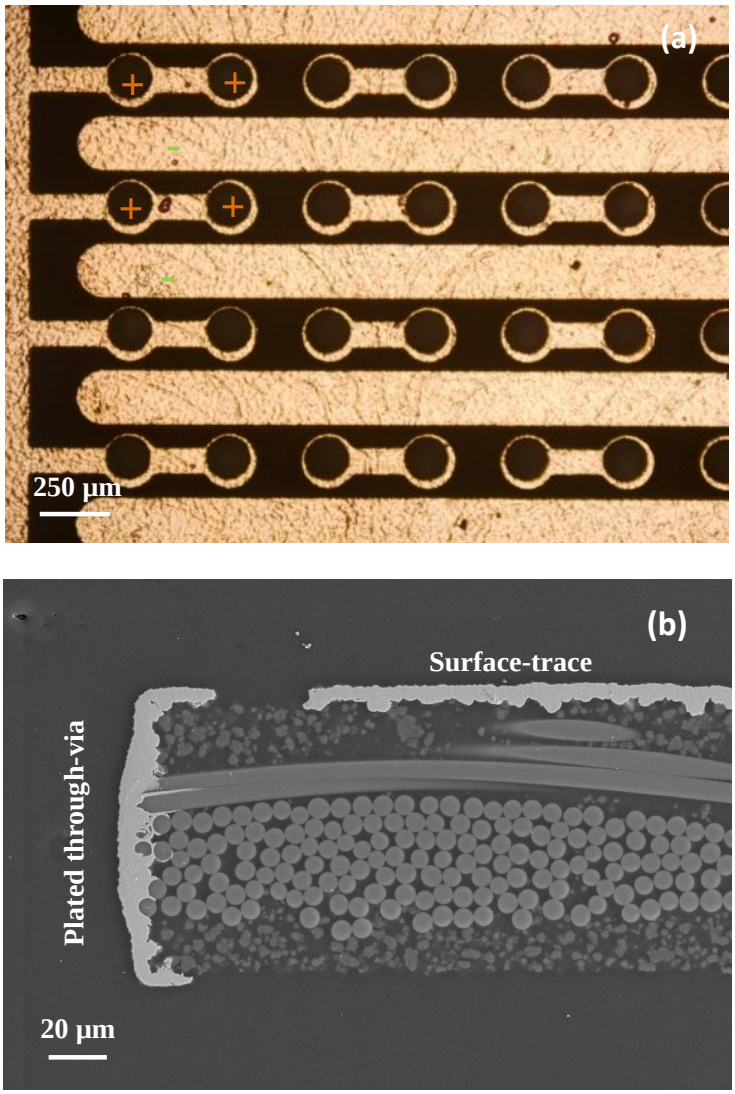

Figure 5.6. Through-via to surface-trace test structure: (a) optical image of the surface and (b) cross-sectional SEM image.

5.7 Accelerated Testing

Five samples of through-via to through-via geometry with spacings of 100 and 150 µm, and five samples of through-via to surface-trace geometry in material A and B were subjected to THB test (85°C and 85% RH with 100V DC bias) for a maximum duration of 1000 h (Section 3.9.1).

5.8 Accelerated Testing Results

5.8.1 Through-via to Through-via Structures

Insulation failures based on a failure criterion of 1 MΩ for the two conductor spacings (100 µm and 150 µm) for the through-via to through-via test structures for materials A and B are summarized in Table 5.4.

Table 5.4. Insulation measurement results based on a failure criterion of 1 MΩ for through-via to through-via test structures.

Substrate material	No. of failures/ Total no. of coupons	
	100 µm	150 µm
Material A	5/5	4/5
Material B	5/5	2/5

The insulation resistance measurements indicated that all five test coupons with through-via spacing of 100 µm in either substrate material type exhibited insulation failures. Test structures in Material A were found to exhibit failures within 24 - 48 h of test with four out of five coupons failing within 24 h. Test structures with through-via spacing of 100 µm in material B exhibited relatively longer time to failure with insulation failures occurring between 48-168 h.

For the test structures with conductor spacing of 150 µm, four coupons exhibited failures in material A. Two coupons failed within 24 h of test and the other two failures occurred after 120 h and 288 h, respectively. For material B, the first insulation failure occurred after 264 h and the second failure occurred after 504 h.

5.8.2 Through-via to Surface-trace Structures

The insulation measurement results based on a failure criterion of 1 MΩ for through-via to surface-trace geometry test structures subjected to THB test is given in Table 5.5.

Table 5.5. Insulation measurement results based on a failure criterion of 1 MΩ for through-via to surface-trace test structures.

Substrate	No. of failures/ Total no. of coupons
Material A	0/5
Material B	0/5

In THB test, either substrate material did not exhibit any insulation resistance failures (resistance change to 1 MΩ) during the accelerated test up to 1000 h.

5.9 Discussion

5.9.1 Conductor Spacing and Geometry Effects on Reliability

The through-via to through-via test structures in either substrate material exhibited insulation failures (1 MΩ) (Table 5.4). The test structures with 100 µm spacings in material A exhibited short failure times and for the test structures with 150 µm, two test coupons also exhibited failures within 24 h. In either substrate material, the test structures with 100 µm exhibited short failure times. For CAF failures, with all failures occurring within 48 h with 100 µm spacings, it would be expected that all test structures with 150 µm spacings fail within 2 – 5 times the failure time. However, such dependence on spacing was not observed. Possible reasons for the occurrence of short failure times are described in Section 5.10 based on failure analysis.

The through-via to surface-trace test structures exhibited better insulation reliability in spite of the smaller conductor spacing (75 µm) in comparison to the through-via to through-via test structures with spacings of 100 and 150 µm. One possible reason is the lack of direct contact of the glass fibers with the surface-traces (Figure 5.6), which minimizes electrical shorts. Lando et al. [7] also reported that lack of contact leads to better reliability in surface-trace geometry. The other reason is the electric field in through-via to surface-trace geometry is weaker compared to through-via to through-via geometry. It is to be noted that the through-via to surface-trace geometry test structures also have lesser number of possible failure sites compared to the through-via to through-via test structures. The other reason is related to drilling-induced fracture with smaller spacings in through-via to through-via test structures as found from cross-sectional analysis, which is discussed further in failure analysis (Section 5.10).

5.9.2 Substrate Material Effects on Reliability

Based on *in-situ* resistance measurements, substrate material B was found to exhibit better insulation reliability than material A. The results were consistent in both through-via to through-via geometry at both via spacings and with the through-via to surface-trace geometry in either accelerated tests. Substrate material B exhibited a higher glass transition temperature and a lower CTE compared to material A (Table 5.1). The difference in glass transition temperature and CTE between the two materials stems from the resin chemistry and differences in inorganic filler content in the resin (Figure 5.7). The lower CTE of material B is due to the presence of silica filler particles, which reduces the thermal mismatch strain compared to material A with higher CTE. A previous study on evaluation of halogen-free laminates indicated that the addition of silica fillers in the resin system prolongs the time to delamination at both 260 and 288˚C [12]. Therefore, material B is expected to have higher thermal stability compared to material A.

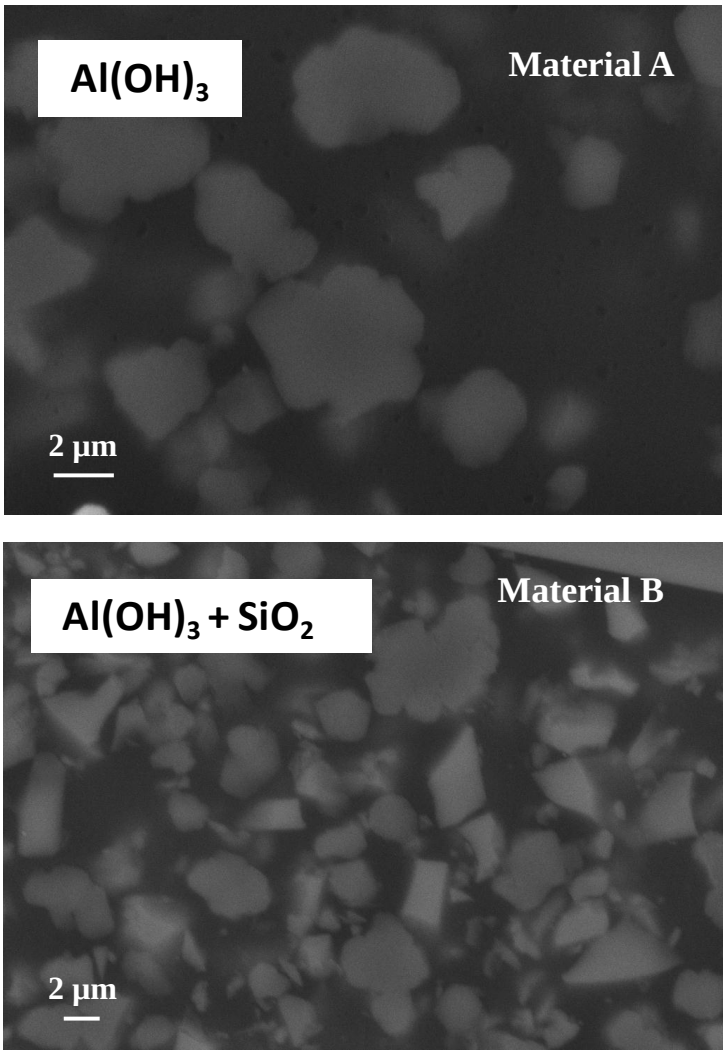

Figure 5.7. SEM images of the resin matrix in material A and material B showing differences in filler content.

It was observed that moisture content in material B was approximately two times the moisture content compared to material A (Figure 5.2). The moisture sorption trend for the two materials indicate that the moisture content change in material A is minimal after the initial sorption increase, while material B showed a slow increase after the initial sorption, possible reasons for such behavior were previously explained. Information on the difference between two material systems was not available due to the proprietary

nature of the resin formulation. Besides differences in resin system and the curing agents, higher cross-link density in epoxy leading to increase in free volume and filler interface interaction with moisture, have both been found to influence moisture uptake of the substrates [88]-[92]. In spite of its relatively higher moisture sorption, material B was found to exhibit better reliability. The higher thermal stability and lower CTE are the possible reasons for the better reliability performance of material B.

5.10 Failure Analysis and Characterization

5.10.1 Through-via to Through-via Test Structures

Optical images recorded using transmission light source of the failed test coupons with through-via to through-via geometry are shown in Figure 5.8. Based on optical inspection, failures were observed in both through-via orientations (Figs. 5.8a and b), which is expected with the improved test design used in this study. In material A, four out of the five failures occurred along the same orientation for the test structures with 100 µm spacings and two out of the four failures occurred along the same orientation. In material B, three out of five failures occurred along the same orientation with 100 µm spacing, and the two failures with 150 µm spacing also occurred along the same direction.

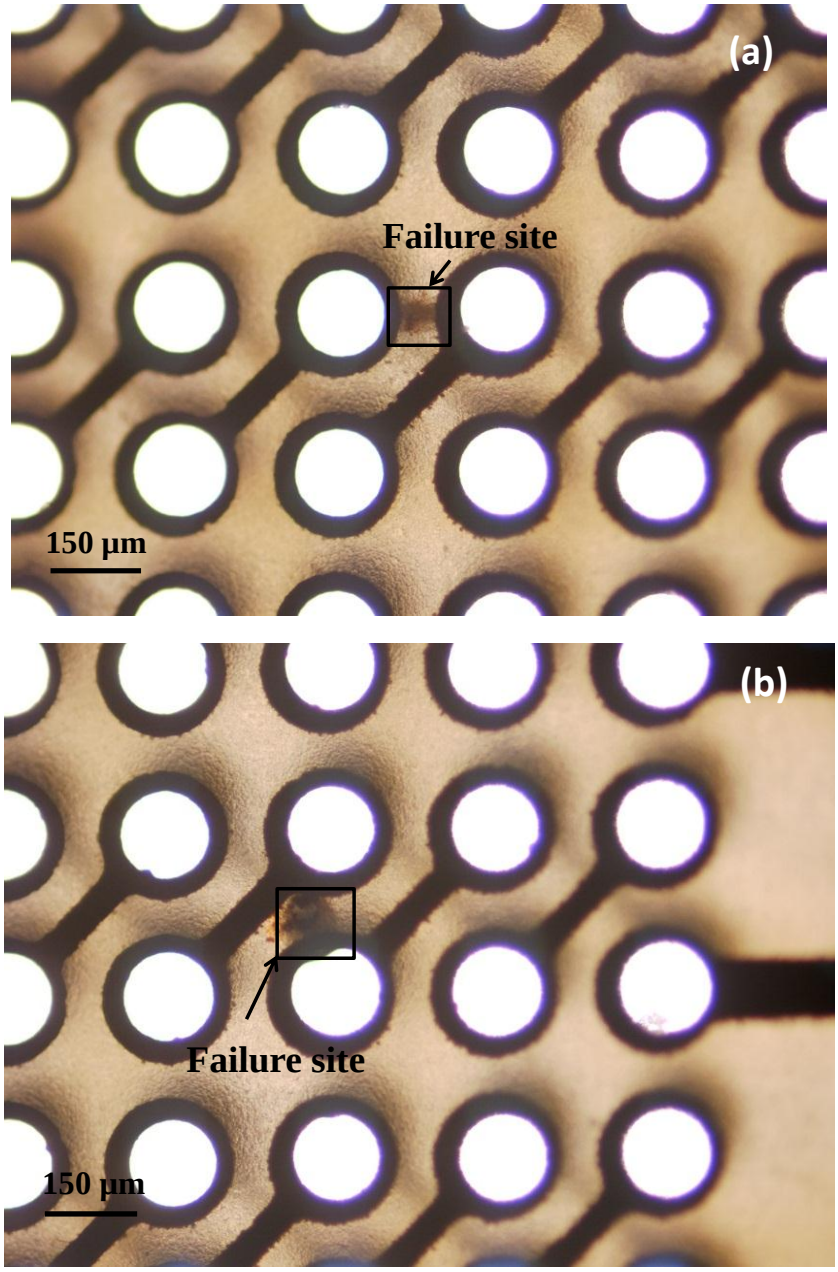

Figure 5.8. Optical transmission images of test coupons with insulation failures in (a) horizontal and (b) vertical directions.

After the identification of the failure sites, the test coupons were cross-sectioned and observed under SEM. SEM analysis of the failure sites in the samples which displayed short failure times revealed the presence of cracks in the resin matrix and along the resin-glass fiber interface in either substrate materials (Figure 5.9a and b).

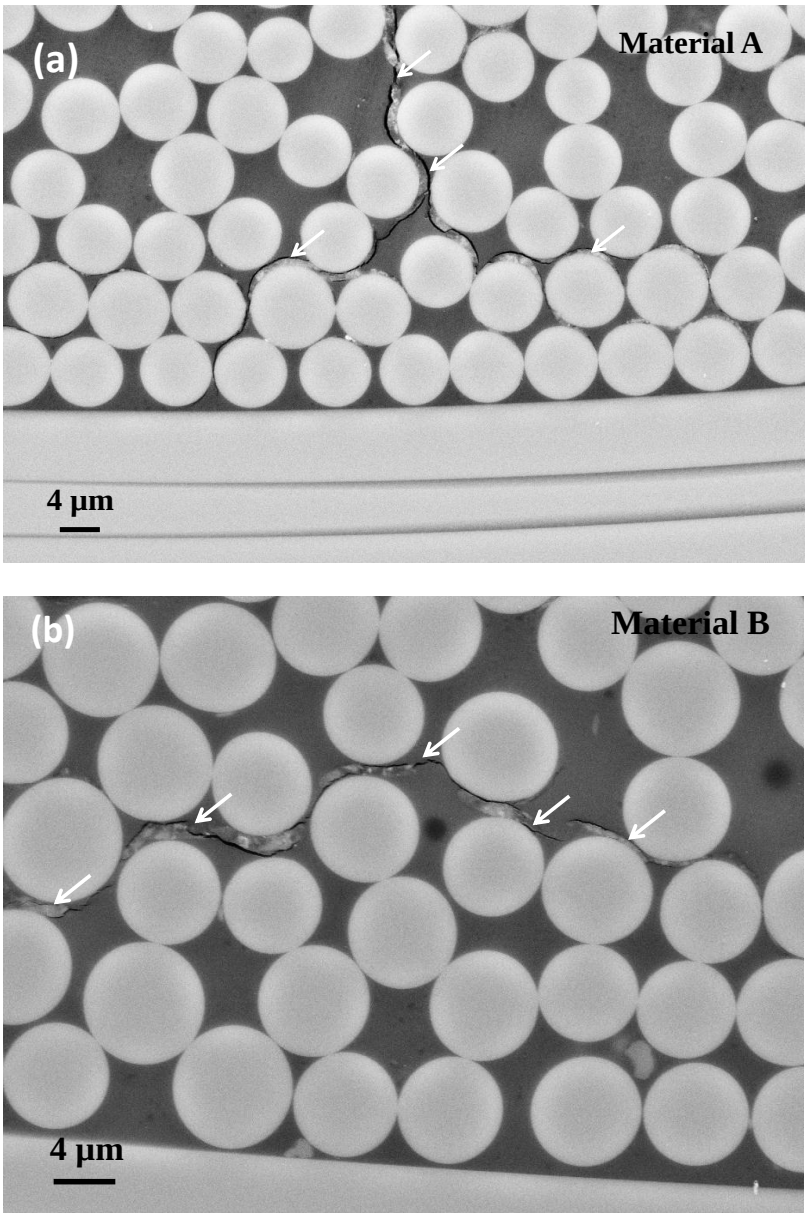

Figure 5.9. Cross-sectional SEM image of failure sites showing cracking in resin and interface: (a) material A and (b) material B.

The presence of interfacial cracks lead to deposition of copper during the through-via plating process. While CAF formation is typically confined to the interfacial region surrounding the glass fibers, the cross-sectional SEM analysis indicated the presence of residue in the cracks within the polymer matrix in addition to the glass fiber-resin

interface region. EDS characterization performed on the residue observed near cracks revealed the presence of copper, indicating possible plating deposition within the cracks (Figure 5.10).

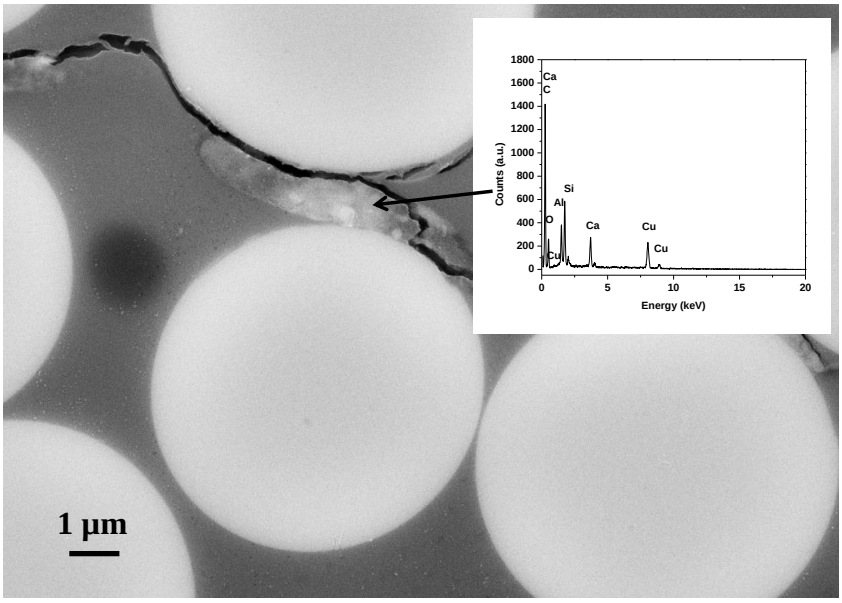

Figure 5.10. EDS characterization in the region near cracks in the resin.

The presence of cracking within resin during thermal testing was previously observed in halogen-free laminates, where degradation within the epoxy/epoxy interface in addition to glass fiber/epoxy interface in substrates consisting of aluminum hydroxide fillers. Such defects appear to be characteristic of halogen-free substrates as a result of the high filler content in the resin matrix [12]. Cracking within matrix and the interface, and resulting plating deposition within the cracks are presumed to be the reasons for short time to failure with small through-via spacings. Although short failure times were observed in test structures with 100 µm spacings, the test structures with 150 µm spacings were found to exhibit better reliability. The results indicated that the crack length is a function of the spacing between the through-vias. The through-via to surface-

trace test structure geometry with via to via spacing of 300 µm was found to display significantly better reliability.

5.10.2 Through-via to Surface-trace Test Structures

While there were no insulation failures based on resistance drop to 1 MΩ in the through-via to surface-trace test structures in THB test, optical inspection of test structures in material A revealed the occurrence of electrochemical migration (Figure 5.11). The filaments formed were not found to result in burnout failures during the accelerated test as was observed in the through-via to through-via test structures. The thin nature of the filaments as seen in Figure 5.11, did not result in drastic changes in insulation resistance, therefore, could not be detected electrically. Ready et al. [78] also noted that the CAF formed in SIR test coupons could not be detected based on discrete insulation resistance measurements. Optical inspection of material B, however, did not reveal any presence of electrochemical migration.

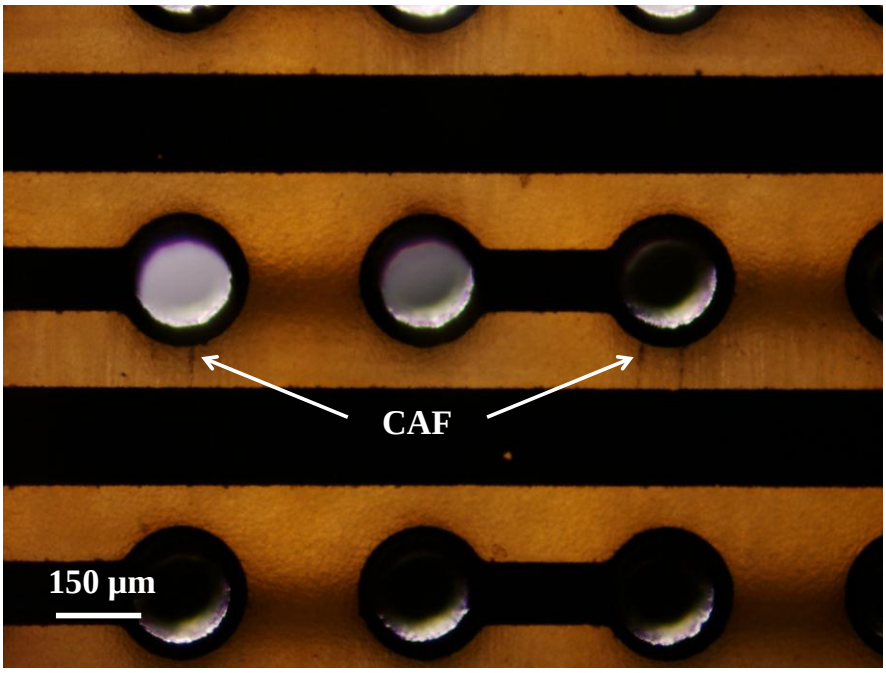

Figure 5.11. CAF formation in through-via to surface-trace test structure.

5.10.3 CAF Characterization

A high resolution optical image of CAF along the glass fiber interface is shown in Figure 5.12. Detection of CAF in the substrates was relatively more difficult due to the smaller fiber diameters. The average diameter of individual glass fibers in the matrix is approximately 6 µm and it was observed that the small glass fiber thickness resulted in smaller interfaces where CAF formation occurred.

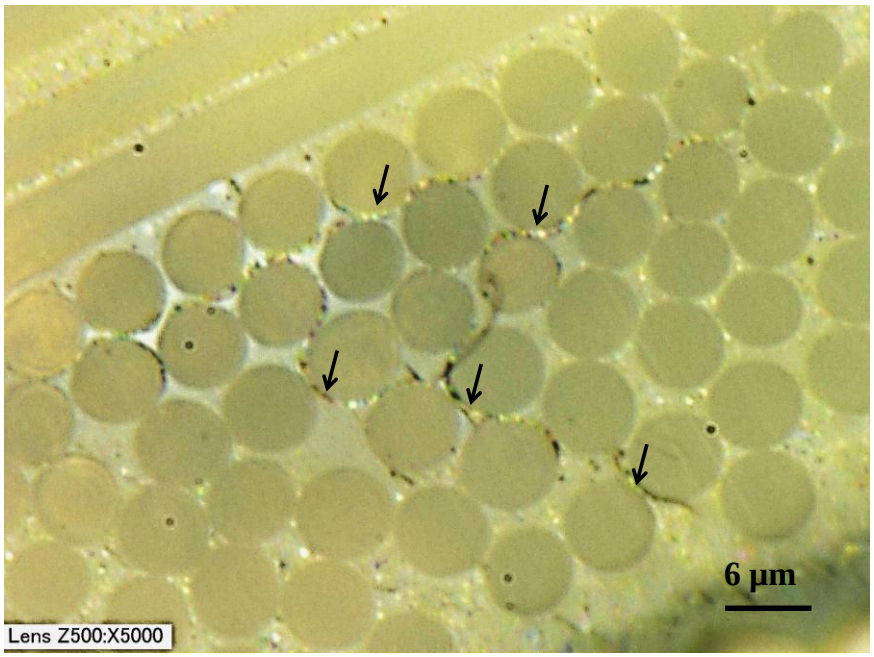

Figure 5.12. Optical image of CAF in the glass fiber-resin interface.

Cross-sectional SEM image of the sample is shown in Figure 5.12. The higher magnification image shows the separation between the organic resin and the glass fiber where the compound is present.

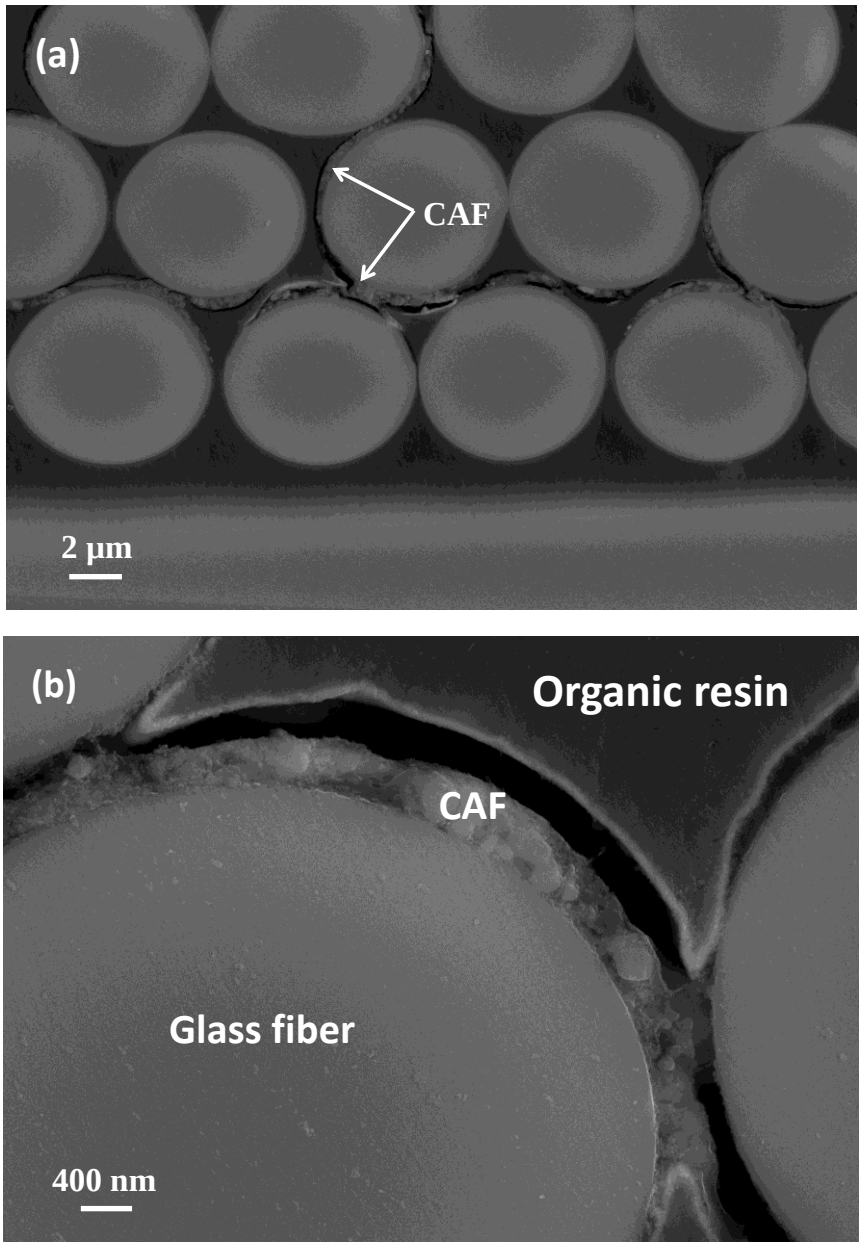

Figure 5.13. SEM images: (a) and (b) CAF in the glass fiber-resin interface at different magnifications.

Elemental characterization was performed on the cross-sections using EDS. The elemental spectra obtained from the resin matrix and the CAF regions are shown in Figure 5.14a and b, respectively. The EDS spectrum obtained from the matrix (Figure 5.14a) revealed the presence of silicon, calcium, aluminum and oxygen peaks from

interaction of electrons with the epoxy resin, glass fibers and aluminum hydroxide filler particles. The halogen-free epoxy resins as verified using EDS did not consist of bromine. Bromine and aluminum have similar x-ray emission characteristics; the *Lα* of bromine (1.48 keV) and the *Kα* of aluminum (1.486 keV) lie close in the energy spectra. There is *Kα* peak for bromine at 11.90 keV, which can be used to distinguish bromine from aluminum [12]. Therefore, the EDS spectrum was obtained up to 20 keV to verify the absence of bromine in CAF. The EDS spectrum obtained from the CAF region (Figure 5.14b) revealed the presence of copper and chlorine in addition to the other elements found in the resin matrix and glass fibers. The spot size where the x-ray generation occurred was approximately 10 μm in diameter in the Zeiss Ultra60 SEM. The intensity of copper and chlorine was relatively less due to masking by the other elements from the resin and glass fibers. The EDS analysis indicated the likelihood of chloride-containing copper compound.

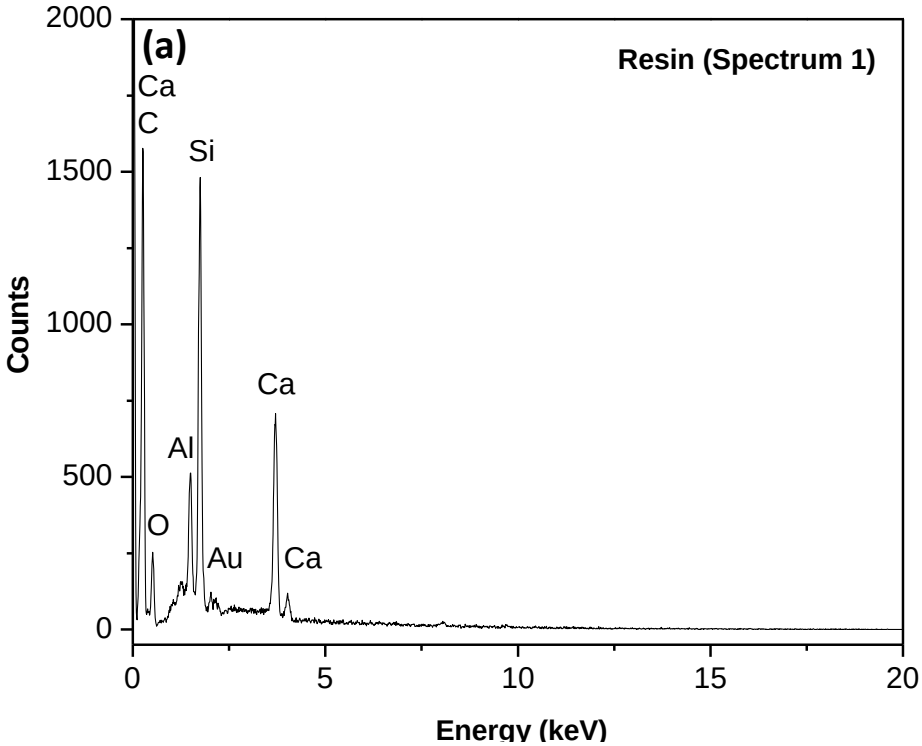

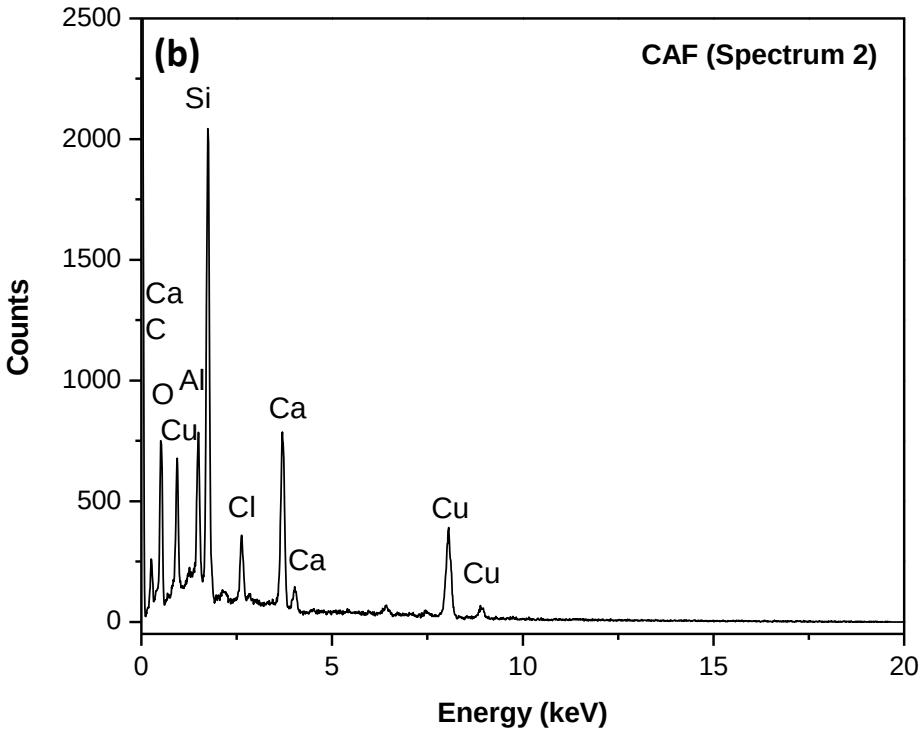

Figure 5.14. EDS characterization: (a) resin and (b) CAF region.

5.11 Potential-pH diagrams for Cu-Cl-H_2O

In this section, potential-pH diagrams were generated by varying the parameters such as temperature and chloride concentration to understand the thermodynamic behavior of copper in different conditions. In this study, EDS analysis of CAF in the halogen-free epoxy substrates revealed the presence of chlorine in CAF region. The extractable chloride content in halogen-free epoxy resins (Table 5.3) was approximately 3 – 4 times lesser than the halogenated epoxy (Table 4.3) based on extractable ion content analysis. Therefore, potential-pH diagrams were generated to examine the different compounds that are favored with different concentration of chloride ions and temperature.

Potential-pH diagrams [18] predict the thermodynamic behavior of metals under given conditions of potential and pH. The vertical axis in the plot is the potential and the horizontal axis is the pH. The lines in the plot represent either chemical or

electrochemical reactions that occur under the given conditions of temperature, ion concentration, and pH. The spontaneity of the reactions can be predicted by calculation of Gibbs free energy change. If the change in Gibbs free energy is negative ($\Delta G < 0$), the reaction is favored. The Gibbs free energy for electrochemical reactions is described using the following equation:

$$\Delta G^0 = -nFE^0 \qquad (5.2)$$

Where n is the number of electrons passing through the circuit, F is the Faraday's constant and E is the electromotive force. The equation described above is applied for standard states. For non-standard states, the change in free energy is given by,

$$\Delta G = -nFE^0 - \mathrm{RTln}\left(\frac{a^n_{cathode}}{a^n_{anode}}\right) \qquad (5.3)$$

Where $a^n_{cathode}$ and a^n_{anode} are the activities of the products and reactants at cathode and anode, respectively. The potential is described using the Nernst equation as,

$$E = E^0 - \left(\frac{RT}{nF}\right)\ln\left(\frac{a^n_{cathode}}{a^n_{anode}}\right) \qquad (5.4)$$

The potential-pH diagrams were constructed using software (HSC Chemistry 5.11) by varying either the temperature or the chloride concentration to analyze the effect on thermodynamic stability of the phases.

5.11.1 Effect of Chloride Concentration

In this study, the effect of chloride ion concentration on corrosion behavior of copper was investigated by varying the concentration from 10^{-3}M to 10^{-5}M, (~35 ppm -

0.35 ppm) to investigate the decreasing concentration of chloride ions on thermodynamic stability of solid phases that form near the anodic region. For convenience, the copper concentration was fixed at 1M, the temperature was fixed at 25°C, and only aqueous ions or solid phases were considered in generation of such diagrams. The potential-pH diagrams of Cu with different concentrations are shown in Figure 5.15.

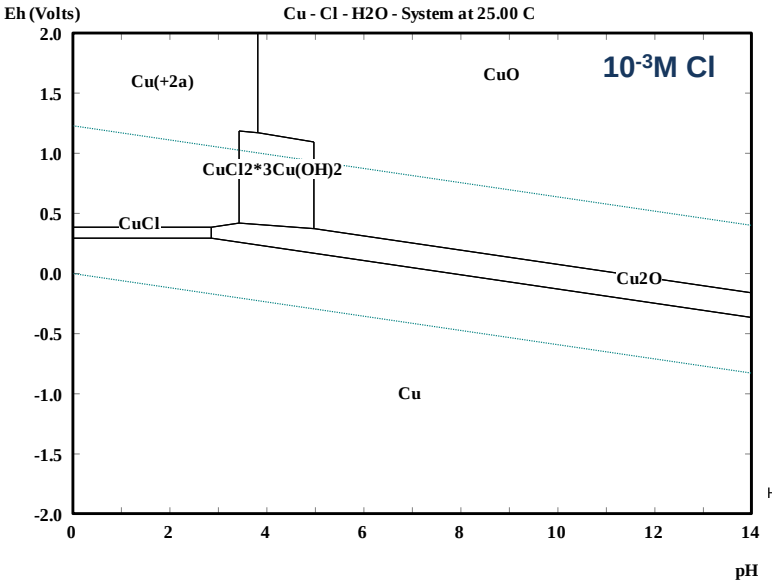

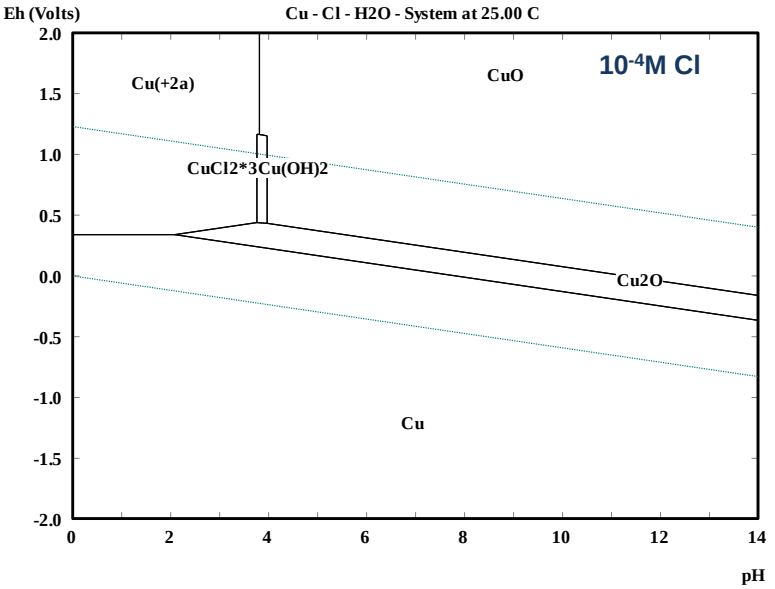

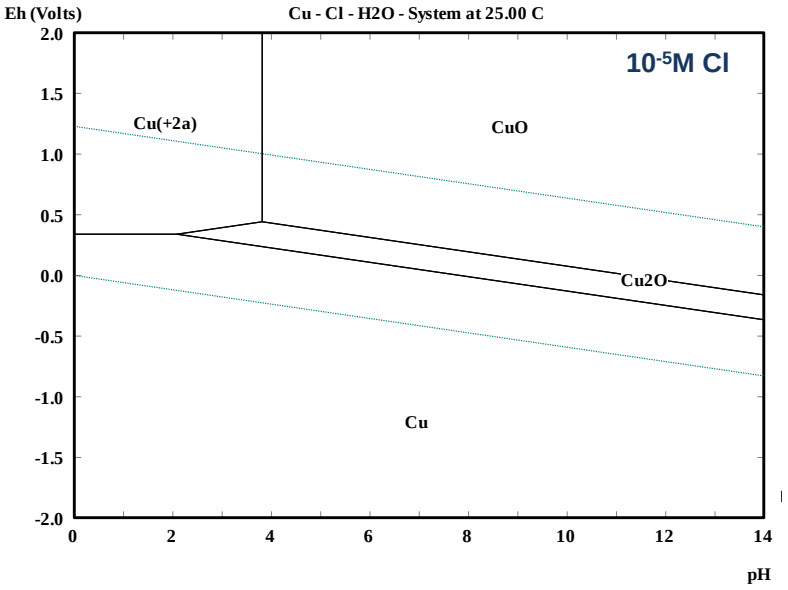

Figure 5.15. Potential-pH diagrams for the ternary Cu-Cl-H_2O system at 25°C with Cl^- concentration of 10^{-3}M, 10^{-4}M, and 10^{-5}M.

The compound ($CuCl_2.3Cu(OH)_2$) is found to be stable over a wide range of pH at a chloride concentration of 10^{-3}M and the stability of the compound decreases with reducing chloride concentration. The compound appears to be thermodynamically unfavorable at a chloride concentration below 10^{-4}M. Such diagrams are useful tools for predicting the thermodynamic behavior of metals; however, kinetic limitations need to be considered. The corrosion behavior of copper in chloride has also been investigated by several researchers [61]-[66]. Previous studies report corrosion behavior in chloride concentrations in the range of 0.1 M and generally higher than 1 M. Organic substrates in electronic packages and boards consist of much smaller chloride ion content. The maximum concentration allowed in halogen-free substrates is 900 ppm, which refers to both bound and hydrolysable chloride content in the resin matrix. The hydrolysable chloride content in the substrates is known to affect the corrosion behavior of copper. Previous studies have reported that epichlorohydrin (C_3H_5ClO) used in manufacturing of epoxy resins is the source of chloride ions and around 100 - 200 ppm of hydrolysable

chloride is available in traditional epoxy boards with the total content in the range of 1000 – 2000 ppm in halogenated substrates [41]. However, recently improved materials have significantly reduced chloride concentrations in the range of 0.1 to 10 ppm. Chloride ions can also be introduced from various other sources besides the epoxy resin itself. The other sources of chloride ions are from the copper etching solution chemistry and the etching process that utilizes chloride-based chemistry such as cupric chloride or ferric chloride. In addition, cleaning and degreasing agents such as hydrochloric acid, palladium chloride in electroless copper plating process could also introduce chloride ions in to the board [93]. Water soluble flux constituents have also been identified as a source of halide (chloride ions) in the board, which diffuse in to the board during high temperature processes when the substrates are above the T_g [41], [43]. Ternary Cu-Cl-H_2O system with chloride concentration of 35 ppm at 25°C has previously been used to explain electro dissolution of copper near the anodic region in PWBs [41].

The concentration of extractable chloride ion in this study for the halogenated and halogen-free substrates is approximately in the range of 0.42 to 1.68 ppm. EDS analysis of CAF formed in either substrates (halogenated and halogen-free epoxy substrates) indicate the formation of chloride containing copper compound in this study. Similarly Caputo [43] reported total extractable chloride content in their boards in the range of 0.19 to 0.67 ppm using ion chromatography. The extractable chloride content was found to vary with different types of water soluble fluxes. EDS characterization in their study also revealed the presence of copper and chlorine in CAF region [43]. The elemental characterization results indicate the formation of chloride containing copper compound in the presence of relatively small amount of chloride (approximately 10^{-4} to 10^{-5} ppm) in the substrates. While the potential-pH diagrams generated are fixed concentration of ions, the actual concentration of ions at the interface depends on the diffusion and migration of chloride ions in the presence of an electric field. The net flux of the ions is related to the potential and the concentration gradients, which is related to parameters such as the

concentration of ions, diffusivity, potential gradient, mobility of ions, etc. In this study, voltage gradient of 0.5 - 1V/μm was used for studying CAF reliability, therefore migration and diffusion of ions can drastically alter the concentration of ions near the interface, thereby favoring the formation of stable phases near the anode. In the absence of chloride, copper can form compounds such as $Cu(OH)_2$ in the presence of water, previously reported by DerMarderosian [49], which can also result in insulation failures in substrates. As mentioned previously, the potential-pH diagrams in this study were generated with fixed temperature and concentration, the actual potential and pH may shift based on rate of reactions, thereby altering the stability and favoring the formation of certain phases near the anode.

5.11.2 Effect of Temperature

The temperature in actual electronic systems could vary based on several factors. The operating environment which the devices are exposed to can influence temperature and as the devices are powered up and down, heating of the devices due to power dissipation results in variation in temperatures. Such temperature variations can also influence the thermodynamic stability of compounds. Additionally, accelerated life tests are also run at higher temperatures (65°C or 85°C) for studying CAF reliability. Additionally, highly accelerated tests are carried out at even higher temperatures (110°C or 130°C). Potential-pH diagrams were generated at different temperatures of interest to investigate the stability of phases at different temperatures. For generating the potential-pH diagrams, the copper concentration was fixed at 1M and the chloride concentration was fixed at 10^{-3}M (~35 ppm) for convenience. The potential-pH diagrams at different temperatures are shown in Figure 5.16.

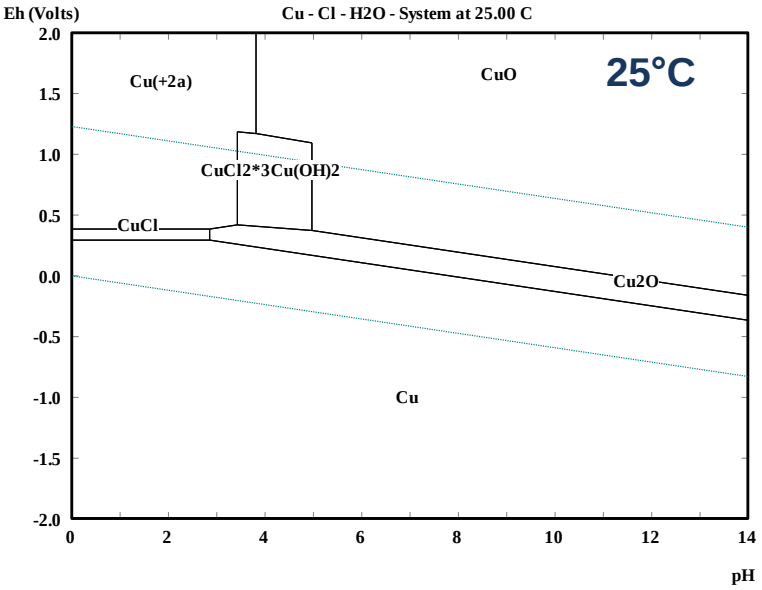
Eh (Volts)
Cu - Cl - H2O - System at 25.00 C
25°C
Cu(+2a)
CuO
CuCl2*3Cu(OH)2
CuCl
Cu2O
Cu
2.0
1.5
1.0
0.5
0.0
-0.5
-1.0
-1.5
-2.0
0
2
4
6
8
10
12
14
pH

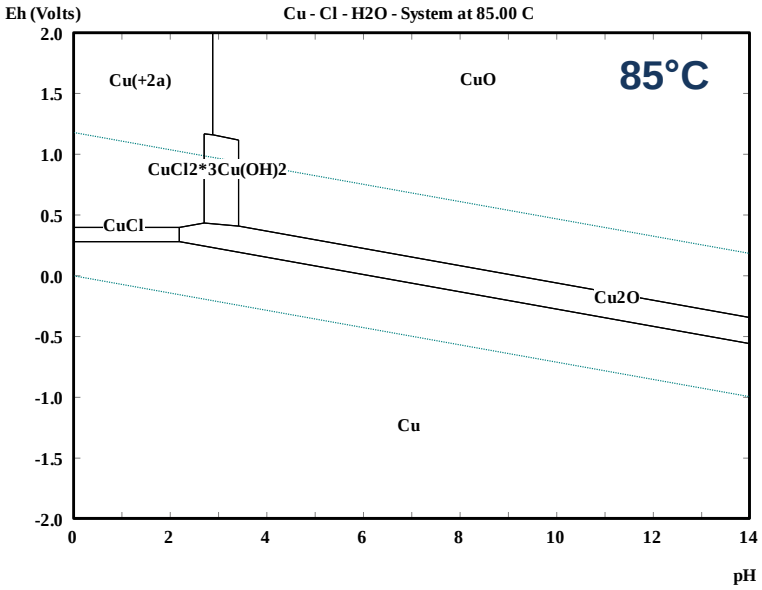
Eh (Volts)
Cu - Cl - H2O - System at 85.00 C
85°C
Cu(+2a)
CuO
CuCl2*3Cu(OH)2
CuCl
Cu2O
Cu
2.0
1.5
1.0
0.5
0.0
-0.5
-1.0
-1.5
-2.0
0
2
4
6
8
10
12
14
pH

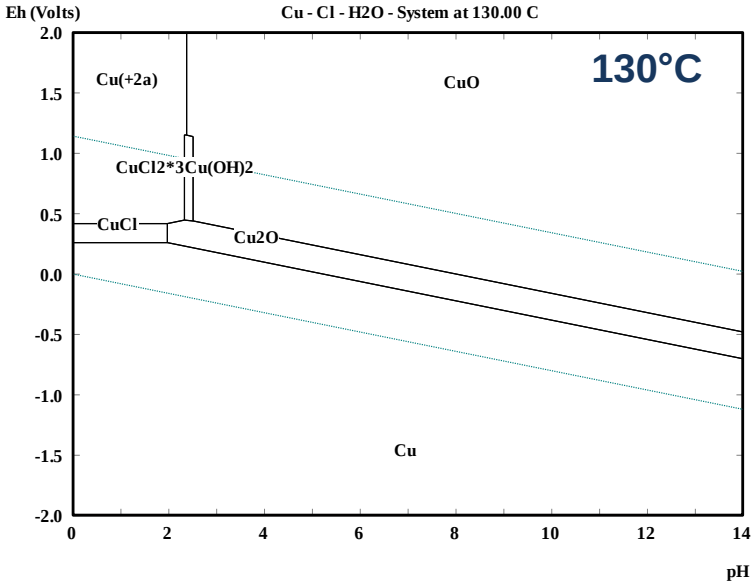

Figure 5.16. Potential-pH diagrams for the ternary Cu-Cl-H_2O system with 10^{-3}M Cl^- concentration at different temperatures: 25°C, 85°C, and 130°C.

In the temperature range of interest, the formation of $CuCl_2.3Cu(OH)_2$ is favored and the stability of $CuCl_2.3Cu(OH)_2$ is found to decrease with increasing temperature. Similar trend was reported in a study on copper corrosion behavior with chloride concentrations of 0.2 M and 1.5 M in the temperature range of 5 - 100°C. $CuCl_2.3Cu(OH)_2$ was reported to be the only stable solid copper-chloride phase that formed under the concentration of the chloride [94], [95]. In this study, EDS analysis revealed the formation of chloride containing copper compounds at different test temperatures (85°C and 130°C) used for CAF reliability study. While the potential-pH diagrams generated here consider the temperature used for tests, the actual temperature could be different at electrolytic cell formed near the interface.

5.12 Chapter Summary

This chapter reported the insulation reliability of fine-pitch wiring (through-vias and surface-traces) in two different halogen-free epoxy resin systems using an improved

test structure design. In accelerated testing, the through-via to through-via test structures with 100 µm exhibited short mean time to failure in either substrates with most failures occurring within 120 h of testing. At a through-via spacing of 150 µm, there were lesser number of failures indicating better reliability behavior with a larger conductor spacing. Cross-sectional analysis of the failure sites in the through-via to through-via test structures revealed the presence of cracks within the resin matrix and at glass fibers/resin interface where copper was observed. This resulted in preferred failure sites reducing the time for insulation failures. The results indicate that reliable fine-pitch vias may not be achieved due to the enhanced degradation observed with smaller via spacings.

Based on accelerated testing results, it was also found that the substrate material system properties influenced the reliability. Substrate material with high T_g (165°C) exhibited better insulation reliability compared to the material with lower T_g (145°C) in spite of its relatively higher moisture sorption. This is likely due to the enhanced thermal stability from the addition of SiO_2, which improves the thermal stability and time to degradation. The through-via to surface-trace geometry in either substrates did not exhibit any insulation failures during the test. However, CAF formation was visible in optical microscopy inspection of the through-via to surface-trace test structures in the substrate material. Elemental characterization using EDS revealed the presence of copper and chlorine in the CAF region in halogen-free epoxy substrates with significantly smaller chloride content compared to halogenated-epoxy substrates.

CHAPTER 6

RELIABILITY OF FINE-PITCH THROUGH-VIAS IN HALOGEN-FREE CYCLO-OLEFIN POLYMER SUBSTRATE

6.1 Chapter Overview

This chapter discusses the reliability investigation conducted in a glass fiber-reinforced halogen-free cyclo-olefin polymer substrate. The test structures for investigating reliability included through-via to through-via geometry with conductor spacing of 100, 150 and 200 µm. Reliability was investigated using THB test for 1000 h and B-HAST for 100 h. The accelerated test results and substrate material influence on insulation reliability will be discussed.

6.2 Substrate Material

The substrate was a glass fiber reinforced cyclo-olefin polymer resin system. The resin system incorporated halogen-free inorganic fillers ($Mg(OH)_2$) for achieving flame retardant property. Cyclo-olefin polymer is a relatively new class of material, which has recently gained attention as electronic packaging substrates due to its superior electrical properties. Cyclo-olefin polymer is an amorphous polymer with a bulky ring structure in the main chai and was discovered from ring opening polymerization of norbornene (NB). Synthesis of cyclo-olefin polymer from dicyclopentadiene (DCPD) is shown in Figure 6.1. The glass transition temperature of this polymer can be tailored by changing the R groups [96].

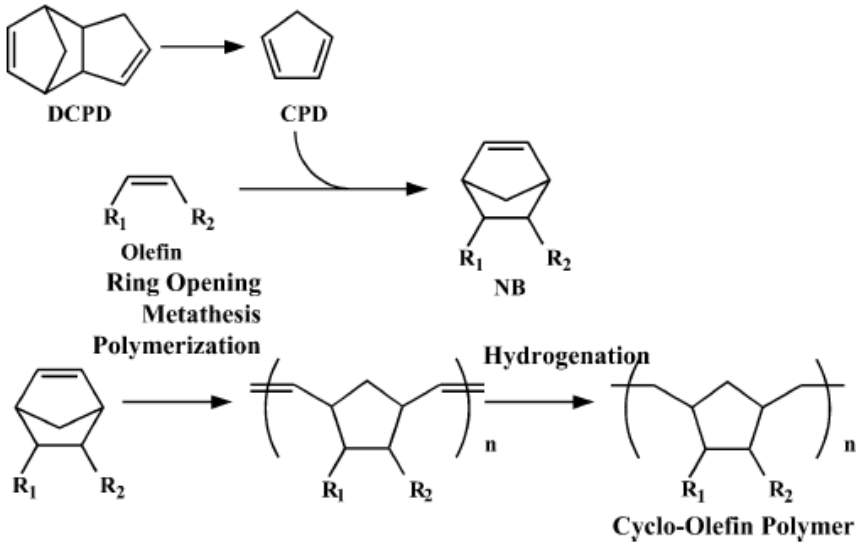

Figure 6.1. Synthesis of cyclo-olefin polymer [96].

Some of the important properties of cyclo-olefin polymer include high transparency, low water absorption, high heat resistance and good electrical insulation property. The high thermal stability enables the polymer to be used across a wide range of temperature. Cyclo-olefin polymer also exhibits low dielectric constant and low loss tangent even at high frequencies [96]. The key properties of the substrate used in this study are summarized in Table 6.1.

Table 6.1. Material properties of cyclo-olefin polymer substrate.

Parameter	Value
CTE (ppm/°C)	12
T_g (°C), TMA	170
Dk (1 GHz)	4.2

6.3 Moisture Sorption

The moisture sorption of the cyclo-olefin polymer substrate was studied using gravimetric measurement (Section 3.3). The average increase in moisture sorption with time after exposure to 85°C and 85% RH is summarized in Table 6.2. There were significant errors associated with measurements due to the extremely low sorption of the cyclo-olefin polymer system. Additionally, the substrate thickness is 100 µm, which can result in additional errors in measurements [37]. Although the measurements in Table 6.2 indicate an increase in moisture content with time, the average moisture sorption varied between 0.01 to 0.11 wt% during the measurement at different time intervals, showing no significant increase with time after the initial increase in weight.

Table 6.2. Moisture sorption at 85% RH and two test temperatures.

Temperature (°C)	**Moisture sorption [M_t (wt%)]**		
	24 h	**100 h**	**1000 h**
85	0.05 ± 0.03	0.05 ± 0.02	0.09 ± 0.04
130	0.08 ± 0.01	0.08 ± 0.03	-

6.4 Extractable Ion Content

The results of ion analysis performed using the procedure described in Section 3.4 are summarized in Table 6.3. Possible errors associated with determination of extractable ion content were discussed previously in Section 4.4.

Table 6.3. Extractable ion content in cyclo-olefin polymer substrate.

Sample	**Br^- (µg/cm^2)**	**Cl^- (µg/cm^2)**
Cyclo-olefin polymer	< 0.01	0.182

6.5 Test structure design and fabrication

The test structure design used for investigating CAF is same as previously described in Chapter 4 (Section 4.5). The test structures were fabricated using subtractive etching process (Section 3.7.1). An optical image of the portion of the fabricated test coupon and a cross-sectional SEM image with copper plated-through-vias in the test structure are shown in Figure 6.2a and b.

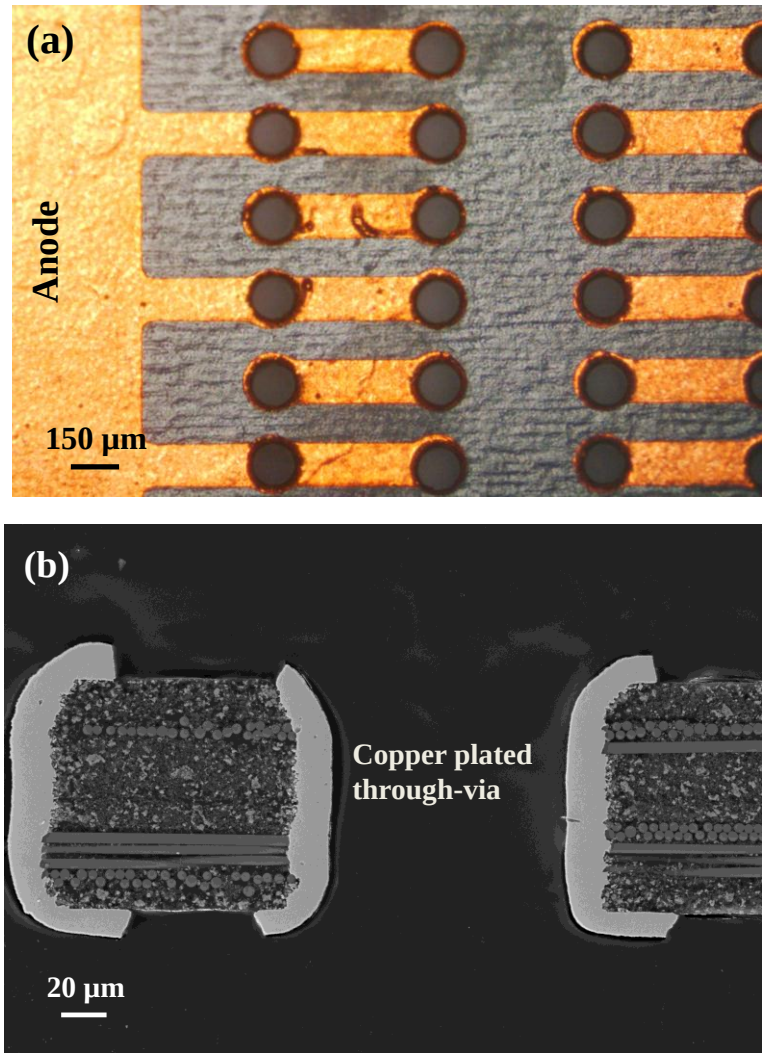

Figure 6.2. Test structure: (a) optical image with alternate anode and cathode configuration and (b) cross-sectional SEM image showing a plated-through-via.

6.6 Accelerated Testing

The accelerated testing parameters are described as follows:

1. Five test samples each with three through-via spacings (100, 150 and 200 µm) were subjected to THB test (85°C and 85% RH with 100V DC bias) for a maximum duration of 1000 h (Section 3.9.1).
2. Five test samples each with two through-via spacings (100 and 200 µm) were subjected to B-HAST (130°C, 85% RH and 2 atm with 100V DC) for a maximum duration of 100 h (Section 3.9.2).

6.7 Accelerated Testing Results

The insulation measurement results for a total of five test coupons for each conductor spacing observed is summarized in Table 6.4. The failure criterion is a resistance drop to 1 MΩ. The average initial resistance of all test coupons before temperature and humidity test was higher than 10^{10} Ohms.

Table 6.4. Insulation measurement results based on a failure criterion of 1 MΩ in accelerated testing.

Through-via spacing (µm)	No. of failures/ total no. of coupons	
	THB	B-HAST
100	0/5	0/5
150	0/5	-
200	0/5	0/5

Based on insulation resistance measurements, there were no insulation failures (1 MΩ) in this substrate.

6.8. Discussion

The test structures were found to exhibit stable insulation resistance with all through-via spacings in either test condition. Based on gravimetric measurements, the moisture sorption content was found to be less than 0.1 wt%. The low moisture content is due to the bulky structure and the absence of polar groups in the polymer. Substrates such as BT, CE and polyimide that display low moisture absorption and high glass transition temperatures have previously been reported to exhibit high reliability against CAF failures [19]-[21]. Cyclo-olefin polymer displayed the lowest moisture sorption in comparison to previously reported substrate materials. The low moisture uptake due to lack of polar groups minimizes swelling of resin and chemical interaction with absorbed moisture is minimized. Epoxy resins, on the other hand, consist of polar groups that chemically interact with water, resulting in hygroscopic strain, the magnitude of which can be comparable to thermal strains resulting from mismatch of CTE [97]. The reduced chemical interaction of non-polar groups in the substrates results in smaller hygroscopic stresses at the interface. Additionally, the rate of hydrolysis of interfacial bonds (hydrolysis of silane coupling agents) is a function of the moisture content at the resin-glass fiber interface [85]. Low concentration of water at the resin-glass fiber interface slows down the chemical degradation process, thereby delaying the path formation for electrochemical migration.

The substrates incorporated thinner glass fibers in comparison to the epoxy substrates studied. Thinner glass substrates are known to reduce the force required for drilling and cause lesser interfacial damage between the fibers [27]. On the other hand, several layers of glass fibers enable more interfaces for CAF formation. The extractable chloride content in the substrate was found to be similar to the epoxy substrates (Table 6.3) and higher compared to halogen-free epoxy substrates. However, insulation measurements during accelerated testing did not show significant changes in electrical resistance behavior in the substrate. Additionally, high temperature reliability test (B-

HAST) also did not reveal significant changes in insulation resistance at the higher test temperature. The CTE of the substrate is 12 ppm/°C (Table 6.1), which also results in lower contribution to thermal strain (ε^T). The polymer also exhibited relatively high glass transition temperature (170°C) and the enhanced thermal stability of the resin minimizes the thermal strain resulting from lead-free reflow process resulting in high reliability eveb at high temperatures.

6.9 Chapter Summary

In summary, the CAF reliability of fine-pitch through-vias in a glass fiber reinforced cyclo-olefin polymer substrate was investigated. The test structure design for accelerated tests CAF consisted of through-via to through-via geometry with 100 through-vias with conductor spacings of 100, 150 and 200 μm. Based on accelerated tests insulation measurements, all test structures were found to exhibit stable insulation resistance at the two different test conditions. Gravimetric measurements indicated extremely low moisture sorption content at the test conditions. The insulation reliability behavior of the substrate is believed to be a function of the low moisture sorption and high thermal stability of the resin system.

CHAPTER 7

CONCLUSIONS

It has been reported that approximately 26% of the failures in electronic systems are related to substrates. Insulation failures resulting from electrochemical migration of copper in the presence of temperature, humidity and bias voltage resulting in formation of a conductive copper salt are referred to as conductive anodic filament (CAF) failures. CAF failures have been recognized as one of the major threats to miniaturization of electronic systems. The advent of new materials for organic substrates due to environmental regulations challenges in achieving high reliability. This study investigated the effect of small conductor spacings (75 – 200 µm) and influence of substrate material properties on insulation reliability and chemical nature of CAF failure using accelerated testing.

The first part of the study investigated the reliability of through-vias with spacings of 100, 150 and 200 µm in brominated-epoxy substrates (Tg: 150°C and moisture sorption: 0.6 wt%) using two different test conditions. The test structures with 100 µm spacing were found to exhibit insulation failures with short time to failure, which was found to be driven by enhanced drilling-induced defects. The test structures with 150 and 200 µm spacings exhibited better reliability. Elemental characterization of CAF revealed the presence of copper and chlorine in the failure region indicating the formation of a chloride containing CAF compound. Impedance spectroscopy measurements at 50mV AC over a frequency range of 10^{-1} to 10^{5} Hz in test structures revealed significant differences in impedance response for the three samples (control, CAF growth and insulation failure) before and after exposure to humidity.

The second part of the study reported the reliability of fine-pitch wiring (through-vias and surface-traces) in two different halogen-free epoxy substrates with conductor

spacing of 75 - 150 µm. The through-via to through-via test structures with 100 µm exhibited short mean time to failure in either substrates with most failures occurring within 120 h in either substrate system in spite of its lower moisture sorption (0.2 – 0.4 wt%). At a through-via spacing of 150 µm, there were lesser number of failures. Cross-sectional analysis of the failure sites revealed the presence of cracking within the resin and interface, and the presence of copper in cracks, resulting in preferred failure sites. Substrate material with high T_g (165°C) was found to exhibit better insulation reliability compared to the material with lower T_g (145°C) in spite of its relatively higher moisture sorption. The through-via to surface-trace geometry in either substrates did not exhibit any insulation failures during the test. However, CAF formation was visible under optical inspection. Elemental characterization of CAF revealed the presence of copper and chlorine even with significantly lesser extractable chloride content compared to the halogenated-epoxy substrates.

The final study reported the reliability of fine-pitch through-vias (spacings: 100, 150 and 200 µm) in cyclo-olefin polymer substrates and demonstrated a potential solution for achieving high reliability at small conductor spacings. The substrate exhibited the lowest moisture sorption (< 0.1 wt%) and high thermal stability. All test structures were found to exhibit stable insulation resistance. The insulation reliability behavior of the substrate was due to the low moisture sorption and high thermal stability of the resin system.

This study suggests that CAF reliability is a serious concern when moving to smaller conductor spacings with mechanically-drilled through-vias in glass fiber reinforced organic substrates. Potential solutions for mitigating CAF failures at small spacings based on this study include minimizing fracture by drilling process optimization, exploring alternate via drilling methods such as laser via drilling to achieve small conductor spacings, and using low moisture uptake substrates such as cyclo-olefin polymers.

CHAPTER 8

FUTURE WORK

This study investigated the insulation reliability of mechanically-drilled fine-pitch through-vias in thin substrates. While mechanical drilling remains the preferred low-cost method for through-via formation in substrates, sufficient reliability could not be achieved at small conductor spacings. Smaller through-via diameters and spacings can be achieved using laser drilling process. Therefore, it is necessary to investigate the reliability of laser-drilled through-vias with small conductor spacings in thin substrates.

It would be useful to evaluate both thinner glass fibers for the same substrate thicknesses to minimize drilling induced defects and thin butter-coat layers to prevent CAF formation between through-vias and surface-traces. It would also be useful to investigate the effect of mechanical properties of the halogen-free resin systems that include high filler content for improving thermomechanical properties on drilling induced fracture and insulation reliability for small via spacings.

This study revealed the formation of chloride-containing copper compounds in halogenated and halogen-free epoxy resin based substrates. It would be useful to investigate if compounds such as copper hydroxide can form in the absence of sufficient concentration of chloride and bromide ions that can result in insulation failures.

REFERENCES

[1] R. R. Tummala and E. J. Rymaszewski, *Microelectronics Packaging Handbook*. New York: Van Nostrand Reinhold, 1989.

[2] International Technology Roadmap for Semiconductors, ITRS 2010 Edition.

[3] V. Sundaram, R. R. Tummala, F. Liu, P. A. Kohl, J. Li, S. A. Bidstrup-Allen, and Y. Fukuoka, "Next-generation microvia and global wiring technologies for SOP," *IEEE Transactions on Advanced Packaging,* vol. 27, no. 2, pp. 315-325, May 2004.

[4] G. Lee, P. Liang, and J. Lin, "A thermally enhanced halogen free laminate material to reduce the impact of lead free process," in *Microsystems, Packaging, Assembly & Circuits Technology Conference,* 2008, pp. 167-170.

[5] M. Rakotomalala, S. Wagner, and M. Döring, "Recent developments in halogen free flame retardants for epoxy resins for electrical and electronic applications," *Materials*, vol. 3, no. 8, pp. 4300-4327, 2010.

[6] L. J. Turbini, "Processing and material issues related to lead-free soldering," *Lead-Free Electronic Solders.* Springer US, 2007, pp. 147-154.

[7] D. J. Lando, J. P. Mitchell, and T. L. Welsher, "Conductive anodic filaments in reinforced polymeric dielectrics: formation and prevention," in *17th Annual IEEE Proceedings of Reliability Physics,* 1979, pp. 51–63.

[8] A. Caputo, L. J. Turbini, and D. D. Perovic, "Design limitations related to conductive anodic filament formation in a micro-world," *Microsystem Technologies - Special Issue on MicroNanoReliability,* vol. 15, no.1, pp. 39-44, 2009.

[9] K. Ramachandran, F. Liu, V. Sundaram, and R. Tummala. "Conductive anodic filament reliability of small and fine-pitch through-vias in halogen-free organic packaging substrate," *IEEE Transactions on Components, Packaging and Manufacturing Technology*, vol.3, no. 2, pp. 282-288, 2013.

[10] L. D. Olson, *Electronic Materials Handbook Volume 1, Packaging, Materials: Resins and Reinforcements*. Park, OH: ASM International, 1989, pp. 534-537.

[11] E. P. Plueddemann, *Silane Coupling Agents*. New York: Plenum press, 1991.

[12] D. Y. H. Lau, "Evaluation of halogen-free laminates used in handheld electronics." M.S. thesis, Mech. Eng, University of Waterloo, 2009.

[13] L. J. Turbini, "Chemical changes for lead-free soldering and their effect on reliability," *Lead-Free Solders: Materials Reliability for Electronics*. pp. 179-194, 2012.

[14] S. P. Muraka, I. V. Verner, and R. J. Gutmann, *Copper - Fundamental Mechanisms for Microelectronic Applications*. New York: John Wiley and Sons Inc, 2000.

[15] G. T. Kohman, H. W. Hermance, and G. H. Downes, "Silver migration in electrical insulation," *Bell System Technical Journal*, vol. 34, pp. 1115-1147, 1955.

[16] P. J. Boddy, R. H. Delaney, J. N. Lahti, E. F. Landry, and R. C. Restrick. "Accelerated life testing of flexible printed circuits," in *14th Annual IEEE Reliability Physics Symposium*, 1976, pp. 108-117.

[17] J. N. Lathi, R.H. Delaney, and J. N. Hines, "The caracteristic wear-out process in epoxy glass printed circuits for high density electronic packaging," in *17th Annual Proceedings of Reliability Physics*, 1979, pp. 39-43.

[18] M. J. N. Pourbaix, *Atlas of Electrochemical Equilibria in Aqueous Solutions*. New York: Pergamon Press, 1966, pp. 384-392.

[19] B. S. Rudra, M. G. Pecht, and D. Jennings, "Assessing time-to-failure due to conductive filament formation in multi-layer organic laminates," *IEEE Transactions on Components, Packaging and Manufacturing Techniques-Part B*, vol. 17, pp. 269-276, Aug 1994.

[20] P. C. Liu, D. W. Wang, E. D. Livingston, and W. T. Chen, “Moisture absorption behavior of printed circuit laminate materials,” *Advances in Electronic Packaging*, vol.4, no. 1, pp. 435-442, 1993.

[21] W. J. Ready, “Factors which enhance conductive anodic filament (CAF) formation,” M.S. thesis, Met. Eng., Georgia Institute of Technology, Atlanta, GA, 1997.

[22] C. Cohn and H. Kimbara, "Via to via isolation vs. quality of via formation in organic substrates," in *Electronics Packaging Technology Conference*, 2007, pp. 86-93.

[23] K. Sauter, “Electrochemical migration testing results: Evaluating PCB design, manufacturing process and laminate material impacts on CAF resistance,” *CircuiTree*, pp. 10-19, 2002.

[24] A. Brewin, Z. Ling, and C. Hunt, "Susceptibility of glass-reinforced epoxy laminates to conductive anodic filamentation," *NPL Report MATC(A) 155*, 2004.

[25] L. S. Chan, "Effects of curing agents and drilling methods on CAF formation in halogen-free laminates," M.S. thesis, Mech. Eng, University of Waterloo, 2011.

[26] K. Demir, K. Ramachandran, Y. Sato, Q. Chen V. Sukumaran, R. Pucha, V. Sundaram, and R. Tummala, "Thermomechanical and electrochemical reliability of fine-pitch through-package-copper vias (TPV) in thin glass interposers and packages," in *Proceedings of the 63rd IEEE Electronic Components and Technology Conference, Las Vegas, NV*, 2013.

[27] B. K. Hinds and M. Treanor, “Drilling of printed circuit boards: factors limiting the use of smaller drill sizes,” *Proceedings of the Institution of Mechanical Engineers Part B Journal of Engineering Manufacture*, vol. 214, no. 1, pp. 35–45, 2000.

[28] K. Karavakis and S. Bertling, "Conductive anodic filament (CAF): the threat to miniaturization of the electronics industry," *CircuiTree*, vol. 17, pp. 70, 2004.

[29] P. Johander, P. Tegehall, A. A. Osman, G. Wetter, and D. Andersson, "Printed

circuit boards for lead-free soldering: materials and failure mechanisms," *Circuit World*, vol. 33, pp. 10-16, 2007.

[30] K. Rogers, C. Hillman, and M. Pecht. "Hollow fibers can accelerate conductive filament formation," *Practical Failure Analysis*, vol. 1, no. 4, pp. 57-60, 2001.

[31] M. Pecht, C. Hillman, K. Rogers and D. Jennings, "Conductive filament formation: a potential reliability issue in laminated printed circuit cards with hollow fibers," *IEEE Transactions on Electronics Packaging Manufacturing*, vol. 22, no. 1 pp. 80-84, Jan 1999.

[32] H. Su, X. Zhong, G. Zhan, Y. Yu, and W. Gan, "Improvement of interface interaction and conductive anodic filament resistance through amphiphilic oligomeric silane," *Journal of Applied Polymer Science*, vol. 122, iss. 4, pp. 2317–2324, 2011.

[33] D. J. Boday and J. Kuczynski, "Hydrophobic silane coating for preventing conductive anodic filament (CAF) growth in printed circuit boards," *U.S. Patent Application*, 12/718,213.

[34] P. C. Liu, D. W. Wang, S. J. Fuerniss, M. D. Poliks, J. Orbzut, L. M. Siperko, W. T. Chen, R. D. Havens, and R. M. Murcko, "Moisture absorption and its effect on the performance of printed circuit materials," in *Materials Research Society Symposium Proceedings*, vol. 323, 1994, pp. 309-319.

[35] K. M. Takahashi, "Conduction paths and mechanisms in fr-4 epoxy / glass composite printed wiring boards," *Journal of the Electrochemical Society*, vol. 138, no. 6, pp. 1587-1593, 1991.

[36] D. R. Lefebvre, K. M. Takahashi, A. J. Muller, and V. R. Raju, "Degradation of epoxy coatings in humid environments: the critical relative humidity for adhesion loss," *Journal of Adhesion Science and Technology*, vol. 5, no. 3, pp. 201-227, 1991.

[37] X. Fan, "Mechanics of moisture for polymers: fundamental concepts and model study," in *International Conference on Thermal, Mechanical and Multi-Physics Simulation and Experiments in Microelectronics and Micro-Systems*, 2008, pp. 1-14.

[38] H. Murai, T. Fukuda, and T. Fischer, "Evaluation of CAF property for very narrow TH pitch," in *Proceedings of IPC Annual Meeting*, 2008.

[39] L. Fu, J. Qu, and H. Chen, "Mechanical drilling of printed circuit boards: the state-of-the-art", *Circuit World*, vol. 33, iss: 4 pp. 3 – 8, 2007.

[40] L. Gopalakrishnan, M. Hu, and M. Brillhart, "Conductive anodic filament formation - effect of feature sizes on product reliability," in *SMTA International Conference Proceedings*, 2004, pp. 429-437.

[41] W. J. Ready and L. J. Turbini, "The effect of flux chemistry, applied voltage, conductor spacing, and temperature on conductive anodic filament formation," *Journal of Electronic Materials*, vol. 31, no. 11, pp. 1208-24, 2002.

[42] G. Parry, P. Cooke, A. Caputo, and L. J. Turbini, "The effect of manufacturing parameters on board design on CAF evaluation," in *Proceedings of the International Conference on Lead-free Soldering*, 2005.

[43] A. Caputo, "Conductive anodic filament (CAF) formation," Ph.D. dissertation, Mat. Sci. Eng, University of Toronto, 2012.

[44] IPC-TM-650 2.6.25, "Conductive anodic filament (CAF) resistance test: X-Y axis," The institute for interconnecting and packaging, electronic circuits, IPC, Northbrook, IL, 2003.

[45] B. Sood and M. Pecht, "Conductive filament formation in printed circuit boards: effects of reflow conditions and flame retardants." *Journal of Materials Science: Materials in Electronics*, vol. 22, pp. 1602-1615, 2011.

[46] G. E. Balcome, P. K. Brett, J. Kuczynski, T. G. Ryks, and T. J. Tofil, "Preventing conductive anodic filament (CAF) formation by sealing discontinuities in glass fiber bundles," *U.S. Patent 20,130,052,409*, 28 Feb. 2013.

[47] L. Zhang, "Barrier layer to prevent conductive anodic filaments." *U.S. Patent No. 8,143,532*. 27 Mar. 2012.

[48] X. C. Wang , Z. L. Li , T. Chen , B. K. Lok, and D. K. Y. Low, "355nm DPSS UV laser cutting of FR4 and BT/epoxy-based PCB substrates," *Optics and Lasers in Engineering*, vol. 46, iss. 5, pp. 404–409, 2008.

[49] A. DerMarderosian, "Raw material evaluation through moisture resistance testing," in *Proceedings of the IPC Fall Meeting*, 1976.

[50] J. A. Augis, D. G. DeNure, M. J. LuValle, J. P. Mitchell, M. R. Pinnel, and T. L. Welsher, "A humidity threshold for conductive anodic filaments in epoxy glass printed wiring boards," in *3rd International SAMPE Electronics Conference*, 1989, pp. 1023-1030.

[51] J. A. Jachim, G. B. Freeman, and L. J. Turbini, "Use of surface insulation resistance and contact angle measurements to characterize the interactions of three water soluble fluxes with FR-4 substrates," *IEEE Transactions on Components, Packaging, and Manufacturing Technology – Part B*, vol. 20, no. 4, pp. 443-451, Nov 1997.

[52] W. R. Bent and L. J. Turbini, "Identifying the chemicals responsible for conductive anodic filament (CAF) enhancement," in *Proceedings of Surface Mount Technology Association International*, 1999, pp. 359-362.

[53] L. J. Turbini, W. R. Bent, and W. J. Ready, "Impact of higher melting lead-free solders on the reliability of printed wiring assemblies," *Journal of Surface Mount Technology*, pp. 10-14, 2000.

[54] W. J. Ready, "Reliability investigation of printed wiring boards processed with water soluble flux constituents," Ph.D. dissertation, Mat. Sci. Eng, Georgia Institute of Technology, Atlanta, GA, 2000.

[55] W. J. Ready, L. J. Turbini, S. R. Stock, and B. A Smith, "Conductive anodic filament enhancement in the presence of a polyglycol-containing flux," in *IEEE International Reliability Physics Proceedings*, 1996, pp. 267-273.

[56] A. Caputo, L. J. Turbini, and D. D. Perovic, "Conductive anodic filament (CAF) formation part I: the influence of water-soluble flux on its formation," *Journal of Electronic Materials*, vol. 39, no. 1, pp. 85-91, 2010.

[57] A. DerMarderosian, "The electrochemical migration of metals," in *Proceedings of the International Microelectronics Symposium*, 1978, pp. 134-141.

[58] W. J. Ready, S. R. Stock, G. B. Freeman, and L. J. Turbini, "Microstructure of conductive anodic filaments formed during accelerated testing of printed wiring boards," *Circuit World*, vol. 21, iss. 4 pp. 5-9, 1995.

[59] W. Q. Meeker and M. J. LuValle, "An accelerated life test model based on reliability kinetics," *Technometrics*, vol. 37, pp. 133-146, 1955.

[60] A. Caputo, L. J. Turbini, and D. D. Perovic, "Conductive anodic filament formation part ii: electrochemical reactions leading to CAF," *Journal of Electronic Materials*, vol. 39, no. 1, pp. 92-96, 2010.

[61] P. M. May, I. M. Ritchie, and E. T. Tan "The corrosion of copper in ethylene glycol-water mixtures containing chloride ions," *Journal of Applied Electrochemistry*, vol. 21, pp. 358- 364, 1991.

[62] A. L. Bacarella and J. C. Griess, "The anodic dissolution of copper in flowing sodium chloride solutions between 25°C and 175°C," *Journal of the Electrochemical Society*, vol. 120, pp. 459-465, 1973.

[63] L. Brossard, "Anodic dissolution of copper in concentrated LiCl solution at pH between 3 and 7," *Journal of the Electrochemical Society*, vol. 130, pp. 403-405, 1983.

[64] M. Braun and K. Nobe, "Electrodissolution kinetics of copper in acidic chloride solutions," *Journal of the Electrochemical Society*, vol. 126, pp. 1666-1671, 1979.

[65] H. P. Lee and K. Nobe, "Kinetics and mechanisms of Cu electrodissolution in chloride media," *Journal of the Electrochemical Society*, vol. 133, pp. 2035-2043, 1986.

[66] H. P. Lee, K. Nobe, and A.J. Pearlstein, "Film formation and current oscillations in the electrodissolution of Cu in acidic chloride media I. Experimental studies," *Journal of the Electrochemical Society*, vol. 132, pp. 1031-1037, 1985.

[67] A. Caputo, L. J. Turbini, and D. D. Perovic, "Characterization and electrochemical mechanism for bromide-containing conductive anodic filament (CAF) failure," *Journal of Electronic Materials,* vol.40, no.9, pp. 1884-1894, 2011.

[68] T. Aben and D. Tromans, "Anodic polarization behavior in aqueous bromide and bromide/benzotriazole solutions," *Journal of the Electrochemical Society*, vol. 142, pp. 398-404, 1995.

[69] R. L. Brossard, "L'electrodissolution du Cuivre dans les Solutions Bromurees," *Canadian Journal of Chemistry*, vol. 62, no. 1, pp. 36-42, 1984.

[70] D. B. Hibbert, S. Richards, and V. Gonzalves, "The kinetics and mechanism of the corrosion of copper in acidified copper (ii) bromide solution," *Corrosion Science,* vol. 30, pp. 367-376, 1990.

[71] T. L. Welsher, J. P. Mitchell, and D. J. Lando, "CAF in composite printed-circuit substrates: characterization, modeling and a resistant material," in *18th Annual Reliability Physics Symposium*, 1980, pp.235-237.

[72] J. P. Mitchell and T. L. Welsher, "Conductive anodic filament growth in printed circuit materials," in *Proceedings of the Printed Circuit World Convention II*, 1981, pp. 80-93.

[73] M. S. Gandhi, J. McHardy, R. E. Robbins, and K. S. Hill, "Measles and CAF in printed wiring assemblies," *Circuit World*, vol. 18, no. 4, pp. 23-25, 1992.

[74] M. Miyatake, H. Murai, S. Takanezawa, S. Tsuchikawa, M. Takekoshi, T. Kotake, and M. Ose, "Newly developed ultra-low CTE materials for thin core PKG," in *62nd IEEE Electronic Components and Technology Conference,* 2012, pp. 1588-1592.

[75] JEDEC JESD22-A110, Test method A110-B, Highly-Accelerated Temperature and Humidity Stress Test (HAST), Electronic industry alliance, Arlington, VA, 1999.

[76] K. L. Rogers and M. G. Pecht, “A variant of conductive filament formation failures in PWBs with 3 and 4 mil spacings,” *Circuit World*, vol. 32, no.3, pp. 11-18, 2006.

[77] K. L. Rogers, "An analytical and experimental investigation of filament formation in glass/epoxy composites," Ph.D. dissertation, Mech. Eng., University of Maryland, College Park, MD, 2005.

[78] W. J. Ready, L. J. Turbini, R. Nickel, and J. Fisher, “A novel test circuit for detecting electrochemical migration and conductive anodic filament,” *Journal of Electronic Materials*, vol. 28, no. 11, pp. 1158-1163, 1999.

[79] IPC-TM-650 2.3.28A, “Ionic analysis of circuit boards, ion chromatography method,” The institute for interconnecting and packaging, electronic circuits, IPC, Northbrook, IL, 2003.

[80] IPC/JEDEC's J-STD-033B.1: Handling, Packing, Shipping and Use of Moisture/Reflow Sensitive Surface Mount Devices, Arlington, VA, 2007.

[81] Asahi Kasei Microdevices Corporation. *Notes on Mounting and Soldering*. Available http://www.akm.com/akm/en/support/technical/attention/mounting [Accessed: July 1, 2013].

[82] K. Hironaka, "Flame-retardant polyester resin composition, molded article thereof, and method of molding the same." *wipo patent no. 2001025332*, 13 Apr. 2001.

[83] M. R. Vanlandingham, R. F. Eduljee, and J. W. Gillespie, "Moisture diffusion in epoxy systems," *Journal of Applied Polymer Science*, vol. 71, no. 5, pp. 787-798, 1999.

[84] T. C. Wong and L. J. Broutman, "Moisture diffusion in epoxy resins Part I. Non-Fickian sorption processes," *Polymer Engineering & Science,* vol. 25, no. 9, pp. 521-528, 1985.

[85] S. Y. Y. Leung, D. C. C. Lam, and C. P. Wong, "Experimental investigation of time dependent degradation of coupling agent bonded interfaces," in *Proceedings of 51st. IEEE Electronic Components and Technology Conference,* 2001.

[86] K. Ramachandran, F. Liu, P. M. Raj, V. Sundaram, and R. Tummala, "Conductive anodic filament failures in fine-pitch through-via interconnections in organic package substrates," *Journal of Electronic Materials*, vol. 42, iss. 2, pp. 348-354, 2013.

[87] R. A. Gerhardt, "Impedance spectroscopy and mobility spectra," *Encyclopedia of Condensed Matter Physics.* Elsevier Press 2005, pp. 350-363.

[88] Y. Diamant, G. Marom, and L. J. Broutman, "The effect of network structure on moisture absorption of epoxy resins," *Journal of Applied Polymer Science,* vol. 26, no. 9, pp. 3015-3025, 1981.

[89] L. L. Marsh, R. Lasky, D. P. Seraphim, and G. S. Springer, "Moisture solubility and diffusion in epoxy and epoxy-glass composites," *IBM Journal of Research and Development,* vol. 28, no. 6, pp. 655-661, 1984.

[90] W. L. Wu, W. J. Orts, and C. J. Majkzak, "Water absorption at a polyimide/silicon wafer interface," *Polymer Engineering & Science*, vol. 12, pp. 1000–1004, 1995.

[91] T. Nguyen, B. Byrd, D. Alsheh, W. McDonough, and J. Seiler, "Interfacial water and adhesion loss of polymer coatings on a siliceous substrate," in *Proceedings of Materials Research Society*, vol. 385, 1995, pp. 57–63.

[92] M. H. Shirangi and B. Michel, "Mechanism of moisture diffusion, hygroscopic swelling, and adhesion degradation in epoxy molding compounds," *Moisture Sensitivity of Plastic Packages of IC Devices.* Springer, US, 2010, pp. 29-69.

[93] C. Hillman, "Improved methodologies for identifying root-cause of printed board failures." *Microelectronics failure analysis desk reference (5th ed.),* ASM International, Materials Park (OH), 2004, pp. 524-541.

[94] B. Björn and I. Puigdomenech, "Pourbaix diagrams for the system copper-chlorine at 5-100°C," *SKI Report* 98:19, 1998.

[95] B. Björn and S. O. Pettersson, "Pourbaix diagrams for copper in 5 M chloride solution," *SKI Report* 2:23, 2002.

[96] M. Yamazaki, "Industrialization and application development of cyclo-olefin polymer," *Journal of Molecular Catalysis A: Chemical,* vol. 213, no. 1, pp. 81-87, 2004.

[97] H. Ardebili, E. H. Wong, and M. Pecht. "Hygroscopic swelling and sorption characteristics of epoxy molding compounds used in electronic packaging," *IEEE Transactions on Components and Packaging Technologies,* vol. 26, no. 1, pp. 206-214, 2003.